AD-A056 374 CNR INC NEEDHAM MA F/G 20/14
WIDEBAND LINE-OF-SIGHT CHANNEL SIMULATOR.(U)
JUN 78 P A BELLO, D GOLDFEIN, K P JAUNISKIS F30602-75-C-0242
UNCLASSIFIED RADC-TR-78-118 NL

1 OF 2
AD A056374

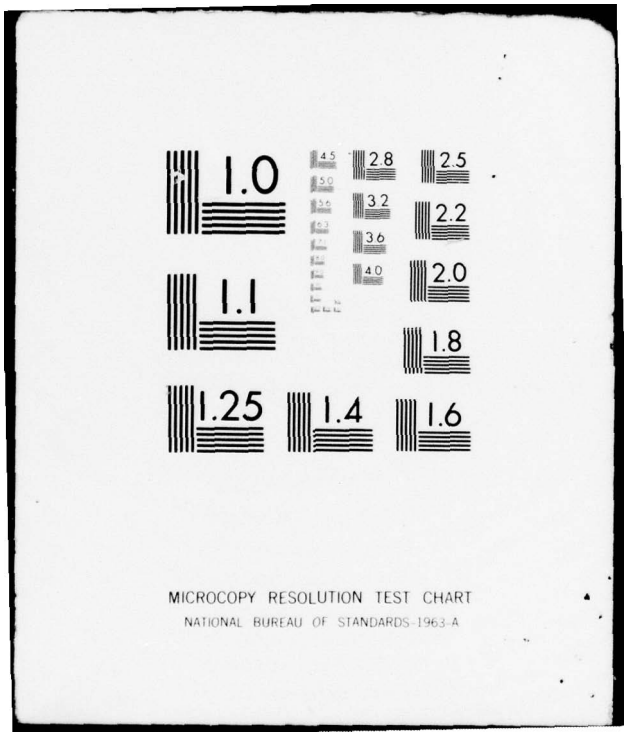
1.0
1.1
1.25
1.4
1.6
1.8
2.0
2.2
2.5
2.8
3.2
3.6
4.0
4.5
5.0
5.6
6.3
MICROCOPY RESOLUTION TEST CHART
NATIONAL BUREAU OF STANDARDS-1963-A

LEVEL II

RADC-TR-78-118
Final Technical Report
June 1978

WIDEBAND LINE-OF-SIGHT CHANNEL SIMULATOR

Phillip A. Bello
David Goldfein
K. Paul Jauniskis
Anthony Lavely

CNR, Inc.

Approved for public release; distribution unlimited.

ROME AIR DEVELOPMENT CENTER
Air Force Systems Command
Griffiss Air Force Base, New York 13441

This report has been reviewed by the RADC Information Office (OI) and is releasable to the National Technical Information Service (NTIS). At NTIS it will be releasable to the general public, including foreign nations.

RADC-TR-78-118 has been reviewed and is approved for publication.

APPROVED: John B. Evanowsky

JOHN B. EVANOWSKY
Project Engineer

APPROVED: Fred I. Diamond

FRED I. DIAMOND
Technical Director
Communications and Control Division

FOR THE COMMANDER: John P. Huss

JOHN P. HUSS
Acting Chief, Plans Office

If your address has changed or if you wish to be removed from the RADC mailing list, or if the addressee is no longer employed by your organization, please notify RADC (DCLF), Griffiss AFB NY 13441. This will assist us in maintaining a current mailing list.

Do not return this copy. Retain or destroy.

UNCLASSIFIED

SECURITY CLASSIFICATION OF THIS PAGE (When Data Entered)

REPORT DOCUMENTATION PAGE

READ INSTRUCTIONS BEFORE COMPLETING FORM

1. REPORT NUMBER: RADC-TR-78-118	2. GOVT ACCESSION NO.
3. RECIPIENT'S CATALOG NUMBER	
4. TITLE (and Subtitle): WIDEBAND LINE-OF-SIGHT CHANNEL SIMULATOR	5. TYPE OF REPORT & PERIOD COVERED: Final Technical Report, Apr 75 - Dec 77
6. PERFORMING ORG. REPORT NUMBER: N/A	
7. AUTHOR(s): Phillip A. Bello, David Goldfein, K. Paul Jauniskis, Anthony Lavely	8. CONTRACT OR GRANT NUMBER(s): F30602-75-C-0242
9. PERFORMING ORGANIZATION NAME AND ADDRESS: CNR, Inc. 220 Reservoir Street Needham MA 02194	10. PROGRAM ELEMENT, PROJECT, TASK AREA & WORK UNIT NUMBERS: 33126F 21570201
11. CONTROLLING OFFICE NAME AND ADDRESS: Rome Air Development Center (DCLF) Griffiss AFB NY 13441	12. REPORT DATE: June 1978
	13. NUMBER OF PAGES: 112
14. MONITORING AGENCY NAME & ADDRESS (if different from Controlling Office): Same	15. SECURITY CLASS. (of this report): UNCLASSIFIED
	15a. DECLASSIFICATION/DOWNGRADING SCHEDULE: N/A

16. DISTRIBUTION STATEMENT (of this Report)

Approved for public release; distribution unlimited.

17. DISTRIBUTION STATEMENT (of the abstract entered in Block 20, if different from Report)

Same

DDC RECEIVED JUL 19 1978 E

18. SUPPLEMENTARY NOTES

RADC Project Engineer: John Evanowsky (DCLF)

19. KEY WORDS (Continue on reverse side if necessary and identify by block number)

Line-of-sight channel simulation
LOS channel measurement
LOS channel modeling
Refractive multipath
Surface multipath
Simulation

20. ABSTRACT (Continue on reverse side if necessary and identify by block number)

This report describes the theoretical background, methods of implementation, and utility of a multi-purpose wiseband LOS (line-of-sight) channel simulation system developed by CNR, Inc. for Rome Air Development Center as a means for evaluating wideband digital modems. The system provides both a channel probing/channel playback capability and a synthetic stochastic channel simulation. Propagation media effects simulated include both multipath due to refractive anomalies (refractive multipath) and scattering off the surface (surface multipath). The types of LOS channels handled by the system include airplane-

DD FORM 1 JAN 73 1473

UNCLASSIFIED

SECURITY CLASSIFICATION OF THIS PAGE (When Data Entered)

78 07 12 018

407 852

airplane, ground-airplane, ground-ground, airplane-satellite. In addition, the simulator allows the introduction of controlled amounts of nonlinearity, phase jitter, and frequency offset. The simulator operates at selectable IF frequencies of 70, 300, or 700 MHz. At the two higher IF frequencies, signal bandwidths up to 100 MHz may be accommodated, while at 70 MHz, bandwidths up to 25 MHz may be handled.

TABLE OF CONTENTS

LIST OF ILLUSTRATIONS

LIST OF ILLUSTRATIONS (Continued)

LIST OF TABLES

EVALUATION

RADC's Technical Program Objective IV, Communication for Command and Control identified a need for media simulators to enable the Air Force to continually provide a capability to evaluate advanced techniques and equipment. The costs and channel characterization problems normally associated with live channel testing can be overcome with the development and application of realistic media simulators which duplicate natural and man-made phenomena. Past experience with channel simulators has dramatically pointed out the great value inherent in the use of this type of device for technique and equipment evaluations.

This effort has provided the RADC Digital Communications Experimental Facility (DICEF) with a system for performing reliable, repeatable simulations for various types of Line-of-Sight (LOS) channels. Immediate applications will include the evaluations of wideband ECCM modems, satellite communications techniques, and point-to-point microwave equipment. In addition, the channel prober/analyzer developed as part of this effort will serve as an invaluable tool for wideband channel characterization.

John B. Evanowsky

JOHN B. EVANOWSKY
Project Engineer

SECTION 1

INTRODUCTION AND SUMMARY

This report will describe the theoretical background, methods of implementation, and utility of a multi-purpose wideband LOS (line-of-sight) channel simulation system developed by CNR, Inc., for Rome Air Development Center as a means for evaluating wideband digital modems. The system provides both a channel probing/channel playback capability and a synthetic stochastic channel simulation. Propagation media effects simulated include both multipath due to refractive anomalies (refractive multipath) and scattering off the surface (surface multipath). The types of LOS channels handled by the system include airplane-airplane, ground-airplane, ground-ground, airplane-satellite. In addition, the simulator allows the introduction of controlled amounts of nonlinearity, phase jitter, and frequency offset. The simulator operates at selectable IF frequencies of 70, 300, or 700 MHz. At the two higher IF frequencies, signal bandwidths up to 100 MHz may be accommodated, while at 70 MHz, bandwidths up to 25 MHz may be handled.

1.1 Background

The development of reliable high-speed digital modems (modulators-demodulators) for use over fading dispersive radio channels can be facilitated greatly with the aid of channel simulators. Two important classes of simulators can be identified:

- Synthetic channel simulation
- Playback or stored channel simulation

In the case of synthetic channel simulation, deterministic or stochastic models are implemented based upon either, or both, theoretical calculations and previously measured statistics. In the case of the playback channel simulation, a long record of parameters characterizing the time-varying system function of a channel (such as tapped delay line weights) are measured with the aid of a channel prober/analyzer and recorded on magnetic tape. This tape is played back into a model of the channel which utilizes the measured parameter values in a corresponding canonic channel model (such as a tapped delay line with weights).

With the playback of a measured and stored channel, there will be identical instantaneous time- and frequency-selective channel conditions as occurred in the field. In the synthetic channel simulation, there will be only statistically similar channel conditions, but they will be adjustable to cover situations expected to occur but not measured due to the limited duration of the field tests. These simulation techniques complement each other in providing tools for modem development.

The simulator described in this report includes both playback channel and synthetic channel simulators and probably represents the most versatile and flexible radio communications channel simulator yet developed. Some of the concepts in the present system design have been developed by Bello [1.1] - [1.7] in previous synthetic and stored-channel simulators he has designed. However, the present equipment represents an expansion of capabilities in terms of simulation bandwidth, flexibility, and operational modes.

1.2 Applicable Channels

The major cost of the simulator is associated with the measurement and simulation of propagation media fading and multipath associated with particular links, namely:

- Ground Aircraft (GA)
- Aircraft-Aircraft (AA)
- Aircraft-Satellite (AS)
- Ground-Ground (GG)

Since propagation media are linear, their input-output behaviors are completely determined by corresponding impulse responses or transfer functions. Because radio channels are time-variant, both the impulse response and transfer function must be regarded as time-variant. It may be shown that the complexity of equipment required to measure, record, and reproduce the characteristics of the propagation channel over a finite bandwidth depends directly upon two gross channel parameters, the multipath spread and the Doppler spread. The multipath spread is a measure of the duration of the impulse response of the channel while the Doppler spread is a measure of the width of the spectrum of a received carrier.

In discussing the values of Doppler spread and multipath spread of a channel and their impact on channel simulator design, it is necessary to distinguish various propagation

modes. For the four canonic LOS channels of interest here (GA, AA, AS, GG), the following three propagation modes are of interest:

- Refractive multipath
- Surface multipath
- Ionospheric scintillation (AS only)

An elevated tropospheric layer with a scale much larger than the wavelength of the carrier can act as a lens which, under proper conditions, focuses the transmitted signal into the receiver over multiple paths. The frequency and intensity of the meteorological conditions which result in such multipath-producing propagation have been studied experimentally [1.8] - [1.21]. The resulting multipath structure has been examined at CNR under three contracts with RADC [1.22] - [1.24], and the numerical results [1.25] agree quite favorably with the experimental data [1.8] - [1.21].

Refractive multipath is a term used to describe the channel characteristics caused by these steep negative gradients in refractive index. The net effect of this gradient is to produce discrete multipath, i.e., a finite set of paths in addition to the direct path between transmitter and receiver. An analysis of the impulse response structure by CNR indicates a maximum of seven paths for a path length of 200 miles. Calculations of multipath are not made beyond 200 miles because the theory assumes a continuous layer and it does not seem likely that layers will extend so long. However, there is a lack of experimental knowledge on layer lengths, so the assumption is purely arbitrary at this point.

Refractive multipath will only occur on LOS paths having an elevation angle of less than 2^{o} - 3^{o}, and is not normally experienced on channels employing a satellite relay which usually do not attempt to communicate at such low elevation angles. On the other hand, the AA, GA, and GG channels perforce operate at low elevation angles of the line-of-sight and thus experience refractive multipath whenever the corresponding propagation conditions exist. On the basis of the propagation model used by CNR, it is found that over most of the world, the worst-case multipath spread is within 65 nanoseconds. The worst Doppler spreads are found to be less than .5 Hz/Mach No./GHz of carrier frequency. Channel measurement would probably be undertaken at speeds of less than Mach .7. For the typical military operating frequency of 8 GHz, we find an expected worst-case Doppler spread of 5.6 Hz.

We consider now the multipath and Doppler spread associated with surface multipath. CNR has carried out considerable study on modeling surface multipath. Although the underlying scattering process which causes this multipath is the same for AS/GS and AA/GA links, operational as well as numerical considerations make the models somewhat different. The AS/GS model was developed at CNR under contract to the Department of Transportation [1.26],[1.27] while the AA/GA model was developed at CNR under contract to RADC [1.29].

The earliest arriving component of the surface multipath is from the "specular" point, i.e., the point of mirror reflection from the surface. Later multipath components come from annular rings at successively large distance from the specular point. There are two sharp contrsts between surface multipath and refractive multipath. First we note the gap in delay between the direct path and the specular delay within which no surface multipath may occur. Refractive multipath is generally clustered soon after the direct path and will frequently be so close as to be unresolvable from the direct path. Second, we note that except for reflections from large objects like mountains or buildings or a "specular" reflection emanating from the average surface around the specular point, the surface multipath consists of a very large number of very small components distributed in delay. Thus it is of a "continuous" nature as opposed to the discrete nature of refractive multipath.

Two other contrasts we wish to make are the behavior of the these modes of propagation as a function of antenna size and operating frequency. Refractive multipath is virtually unaffected by antenna size because the discrete paths are clustered very close to the direct path, deviating only tenths of a degree. Surface multipath is strongly affected by the antenna pattern which can, in principle, be focused to eliminate reflections and scattering from the surface. In practice, antenna sizes are sharply limited for airplane use and surface multipath cannot always be eliminated.

Consider now the effect of changing the operating frequency. In the case of refractive multipath, the relative path delays are to first order, not a function of operating frequency. However, as the operating frequency is lowered sufficiently, the multipath spread will become less than a period of the carrier frequency, and the channel will behave like a single fading path for information transmission. As

the frequency is lowered such that the multipath spread is a small fraction of a carrier frequency period, the fading will disappear because the multipath components will add in-phase.

In the case of surface multipath, the frequency and angle of incidence to the specular point can have a pronounced effect on multipath characteristics. The signal scattered from the surface of the earth (land, water, ice, etc.) has a discrete or specular and a diffuse component. The specular component characterizes the mean signal scattered from the surface, while the diffuse component characterizes the random return due to the roughness of the surface and produces the "continuous" multipath. It may be shown that, for a fixed grazing angle and surface roughness, the multipath will tend to be continuous at the higher (microwave) frequencies and specular or discrete at the lower (UHF) frequencies. For the military links being considered here, there are many naturally-occurring surfaces (e.g., the ocean, hilly terrain, desert, snow drifts, etc.) which will cause diffuse scatter to exist.

The delay difference between the specular and direct signal paths can amount to tens of microseconds for an AS link, while the Doppler difference would be at most 7 Hz/Mach No./GHz of carrier flight for level flight.

We consider now the amount of multipath spread produced by the surface multipath. It has been shown by CNR [1.26] - [1.28] that for sufficiently wide beam antennas and low elevation angles to the satellite, up to 10 μs of multipath spread exist. Since military operational antennas are directive to provide for increased gain, multipath rejection, secure communication, etc. (see [1.30]), multipath spread calculations should be made for typical military situations. It is assumed that the satellite antenna provides broad coverage in a sector which contains the military aircraft, and therefore provides little or no multipath discrimination. However, the aircraft antennas used to communicate with satellites can range from upper hemispherical coverage at UHF to a few degrees beamwidth at the higher microwave frequencies.* The coverage provided by these antennas is indicated

---

*In three years of airborne testing [1.31], blade, dipole, and crossed slot UHF antennas were used to provide upper hemispherical coverage; at S-band, a $\pm 2^{o}$ beamwidth antenna was used. In [1.30], a 32-inch Cassegrain with a 3^{o} beamwidth at SHF was mounted on a KC-135.

in Figure 1.1. Since the antennas are designed for satellite communications, the usual case is for the multipath to occur in a sidelobe, as shown in Figures 1.1(a) and (b). However, when the satellite is at a very low elevation angle, the multipath may occur in the main beam of the antenna, as shown in Figure 1.1(c).

Approximate calculations of multipath spread due to sidelobe illumination have been carried out by CNR for various grazing angles γ and beamwidths θ for diffuse scatter at microwave frequencies. For antenna beamwidths less than about 3^{o}, the maximum (sidelobe) delay spread has been found to be about 200 nanoseconds at an aircraft altitude of 30,000 feet.

If the main beam illuminates the earth's surface as it may when the satellite is near the horizon, the scattered power can be calculated from the scattering cross section, the surface roughness, and the $1/R^2$ losses. In calculating the multipath power, we have assumed worst-case rms surface slope α, i.e.,

$$\alpha = \alpha_{max} = \tan \gamma \qquad (1.1)$$

where γ is the grazing angle to the specular point. (The rougher the surface, the larger the surface area over which scattering takes place and the larger the multipath spread.) When $\alpha > \tan \gamma$, a significant part of the surface becomes shadowed by the surface irregularities, and the multipath power is typically reduced by an order of magnitude [1.31, p. 116]. The results of such an approximate calculation show that, for grazing angles less than about 3^{o}, the multipath spread (defined here as the delay beyond the specular delay at which the multipath power drops to 1/e of its maximum value) is less than 200 ns.

Similarly, one may calculate the Doppler spreads for the cases of sidelobe illumination and mainbeam illumination of the surface at low grazing angles. One may show that, for an 8-GHz carrier frequency and Mach .7, Doppler spreads of less than 10 Hz are predicted for a beamwidth of 3^{o} in the case of sidelobe illumination and for any beamwidth in the case of mainlobe illumination of the surface. Note that the Doppler spread decreases with decreasing grazing angle.

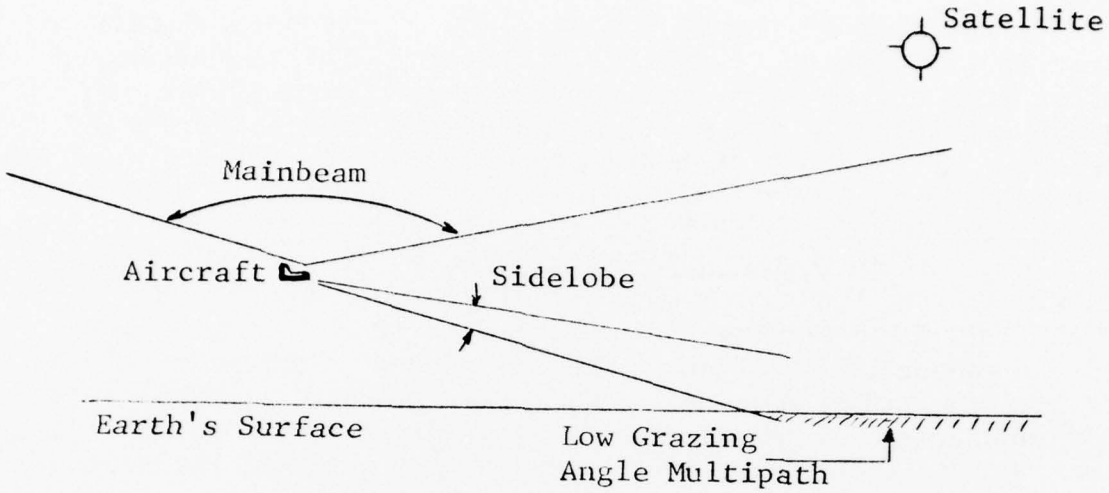

(a) UHF Antenna Coverage

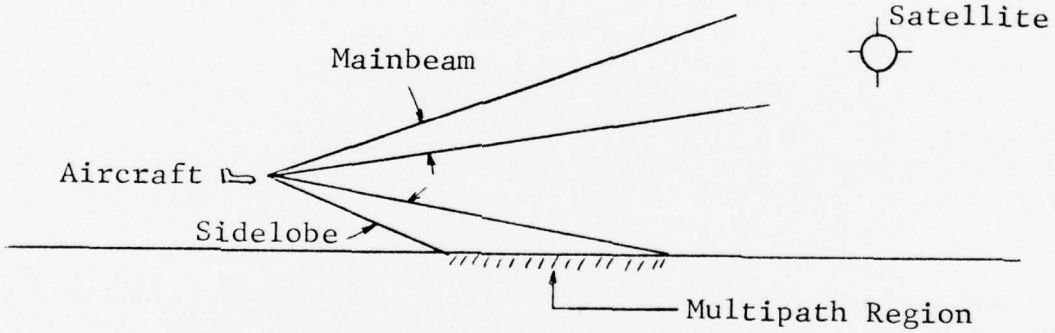

(b) Higher Frequency Microwave Antenna Coverage at High Elevation Angle

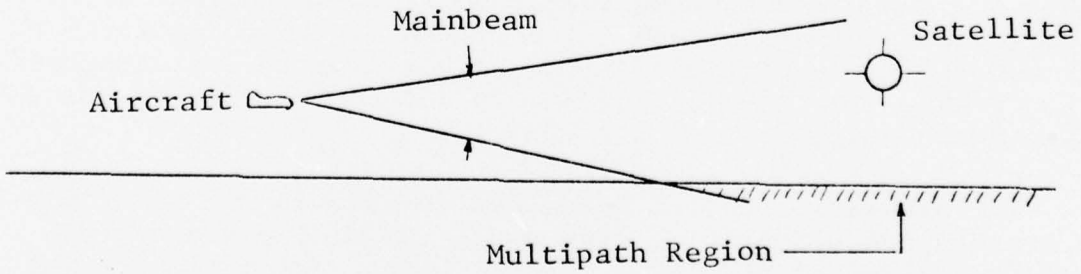

(c) Higher Frequency Microwave Antenna Coverage at Low Elevation Angle

Figure 1.1 Antenna Coverage on Military Aircraft-Satellite Links

In the case of the AA and GA links, surface multipath will occur in addition to refractive multipath. The AA/GA links differ from the AS link, however, in that the multipath is always generated at low grazing angles and within the radio horizon. As a result of these differences, the surface scatter multipath on AA/GA has a specular component which is delayed only a few hundred nanoseconds from the direct path and shifted by at most 10 or 20 Hz. The multipath spread is worst for AA links. For AA links, one may calculate that aircraft at 30,000 feet with antenna beamwidths less than 3^{o} experience diffuse multipath with delay spreads of less than about 150 ns for grazing angles above 1^{o}. At angles below 1^{o}, the diffuse multipath power decreases due to shadowing and due to the tendency of the multipath to be specular near grazing incidence.

Calculations of Doppler spreads indicate small values of the order of these found in other cases, e.g., 10 Hz or less for 8 GHz, Mach .7, and 3^{o} beamwidths.

In the case of GG links with parameters representative of those used in conventional microwave relay communications, multipath spreads and Doppler spreads will be much smaller than those quoted for other links. Calculations are available in a report by CNR [1.22].

As a final channel characteristic, we consider ionospheric scintillation. This phenomenon is of relevance only for AS links in which the LOS pierces regions of the ionosphere which are perturbed anomalously in the vicinity of the equator. From an input-output point of view, the effect is one of causing amplitude and phase fluctuations, i.e., Doppler spread with negligible multipath spread. The effect is quite important at UHF but will be negligible at the higher microwave frequencies, e.g., 8 GHz. The Doppler spread, in any case, is quite low — a few Hz at most.

The simulation system described in this report is designed to measure and playback or synthesize the fading dispersive characteristics of GA, AA, AS, and GG links for various combinations of refractive multipath, surface multipath, and ionospheric scintillation.

1.3 Measurement and Simulation Approach

The problem of channel measurements on fading dispersive channels has been studied extensively by Bello [1.34] - [1.39]. We consider in sequencies the approach used for channel measurement, playback simulation, and synthetic simulation.

1.3.1 Channel Measurement and Playback

The channel measurement approach used here involves transmission of a pseudo-random binary PSK ($0,180^{o}$) with the ($0,180^{o}$) states controlled by the (0,1) states of a maximal length shift register sequence. The receive process is (complex) correlated with delayed replicas of the pseudo-random probing signal to produce lowpass in-phase and quadrature estimates of the channel* time-variant impulse response at a set of equally-spaced delay samples. This set of time-varying samples is digitized and recorded on magnetic tape. In playback, the reverse operation takes place - the tape is played back into a unit that unpacks the samples, filters them, and D/A converts the tape information into the lowpass in-phase and quadrature information needed to drive the analog complex modulators of an analog tapped delay line model of the channel.

To keep the system complexity reasonable, provision is made for separately and simultaneously measuring the surface multipath starting at the earliest arriving specular component and ignoring the "empty" region between the direct/refractive multipath and the surface multipath. By using this procedure, maximum utilization is made of the hardware in measuring and reproducing multipath.

The preceding discussion introduced some of the basic signal processing elements in the channel playback simulation system. However, practical utilization of this system requires the incorporation of additional features for the LOS channels which have moving terminals (GA, AA, AS). The changing path length causes both a time variation in path loss and a time variation in mean path delay for the direct path, refractive multipath, and surface multipath. To handle the time-variant delays, two tracking loops are used which adjust the timing of two separate PN sequence generators. The early tracker removes

*The channel impulse response includes all terminal equipment filters.

the time-variant group delay of the direct/refractive multipath group while the late tracker separately removes the time-variant group delay of the surface multipath. Frequently, refractive multipath will be absent and the direct path alone will be tracked in the early group. The changing path delays also produce Doppler shifts. A Doppler tracking loop is provided to track out the Doppler shift of the direct/refractive multipath group.* Otherwise, the output lowpass filters would have to be made very wide in bandwidth to accommodate this Doppler shift. The Doppler shift of the surface multipath group will differ from that of the direct/refractive multipath group, but for channel measurement with airplanes flying at level height, the differential Doppler will be at most 10 - 20 Hz, and this shift is small enough to be absorbed by the analyzer lowpass filter bandwidth ranges. Therefore, in the interest of cost savings, no separate Doppler tracker is provided for the surface multipath.

In channel playback, ideally, the variable delays and Doppler shifts should be reinserted. It has been found prohibitively expensive to provide time-variable delays covering the range of delays required. Moreover, there appears no need to have this feature, from a modem evaluation point of view. Differential and direct path Doppler may be set manually at measured values recorded in the log of the flight test. Differential delay is fixed but manually-selectable from a range of values. Again, information from the log of the experiment would provide suitable values for this delay. Direct path delay would not be reproduced since it is irrelevant for modem testing. Note that simply setting the bit sync clocks at different rates for the digital modulator and demodulator simulates changing relative path delay.

Path loss variation will be significant only for the AA and GA links where variations of path length greater than 10:1 may occur during a channel measurement period, causing in excess of a 20-dB variation in average SNR during a measurement interval. To make maximum utilization of the dynamic range of the analog correlators employed in the analyzer, an AGC is provided.

---

*Actually, different frequency and time error discriminators are provided for tracking refractive multipath as opposed to tracking a resolvable direct path in order to optimize tracking performance under the fading dispersive conditions of refractive multipath.

Since the path loss variation will be slow, a long time-constant is provided in the AGC. Cases may exist where the fading multipath could have low enough frequency components to be affected by the AGC, and provision is made for recording the gain variations and reproducing them in the channel playback by means of a variable attenuator.

1.3.2 Synthetic Simulation

We consider now the synthetic simulation of the propagation channel. The same tapped delay line is used as in playback simulation, but now the complex tap gains must be generated synthetically.

The two major harmful propagation effects that require some complexity in implementation are refractive and surface multipath. From a mathematical-statistical point of view, these two propagation effects present a study of contrasts. The refractive multipath consists of a small number of individual paths while the surface multipath (aside from a possible specular component) consists of a very large number of small diffuse scattered components and has a continuous type of representation.

From a statistical point of view, the refractive multipath is far more nonstationary than the surface scatter. Consider an AG link. As the airplane passes near the layer of steep negative gradient in refractive index which causes the refractive multipath, multiple ray paths appear, move in delay relative to one another, coalesce, disappear, and new paths appear. As discussed in [1.23], the amplitudes and delays change much slower than the relative phases. Compare this behavior with the surface scatter in an AS link. The airplane antenna is illuminating (through a main or sidelobe) a large portion of the surface of the earth. Many small reflections occur from the surface, and the law of large numbers gives some statistical regularity to the continuum of multipath components. No abrupt changes will be noticed unless the terrain or airplane antenna orientation changes abruptly. Over the ocean, statistical regularity will be the rule rather than the exception.

It may be shown [1.33] that, as the reciprocal channel bandwidth to be characterized becomes small compared to the multipath spread in surface or volume scatter, the tapped delay line model of the channel approaches the case in which the tap gains are complex Gaussian and independent. This is the basic model employed for synthetic simulation of surface multipath.

The complex Gaussian weights are obtained by filtering pseudo-random sequences.

Since the tapped delay line model, with taps spaced 1/W apart and complex weights, provides a perfectly general representation for a linear operation over a bandwidth W, it is possible to find a mathematical relationship between the delays and amplitudes of a discrete set of paths and the complex weights in a tapped delay line model. This relationship is implemented with the aid of a small computer whose input is a tape providing the time-varying path delays and amplitudes associated with the refractive multipath of a given AA/AG/GG scenario. The calculated tap weights are continually generated by the computer and fed as control inputs to the tapped delay line complex modulators. Continuous movement of up to seven discrete paths is provided with the software.

The computer also generates the ionospheric scintillation modulation. The model used involves independent Gaussian noises of different strengths on the in-phase and quadrature inputs of the complex modulator together with a specified nonfading component on the in-phase part.

1.4 Summary of Prober/Analyzer/Simulator System Features

This section summarizes the basic features of the Prober/Analyzer/Simulator system. We consider the prober/analyzer first.

The prober/analyzer has several classes of operating modes:

- Characterization Bandwidth Modes
- IF Frequency Modes
- Integration Time Modes
- Correlator Grouping Modes
- Tracking Modes
- Gain Control Modes

Characterization bandwidths of 25 and 100 MHz may be selected. In the 25-MHz case, an IF frequency of 70 MHz only can be selected, while in the 100-MHz case either 300 MHz or 700 MHz can be selected. It is important to note that the quoted bandwidth characterization, e.g., 100 MHz, is not a nominal characterization but a precise characterization in the sense that the system provides essentially transparent performance over this bandwidth as far as modem error rate reproducibility is concerned in channel playback. (Of course, this

statement is subject to the requirement that sufficient SNR is available during measurement and that the Doppler and multipath spread do not exceed the design values.) Separate IF channelizing filters must be switched in for the 25- and 100-MHz bandwidths to limit alias crosstalk due to the sampling of the impulse response and also separate equalizing filters must be switched into the simulator in the playback mode to counteract the coloring of the prober spectrum. The probing signal in the case of 100-MHz characterization consists of a pseudo-random $(0,180^{o})$ sequence with chip period Δ_0 of 10 ns, i.e., a 100M chips/second rate, while in the 25-MHz characterization, $\Delta = 40$ ns and the chip rate is 25M chips/second. A sequence length of 2047 is used in the 100-MHz mode providing a PN sequence period of 20.47 μs, while in the 25-MHz mode, a sequence length of 511 is used providing a PN sequence period of 20.44 μs.

Analog integrate-and-dump takes place over exactly one PN sequence period at the correlator output. Further integration is done digitally by summing successive analog I&D outputs. It is convenient in discussing system performance to define six modes of operation I - VI, as indicated on Table 1-1, for the various values of total integration time T possible for the system, where $T = I T_0$, $I = 1,2,4,8,16,32$.

Table 1-2 presents the recording time and tape speed for a roll of instrumentation tape for each mode I - VI listed in Table 1-1. Note that because of the approximately 20-μs period of the PN sequence, an ambiguity in multipath delay will occur for paths delayed from the direct path more than 20 μs. This 20-μs ambiguity does not constitute a real limitation to collection of data by the system because long differential delays occur only in the AS channel from which the multipath spread is predicted to be much less than 20 μs. The differential delay can be computed fairly accurately for the radio link geometry so that one may avoid foldover effects for multipath near the 20-μs boundary. In addition, it is only at low grazing angles that any multipath is predicted, and for these grazing angles the differential delay will be smaller than 20 μs.

As discussed above, the channel multipath structure will consist of either a single group of paths or two groups, depending on the simultaneous existence of refractive and surface multipath. Flexibility exists within the analyzer to apportion one subset of the correlators to the early multipath group and one subset to the late multipath group. However, for playback,

TABLE 1-1

DEFINITION OF SOME MODES OF OPERATION OF PROBER/ANALYZER

Mode	Characterization Bandwidth (MHz)	PN Sequence Length	Samples Integrated Prior to Recording
I	100 25	2047 511	1
II	100 25	2047 511	2
III	100 25	2047 511	4
IV	100 25	2047 511	8
V	100 25	2047 511	16
VI	100 25	2047 511	32

TABLE 1-2

DIFFERENTIAL DELAY AMBIGUITY, RECORDING CAPABILITY, AND TAPE SPEED FOR EACH MODE

Mode	Unambiguous Delay Resolution (nearest μs)	Recording Duration of One Roll of Tape	Tape Speed
I	20 μs	15 mins	120 ips
II	20 μs	30 mins	60 ips
III	20 μs	60 mins	30 ips
IV	20 μs	2 hrs	15 ips
V	20 μs	4 hrs	7½ ips
VI	20 μs	8 hrs	3¾ ips

the early group must consist of no more than eight taps in the 100-MHz mode (and two taps in the 25-MHz mode*) because of the physical construction of the simulator. In this split mode of operation, 52.5 ns of refractive multipath (including the equipment channel) can be measured. A direct path is separately measurable when there is no refractive multipath, leaving 31 samples to characterize the surface multipath.

The direct path and surface multipath are separately tracked in delay while only the Doppler shift of the direct path is tracked. Calculations of differential Doppler for collection of data in level flight show that it is small enough to be handled by the bandwidths used in measuring the tap gains. When refractive multipath is present, the fading distortion can affect operation of the coherent direct path tracking. Consequently, alternate delay and Doppler error discriminators more tolerant to multipath and fading are provided and may be selected when refractive multipath is being tracked.

Due to the fact that the path length can change significantly during a collection interval of 30 minutes for AA and AG links, the received signal strength can vary significantly during a run, say, 20 dB. Two modes of gain control are provided, manual and automatic, both over a range of 60 dB. In the AGC mode, a long time constant is used to attempt tracking only the slow path loss variations. However, refractive multipath can vary slowly and, to avoid any possible distortion caused by tracking out refractive multipath fluctuations, the automatic gain fluctuations are recorded on tape and reproduced by a variable attenuator in the channel playback process.

Additional features in the analyzer include a received signal level (RSL) indicator with a LED numeric display, a multipath signal display showing the correlator I&D outputs on an oscilloscope, and a differential path delay indicator with a LED numeric display. Direct-path Doppler may be estimated from the vernier on the Doppler tracking VCXO. There is also an indication for overflow of the A/D converters and underdriving of the correlators.

---

*Because of equipment impulse response spreading, the use of two taps to represent a multipath group appears risky. Thus it may be preferable not to use the 25-MHz mode when both refractive and surface multipath occur.

The simulator has several modes of operation. As far as control of the complex modulators is concerned, there are five basic modes of operation, each one of which may be independently selected for each complex modulator input:

- Playback
- Computer Control
- Synthetic Complex Gaussian
- Calibrate Check
- External Modulation

The playback mode derives its complex modulator input from playback of the recorded multipath analyzer outputs. When this mode is used, an analog equalizer must be switched in to compensate for the non-white prober spectrum. In addition, as pointed out above, if the AGC mode is used in the analyzer, then a gain voltage will be played back to control an output attenuator.

Any set of complex modulator inputs may be controlled by the PDP-11/04 minicomputer provided with the simulator. This computer can provide simulations of refractive multipath, ionospheric scintillation, specular components, arbitrary complex fixed filters, and special programs for checking out the tap modulators and D/A converters. The simulation of refractive multipath utilizes the minicomputer to prepare digital tapes of relative amplitudes and delays of discrete multipath components vs. time, corresponding to a particular scenario of interest. This tape is played back by the minicomputer so that it may generate the complex modulator time-variant gains corresponding to that scenario. Ionospheric scintillation is modeled by use of programs to generate pseudo-random Gaussian modulations.

Special hardware generates the pseudo-random complex Gaussian noise tap modulation used to model surface multipath. The rms Doppler spread of this noise is selected at the front panel in the range 0.1 Hz to 1 kHz. This noise can be reset to the same starting point. A very long PN sequence (shift register length 52) is used to provide an accurate Gaussian probability density, and the period of the PN sequence is very much longer than any measurement interval of interest.

In the calibrate mode, each tap may be set to one of four phases, 0, 180^{o}, 90^{o}, -90^{o}, or OFF manually. By sending a test signal into the simulator and examining the system output for each separate modulator, it is possible to check directly on

the complex modulator performance. This check, in conjunction with similar tests directed from the minicomputer, can be used to isolate and verify performance.

Finally, there is an external modulation mode where the in-phase and quadrature components of any tap complex modulator may be controlled by an external modulation source.

There are two basic differential delay options: a short differential delay for AA and AG links, and a long differential delay for AS links. The value of the short differential delay, implemented with cable, may be selected from the values 100, 200, 300, and 400 ns, while the long differential delay, implemented with SAW devices, may be selected from the values 4.1, 8.1, 12.1, and 16.1 μs.

Figure 1.2, 1.3, and 1.4 show photographs of the fabricated system. Figure 1.2 shows the prober, Figure 1.3 the multipath analyzer, and Figure 1.4 the simulator. The analog and RF signal processing elements are in a double-bay rack cabinet along with the digital signal sources for synthetic surface scatter multipath generation and test modes. The computer and playback tape signal sources are in a second cabinet.

The bulk of the remainder of this report is contained in Section 2 which delves into the theoretical background for the system and develops design criteria based upon the objective of producing a simulator that will allow reproducibility of modem error rate behavior. Section 3 is a relatively brief description of the equipment with tables of specifications.

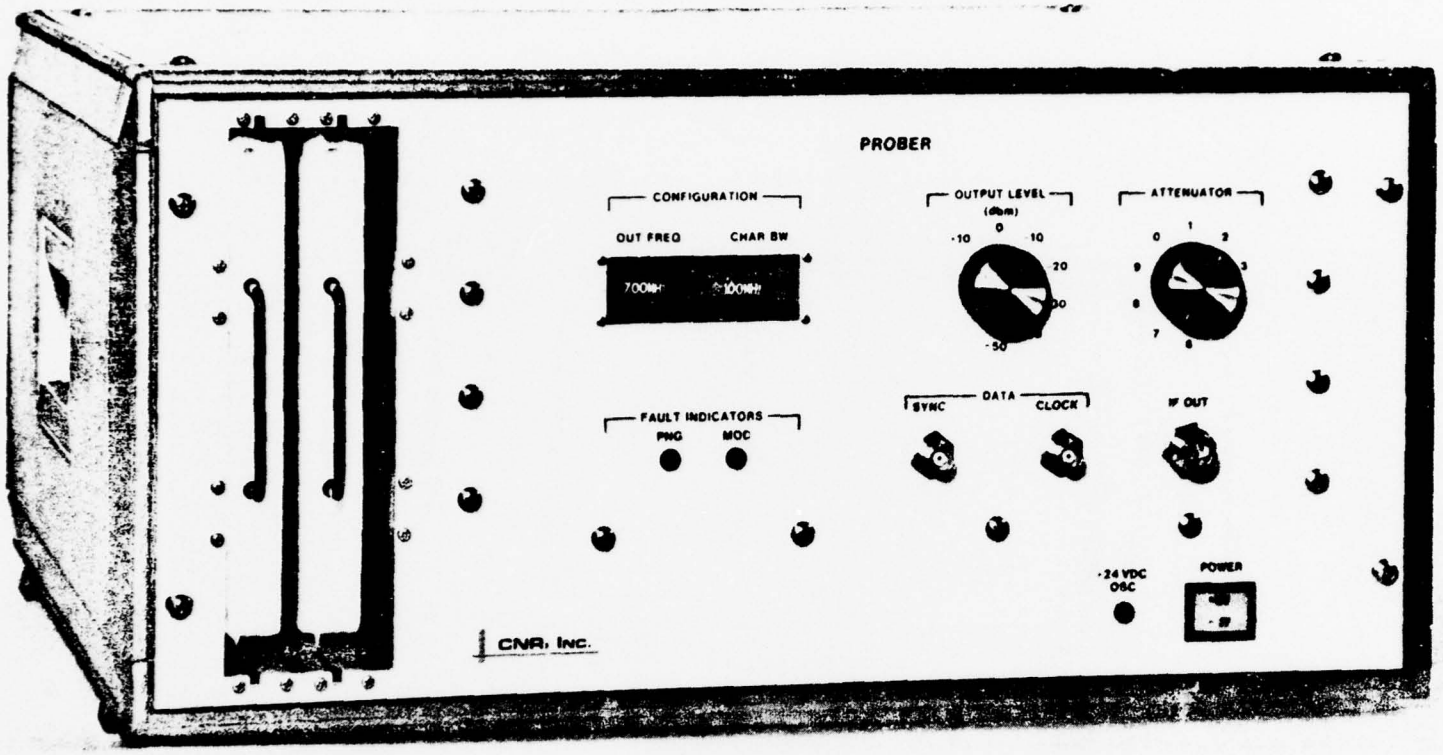

Figure 1.2 LOS Channel Prober

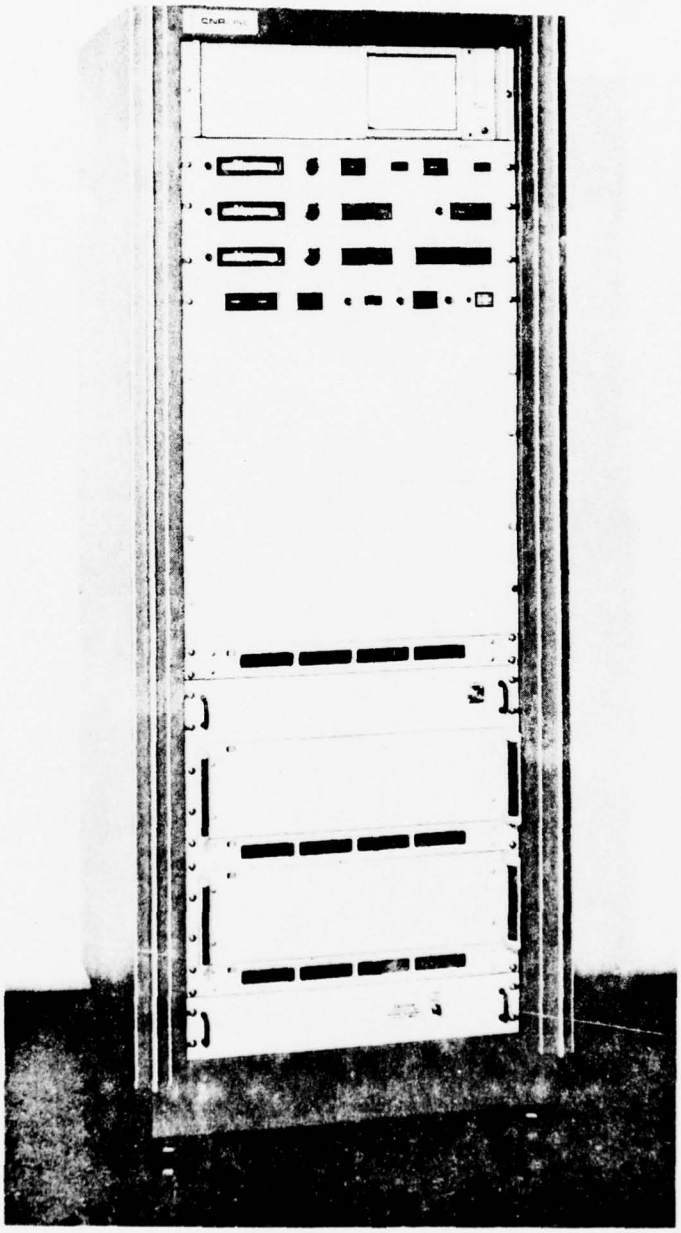

Figure 1.3 Analyzer

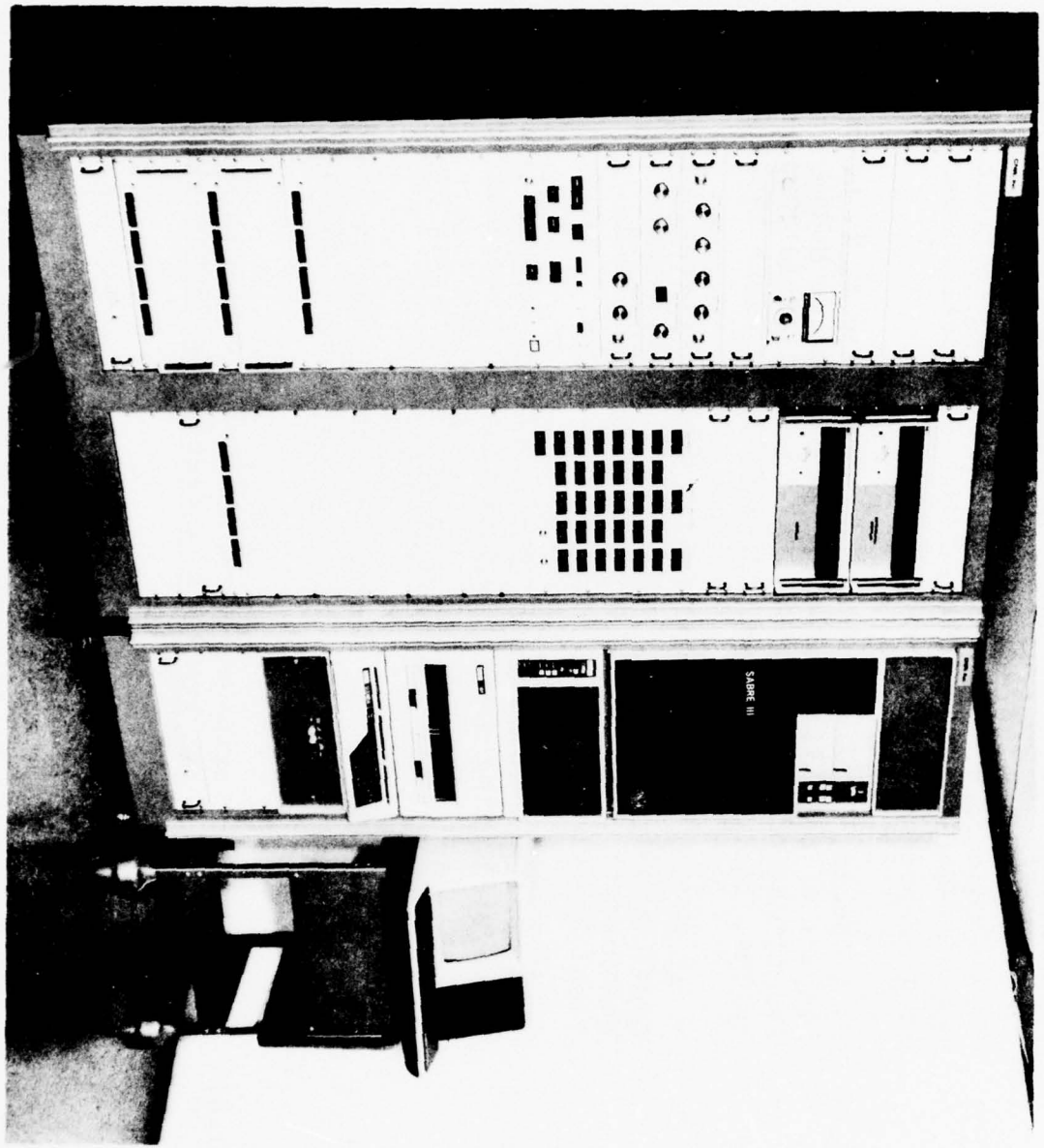

Figure 1.4 LOS Simulator

REFERENCES

[1.1] "Forward Scatter Measurements," Final Report on Contract F19628-71-C-0082 for Rome Air Development Center.

[1.2] "VHF Tactical Channel Simulator," Final Report on Contract DAAB07-71-C-0019 for U. S. Army, Ft. Monmouth, NJ.

[1.3] "Urban Channel Simulator," Final Report on Contract DOT-TSC-84 for Transportation Systems Center, Department of Transportation, Cambridge, MA.

[1.4] P. A. Bello, C. J. Boardman, D. Chase, and J. K. DeRosa, "Impact of Satellite Aeronautical Channel on Modem Specifications," Report No. FAA-RD-74-54, Final Report by CNR, Inc., on Contract DOT-TRC-516-1, March 1974.

[1.5] P. A. Bello, et al., "Underwater Communications," Contract N00140-68-C-0051, and "Generalized Channel Measurement Software," Contract N0060-71-C-0100, Final Reports for Naval Research Labs.

[1.6] P. A. Bello and L. Ehrman, "Troposcatter Modem Performance Prediction with a Complex Gaussian Troposcatter Channel Simulator," Record of the IEEE 1969 International Conference on Communication, pp. 48-11 - 48-16.

[1.7] P. A. Bello and R. W. Pinto, "HF Stored Channel Simulation," Final Report by CNR, Inc. on Contract N00014-74-C-0048 for NRL.

[1.8] F. Ikegami, "Influence of an Atmospheric Duct on Microwave Fading," IRE Trans. on Antennas and Propagation, July 1959, pp. 252 - 257.

[1.9] M. S. Wong, "Refraction Anomalies in Airborne Propagation," Proc. of the IEEE, Vol. 46, September 1958, pp. 1628 - 1638.

[1.10] N. W. Guinard, et al., "Propagation Through an Elevated Duct: Tradewinds III," IEEE PGAP, July 1964, pp. 479 - 490.

[1.11] B. R. Bean and E. J. Dutton, Radio Meteorology, National Bureau of Standards Monograph 92, 1 March 1966.

[1.12] B. R. Bean, et al., "A World Atlas of Atmospheric Radio Refractivity," Essa Monograph No. 1, U. S. Government Printing Office, Washington, DC, 1966.

[1.13] H. T. Dougherty, "A Survey of Microwave Fading Mechanisms, Remedies, and Applications," Essa Technical Report ERL 69-WPL4, U. S. Government Printing Office, Washington, DC, March 1968.

[1.14] E. E. Gossard, "The Reflection of Microwaves by a Refractive Layer Perturbed by Waves," IEEE Trans. on Antennas and Propagation, May 1962, pp. 317 - 325.

[1.15] C. C. Watterson, J. R. Juroshek, and J. L. Demmer, "SHF Bandwidth Study, Phase III," NBS Report 8842, U. S. Department of Commerce, NBS, Boulder, Colorado.

[1.16] M. C. Thompson, Jr., H. B. Janes, L. E. Wood, and D. Smith, "Phase and Amplitude Scintillation of Microwave Signals Over an Elevated Atmospheric Path," Report of NASA Contract Order No. L-31028, ITS, Boulder, CO, 10 May 1971.

[1.17] O. E. DeLange, "Propagation Studies at Microwave Frequencies by Means of Very Short Pulses," BSTJ, January 1952, pp. 91 - 103.

[1.18] A. B. Crawford and W. C. Jakes, Jr., "Selective Fading of Microwaves," BSTJ, January 1952, pp. 68 - 90.

[1.19] G. M. Babler, "A Study of Frequency-Selective Fading for a Microwave Line-of-Sight Narrowband Radio Channel," BSTJ, Vol. 51, No. 3, March 1972.

[1.20] G. M. Babler, "Selectivity Fading Non-Diversity and Space Diversity Narrowband Microwave Radio Channels," BSTJ, Vol. 52, No. 2, February 1973.

[1.21] K. Bullington, "Phase and Amplitude Variations in Multipath Fading of Microwave Signals," BSTJ, Vol. 50, No. 5, July-August 1971, pp. 2039 - 2053.

[1.22] P. A. Bello, J. K. DeRosa, and C. J. Boardman, "Line-of-Sight Wideband Propagation," Final Report by CNR, Inc. on Contract No. F30602-73-C-0013 for Rome Air Development Center, May 1973. RADC-TR-73-167 (AD 762939)

[1.23] P. A. Bello, C. J. Boardman, D. Chase, and J. K. DeRosa, "Line-of-Sight Technical Investigations," Final Report by CNR, Inc. on Contract No. F30602-73-C-0244 for Rome Air Development Center, June 1974. RADC-TR-74-330 (A006104)

[1.24] P. A. Bello, L. W. Pickering, and C. J. Boardman, "Multipath Over LOS Channel Study," Final Report by CNR, Inc. on Contract No. F30602-76-C-0419 for Rome Air Development Center, Nov 77. RADC-TR-77-355 (A048175)

[1.25] J. K. DeRosa, "Tropospheric Refractive Multipath on LOS Links," CNR Executive Software Package No. 9-24.

[1.26] P. A. Bello, C. J. Boardman, D. Chase, and J. K. DeRosa, "Impact of Satellite Aeronautical Channel on Modem Specifications," Final Report by CNR, Inc. on Contract No. FAA-RD-74-54 for DOT/FAA, March 1974.

[1.27] P. A. Bello, "Aeronautical Channel Characterization," IEEE Trans. on Communications, May 1973, pp. 548 - 563.

[1.28] P. A. Bello, D. Chase, J. K. DeRosa, L. J. Weng, and M. G. Bello, "Impact of Satellite Aeronautical Channel on Modem Specification, Phase II: Oceanic Multipath and Modem Concepts," Final Report by CNR, Inc. on Contract No. DOT-TSC-516-2 for DOT/FAA, March 1974.

[1.29] P. A. Bello, J. K. DeRosa, and C. J. Boardman, "Line-of-Sight Wideband Propagation," Final Report by CNR, Inc. on Contract No. F30602-73-C-0013 for Rome Air Development Center, May 1973.

[1.30] NATO/AGARD, "Antennas for Avionics," Conference Proceedings, No. 139, AD-782-310, November 1973.

[1.31] A. L. Johnson and M. A. Miller, "Three Years of Airborne Communication Testing Via Satellite Relay," AFAL Report TR-70-156, November 1970.

[1.32] T. P. McGarty, "Models of Multipath Propagation Effects in a Ground-to-Air Surveillance System," Lincoln Lab., Tech. Note 1974-7.

[1.33] P. A. Bello, "Characterization of Randomly Time-Variant Linear Channels," IEEE Trans. on Comm. Systems, Vol. CS-11, No. 4, December 1963, pp. 360 - 393.

[1.34] P. A. Bello and R. Esposito, "Measurement Techniques for Time-Varying Dispersive Channels," Alta Frequenza, N. 11, Vol. XXXIX, 1970, pp. 980 - 996.

[1.35] P. A. Bello, "The Effects of Oscillator Instability, Time Jitter, and Time-Scale Change Upon Four Channel Probing Techniques," Aspects of Network and System Theory, Holt, Rinehart and Winston, Inc., 1970.

[1.36] P. A. Bello, "Measurement of Random Time-Variant Linear Channels," IEEE Trans. on Information Theory, Vol. IT-15, No. 4, July 1969, pp. 469 - 475.

[1.37] P. A. Bello, "Some Techniques for the Instantaneous Real-Time Measurement of Multipath and Doppler Spread," IEEE Trans. on Comm. Technology, Vol. COM-13, No. 3, September 1965, pp. 285 - 292.

[1.38] P. A. Bello, "On the Measurement of a Channel Correlation Function," IEEE Trans. on Information Theory, Vol. IT-10, No. 4, October 1964, pp. 382 - 383.

[1.39] P. A. Bello, "Measurement of the Complex Time-Frequency Channel Correlation Function," Radio Science J. of Research, NBS/USNC-URSI, Vol. 68D, No. 10, October 1964, pp. 1161 - 1165.

SECTION 2

THEORETICAL BACKGROUND AND DESIGN CONSIDERATIONS

In the discussion below, we first present technical background sections which include a brief discussion of the characteristics of these links and some fundamentals of channel modeling and simulation. Consideration is then given to the effect of simulator nonidealities on reproducibility of modem error rate behavior.

2.1 Characteristics of Links to be Simulated

The LOS communication channels of interest include the following:

- Ground point-to-point microwave links
- Ground-satellite-aircraft UHF and microwave paths
- Aircraft-satellite-aircraft UHF and microwave paths
- Ground to remote-piloted-vehicle (RPV) paths
- Ground-RPV-ground paths
- Aircraft-aircraft paths

Some of these channels are composed of a single link, and others may be subdivided into separate links connected by relays. The major complexity of the simulator is associated with the simulation of propagation media distortion (multipath and fading) associated with particular component links; namely,

- Ground-Aircraft (or RPV) (GA)
- Aircraft-Aircraft (AA)
- Aircraft-Satellite (AS)
- Ground-Ground (GG)

where we have listed acronyms to simplify discussion.

Figure 2.1(a) shows some basic signal processing operations in a single LOS link utilizing a digital modem interfacing at an intermediate frequency (IF). In modeling the effects of the link on the digital modem IF output, it is convenient to regard the signal processing operations as subdivided into a cascade of "channels" as shown in Figure 2.1(b): a transmitter channel, a propagation channel, and a receiver channel.

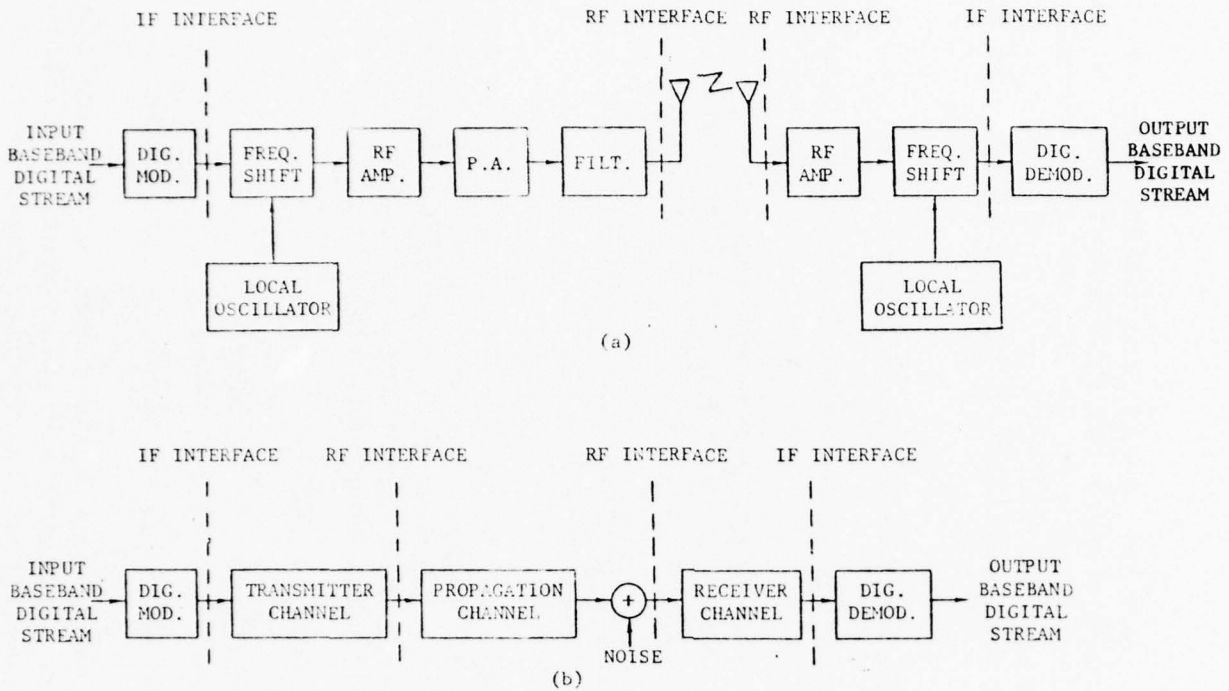

Figure 2.1 Signal Processing in an LOS Channel without Relay Operation

The transmitter channel includes all signal processing operations between the IF input interface and an RF interface defined at the antenna input. These operations include frequency translation, amplification, and filtering. In most cases of interest in LOS links, the filtering in the transmitter channel is mild prior to the power amplifier (PA), which usually operates in a saturated or hard-limiting mode. This type of PA is satisfactory for the constant envelope modulation which is used most often. Filtering is usually excluded from the operations prior to the PA because such filtering will produce amplitude modulation which will be converted into spurious phase modulation by the AM/FM conversion characteristics of the PA. As shown in Figure 2.1(a), filtering is sometimes provided after the PA to limit the radiated spectral splatter.

The receiver channel lumps together all signal processing operations between the output of the receiving antenna and the IF output fed to the modem demodulator. These operations include RF amplification, frequency shifting, and perhaps some IF preamplification. Usually there will be no automatic gain control, a function usually included in the modem demodulator. Under normal operation, the receiver channel and the transmitter channel prior to the PA provide nominally linear operations with some small incidental nonlinearities. Provided the modulation technique is constant envelope and negligible AM is produced by filtering prior to the PA, the complete transmitter channel may be regarded as nominally linear.

When a radio relay is incorporated within the channel as indicated in Figure 2.2(a), additional signal processing functions must be characterized. As indicated in Figure 2.2(b), an additional propagation channel and a "radio relay channel" must be defined. The latter channel characterizes the signal processing of the radio relay, which includes amplification, filtering, frequency shifting, and power amplification. This power amplification is frequently of the saturating type.

The propagation channel includes all the signal processing existing between the input to the transmitter antenna and the output of the receiver antenna. In particular, this component channel includes the fading multipath behavior of the link. Since the propagation channel is linear, its input-output behavior is completely determined by its impulse respose or transfer function. Because radio channels are time-variant, both the impulse response and transfer function must be regarded as time-variant. As will be discussed in Section 2.2,

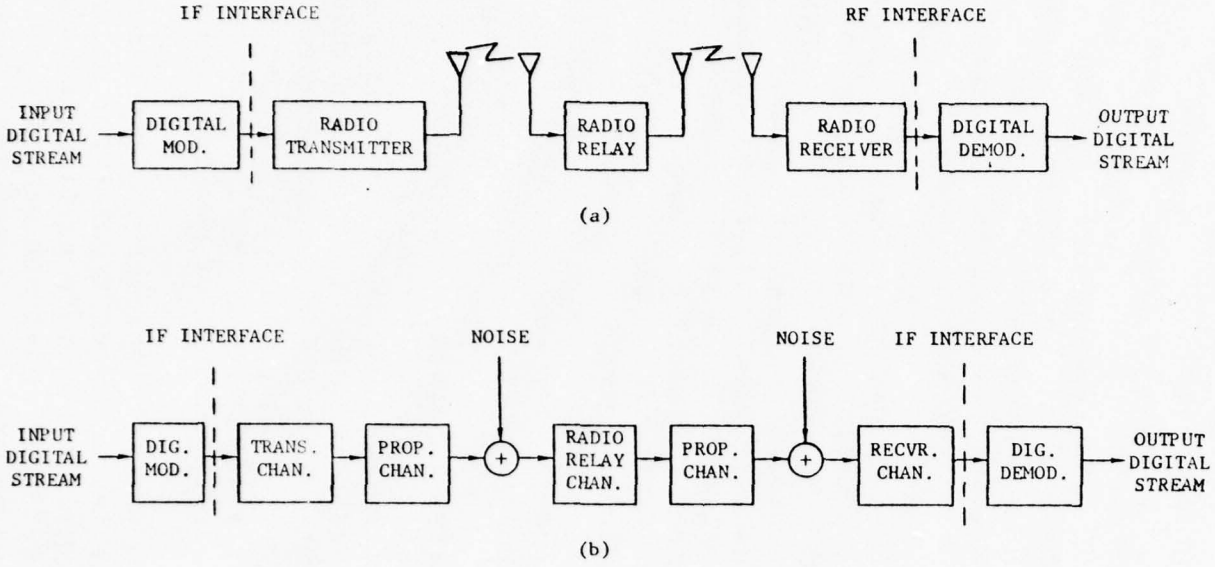

Figure 2.2 Signal Processing in an LOS Channel with Relay Operation

the complexity of equipment provided to measure, record, and reproduce the characteristics of the propagation channel over a finite bandwidth depends directly upon two gross channel parameters, the multipath spread and the Doppler spread. The multipath spread is a measure of the duration of the impulse response of the channel while the Doppler spread is a measure of the width of the spectrum of a received carrier.

In discussing the values of Doppler spread and multipath spread of a channel and their impact on channel simulator design, it is necessary to distinguish various propagation modes. For the four canonic LOS channels of interest here (GA, AA, AS, GG), the following three propagation modes are of interest:

- Refractive multipath
- Surface multipath
- Ionospheric scintillation (AS only)

An elevated tropospheric layer with a scale much larger than the wavelength of the carrier can act as a lens which, under proper conditions, focuses the transmitted signal into the receiver over multiple paths. The frequency and intensity of the meteorological conditions which result in such multipath-producing propagation have been studied experimentally [2.1] - [2.14]. The resulting multipath structure has been explored in great detail at CNR under two contract to RADC [2.15],[2.16], and the numerical results [2.17] agree quite favorably with the experimental data [2.1] - [2.14].

Refractive multipath is a form used to describe the channel characteristics caused by these steep negative gradients in refractive index. The net effect of this gradient is to produce discrete multipath, i.e., a finite set of paths in addition to the direct path between transmitter and receiver. An analysis of the impulse response structure by CNR indicates a maximum of seven paths for a path length of 200 miles. Calculations of multipath are not made beyond 200 miles because the theory assumes a continuous layer, and it does not seem likely that layers will extend so long. However, there is a lack of experimental knowledge on layer lengths, so the assumption is purely arbitrary at this point. Refractive multipath will only occur on LOS paths having an elevation angle of less than 2^{o} - 3^{o} and is not normally experienced on channels employing a satellite relay, which usually do not attempt to communicate at such low elevation angles. On the other hand, the AA, GA, and GG channels perforce operate at low elevation angles of the line-of-sight and thus experience refractive multipath whenever the

corresponding propagation conditions exist. Figure 2.3 presents a plot of maximum delay spread between the latest arriving multipath component and the direct path as a function of path length for some extreme rare refractive gradient conditions. It is seen that over most of the world, the worst-case multipath spread is within 65 nanoseconds. A single rare case reported in Senegal, Africa, yields larger delay spreads. However, this particular combination of events is of extremely low probability of occurrence and should not be used to specify equipment complexity.

Calculations of Doppler spread yield the results shown in Figure 2.4. Disregarding the rare event in Dakar, the worst-case Doppler spreads are seen to be less than .5 Hz/Mach No./GHz of carrier frequency. Channel measurement would probably be undertaken at speeds of less than Mach .7. For the typical military operating frequency of 8 GHz, we find an expected worst case Doppler spread of 5.6 Hz.

We consider now the multipath and Doppler spread associated with surface multipath. CNR has carried out considerable study on modeling surface multipath. Although the underlying scattering process which causes this multipath is the same for AS/GS and AA/GA links, operational as well as numerical considerations make the models somewhat different. The AS/GS model was developed at CNR under contract to the Department of Transportation [2.18],[2.19], while the AA/GA model was developed at CNR under contract to RADC [2.20].

The earliest arriving component of the surface multipath is from the "specular" point, i.e., the point of mirror reflection from the surface. Later multipath components come from annular rings at successively larger distance from the specular point. There are two sharp contrasts between surface multipath and refractive multipath. First we note the gap in delay between the direct path and the specular delay within which no surface multipath may occur. Refractive multipath is generally clustered soon after the direct path and will frequently be so close as to be unresolvable from the direct path. Second we note that except for reflections from large objects like mountains or buildings or a "specular" reflection emanating from the average surface around the specular point, the surface multipath consists of a very large number of very small components distributed in delay. Thus it is of a "continuous" nature as opposed to the discrete nature of refractive multipath.

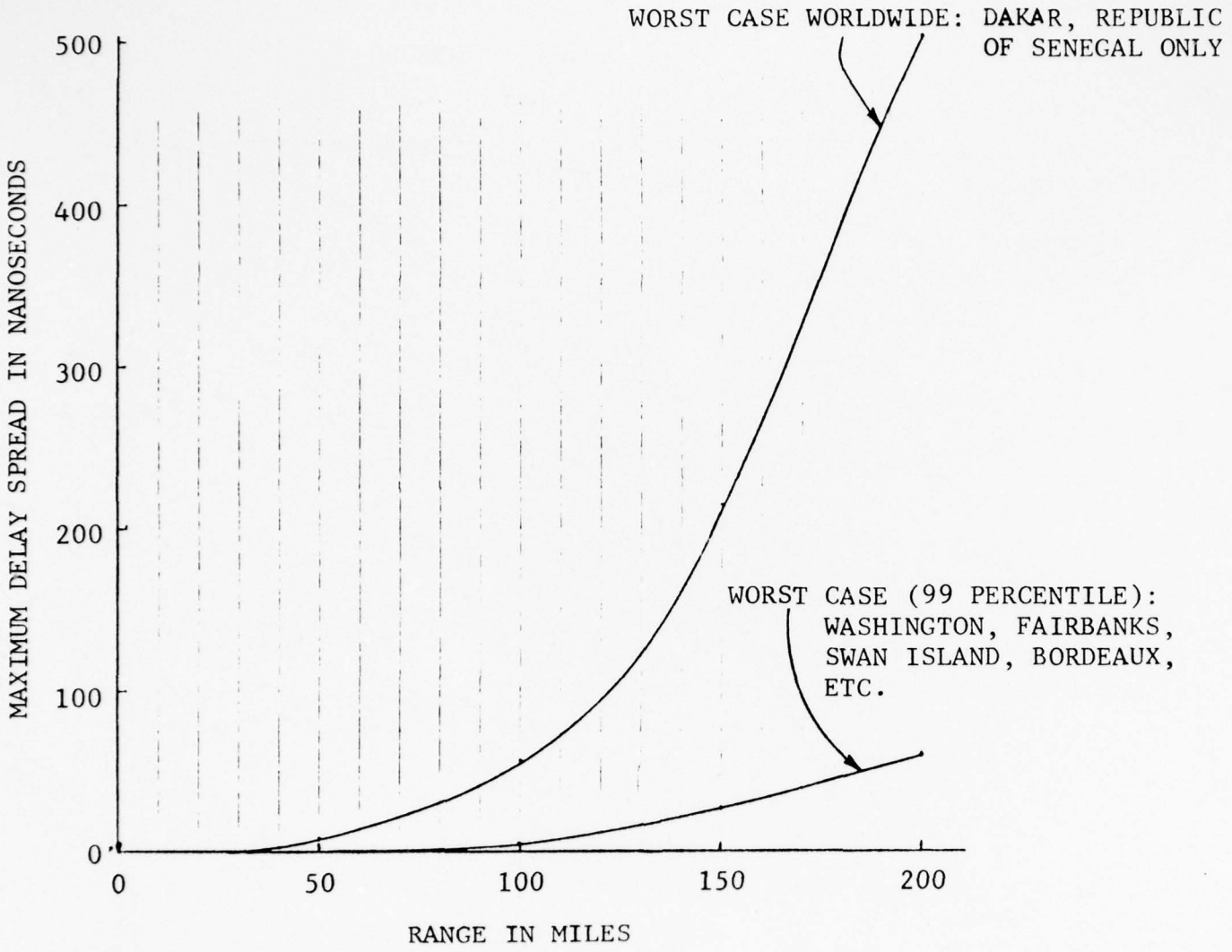

Figure 2.3 Maximum Refractive Multipath Delay Spread on AA/GA Links

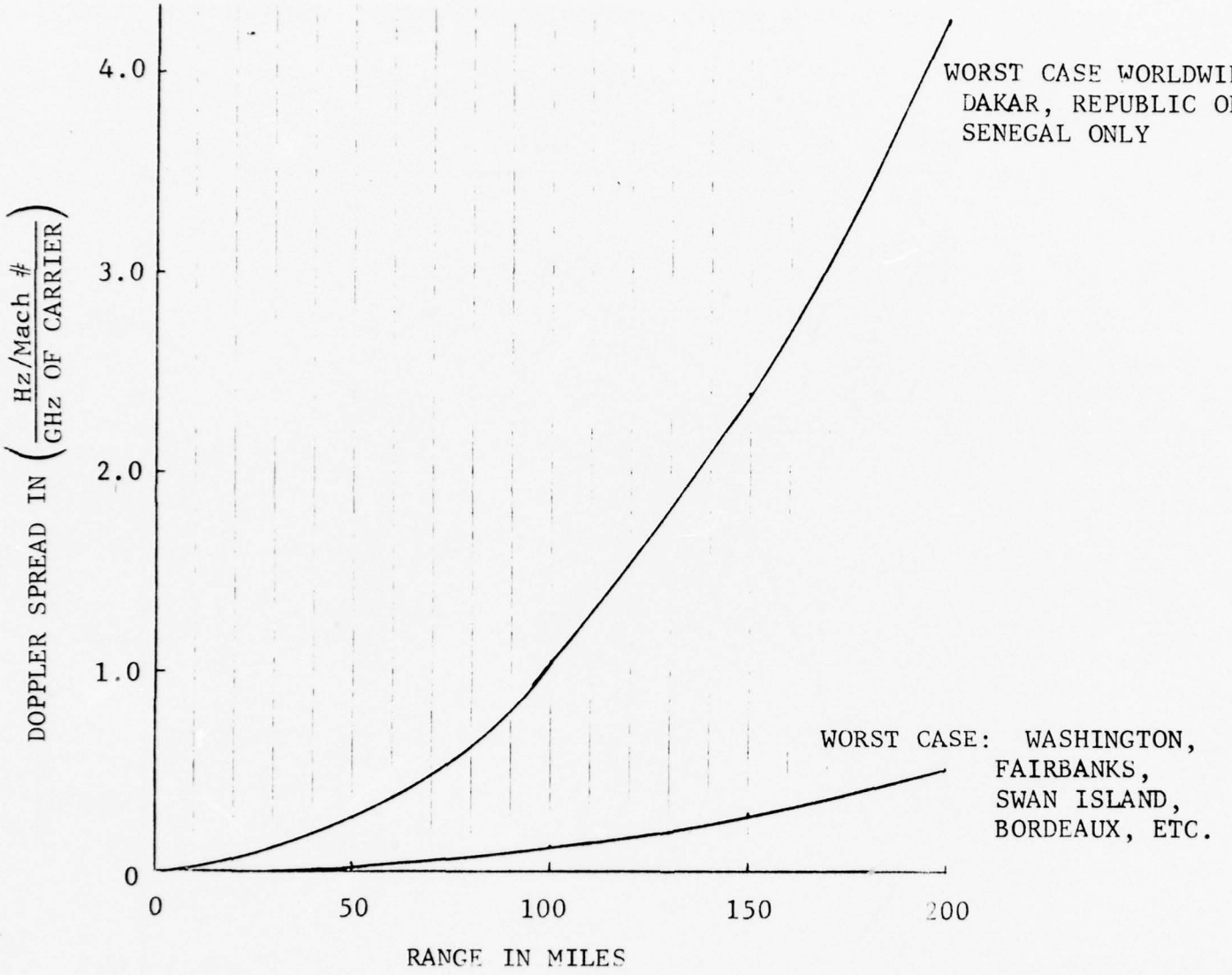

Figure 2.4 Maximum Refractive Doppler Spread on AA/GA Links

Two other contrasts we wish to make are the behavior of these modes of propagation as a function of antenna size and operating frequency. Refractive multipath is virtually unaffected by antenna size because the discrete paths are clustered very close to the direct path, deviating only tenths of a degree. Surface multipath is strongly affected by the antenna pattern which can, in principle, be focused to eliminate reflections and scattering from the surface. In practice, antenna sizes are sharply limited for airplane use and surface multipath cannot always be eliminated.

Consider now the effect of changing the operating frequency. In the case of refractive multipath, the relative path delays are to first order not a function of operating frequency. However, as the operating frequency is lowered sufficiently, the multipath spread will become less than a period of the carrier frequency and the channel will behave like a single fading path for information transmission. As the frequency is lowered such that the multipath spread is a small fraction of a carrier frequency period, the fading will disappear because the multipath components will add in-phase.

In the case of surface multipath, the frequency and angle of incidence to the specular point can have a pronounced effect on multipath characteristics. The signal scattered from the surface of the earth (land, water, ice, etc.) has a discrete or specular and a diffuse component. The specular component characterizes the mean signal scattered from the surface, while the diffuse component characterizes the random return due to the roughness of the surface and produces the "continuous" multipath. A surface is considered "rough" if the rms height, h, of the surface irregularities satisfies the Rayleigh criterion [2.21]:

$$h > \frac{\lambda}{8 \sin \gamma} \qquad (2.1)$$

where λ is the wavelength of the incident radiation and γ is the grazing angle of the incident ray. The rms height above which the scatter is considered diffuse is shown in Figure 2.5 in the frequency range from 1 to 10 GHz. It is seen that a surface with an rms height of 0.5 meter will exhibit some diffuse scatter only for grazing angles above 1^{o} at 10 GHz, above 5^{o} at 1 GHz, and above 10^{o} at 300 MHz. It is evident from Figure 2.5 that, for a fixed grazing angle and surface roughness, the multipath will tend to be continuous at the higher (microwave)

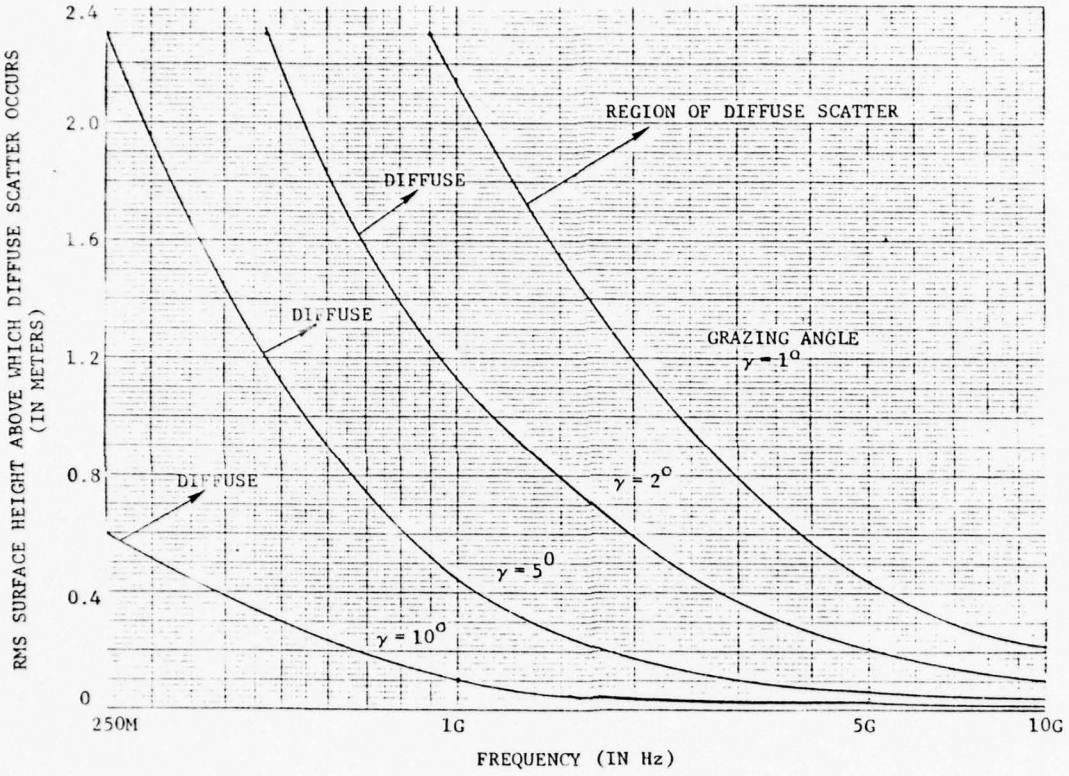

Figure 2.5 Surface Roughness for Diffuse Scatter

frequencies and specular or discrete at the lower (UHF) frequencies. For the military links being considered here, there are many naturally-occurring surfaces (e.g., the ocean, hilly terrain, desert, snow drifts, etc.) which will cause diffuse scatter to exist.

The delay difference between the specular and direct signal paths is shown in Figure 2.6 as a function of distance from the sub-satellite point. The grazing angle γ, which the specular point ray makes with the earth's surface, is also indicated by the dotted lines for the various aircraft altitudes from 10 to 50 thousand feet. It is seen that for the (synchronous) satellite link, tens of microseconds of delay difference can be expected. The amount by which this delay difference changes as the flight progresses can be determined by examination of the legend which indicates the distance traveled in one hour by an RPV, a Mach-1 aircraft, and a Mach-2 aircraft.

The Doppler frequency difference between the direct and specular signals is shown in Figure 2.7 for aircraft altitudes of 30 and 60 thousand feet. Again, a synchronous satellite is assumed, and to get the worst-case (i.e., largest) Doppler difference, the aircraft is assumed to be flying toward or away from the satellite. Note that the curve is normalized to the Mach number of the aircraft and the number of GHz of carrier frequency. Thus, for a Mach-.5 aircraft flying at 30 thousand feet, there is an 18-Hz direct-specular Doppler shift at 10 GHz.

Experiments which verify the theory presented here have been conducted during three years of airborne communication testing via satellite relay [2.22]. Measurements of received signal strength were taken at UHF (250 MHz) on an AS link. The aircraft flew at 30 thousand feet at a velocity of Mach-.7 toward the satellite. Cyclic fades were observed with a rate of about 0.6 Hz above grazing angles of 10^{o} [2.22, p. 55]. From Figure 2.7 it is seen that the predicted Doppler is $(3.5)(0.7)(0.25) = 0.61$ Hz, in agreement with the flight test results. Thus, during the flight test at UHF, a specular multipath component was present to cause cyclic fades with ~0.6 Hz rate

Measurements were also taken at 8 GHz with grazing angles less than 2^{o} (the SHF antenna had a $\pm 2^{o}$ beamwidth). This time fading was experienced but no cyclic variation was present. This indicates that the multipath component was continuous rather than

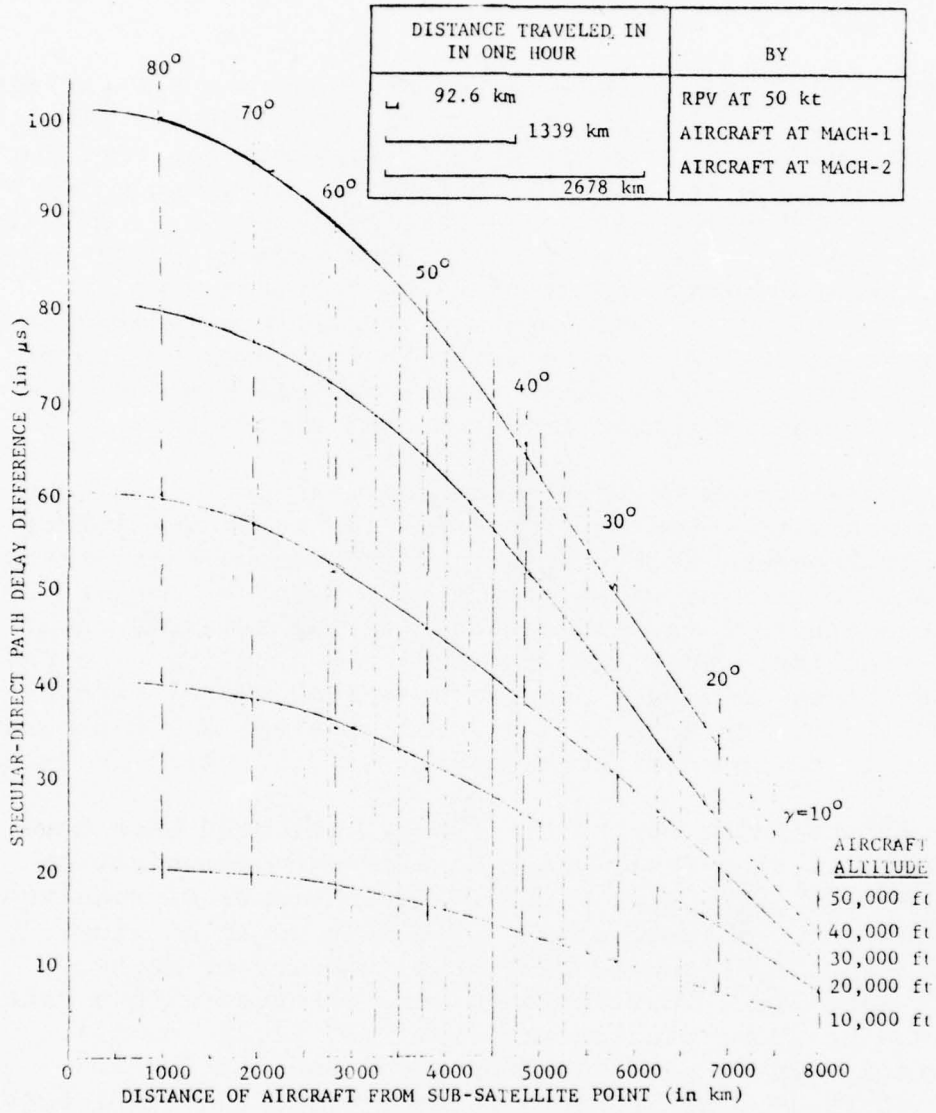

Figure 2.6 Specular-Direct Path Delay on AS Links

SAMPLE CALCULATION
h_A = 30,000 ft
VELOCITY = Mach-0.5
CARRIER FREQUENCY = 10 GHz
DOPPLER = (3.6)(0.5)(10) = 18 Hz

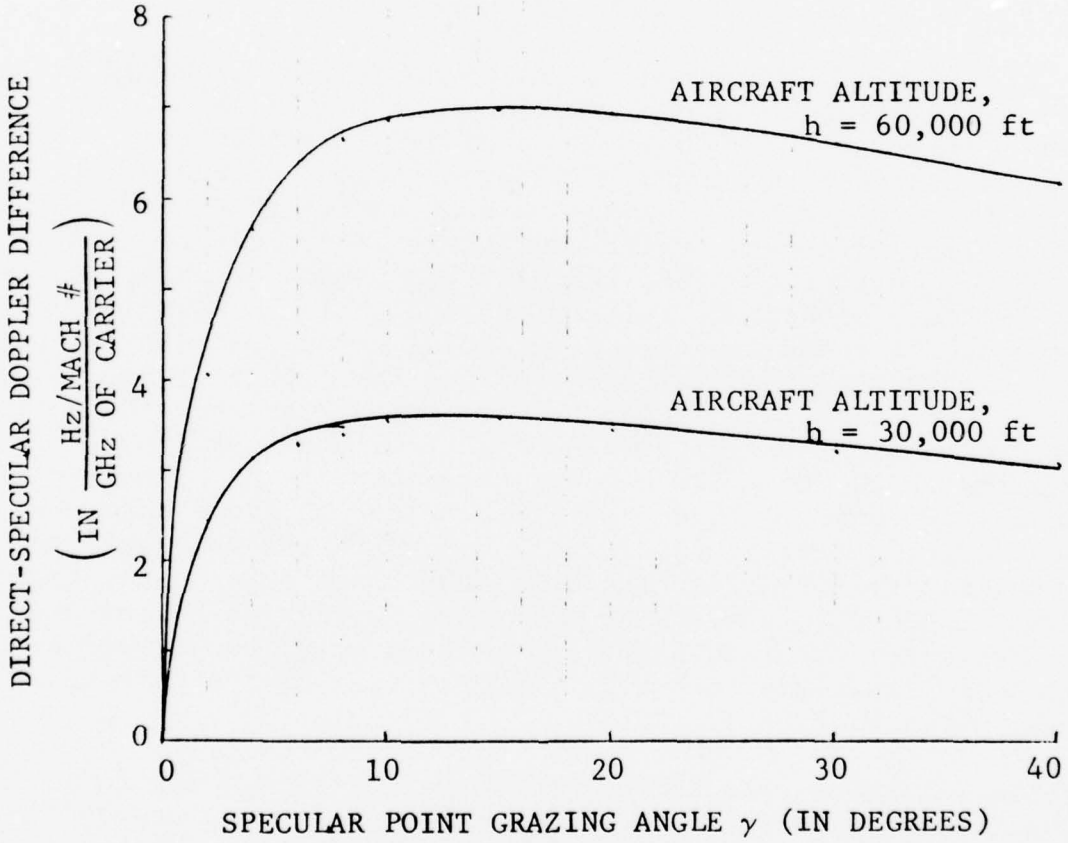

Figure 2.7 Direct-Specular Doppler Difference for Aircraft in Level Flight Flying Toward or Away from Satellite

discrete (specular). It is seen from Figure 2.5 that rms surface heights of 0.2 - 0.4 meter cause specular scatter at UHF (250 MHz) at grazing angles around 10^{o}, but cause diffuse scatter at SHF (8 GHz) at 1^{o} and 2^{o} grazing angles.

It should be noted that the direct-specular Doppler difference or, for short, differential Doppler shown in Figure 2.7 applies to level flight and a synchronous satellite. Nonlevel flight and/or a nonsynchronous satellite can yield much larger values of differential Doppler. Figure 2.7 is of particular interest for channel probing, which would normally be done with an airplane in level flight and a synchronous satellite.

We consider now the amount of multipath spread produced by the surface multipath. It has been shown by CNR [2.18],[2.19] that for sufficiently wide beam antennas and low elevation angles to the satellite, up to 10 μs of multipath spread exist. Since military operational antennas are directive to provide for increased gain, multipath rejection, secure communication, etc. (see [2.23]), multipath spread calculations should be made for typical military situations. It is assumed that the satellite antenna provides broad coverage in a sector which contains the military aircraft and, therefore, provides for little or no multipath discrimination. However, the aircraft antennas used to communicate with satellites can range from upper hemispherical coverage at UHF to a few degrees beamwidth at the higher microwave frequencies.* The coverage provided by these antennas is shown diagrammatically in Figure 2.8. Since the antennas are designed for satellite communications, the usual case is for the multipath to occur in a sidelobe, as shown in Figures 2.8(a) and 2.8(b). However, when the satellite is at a very low elevation angle, the multipath may occur in the main beam of the antenna, as shown in Figure 2.8(c).

Table 2-1 shows calculations of multipath spread due to sidelobe illumination for various grazing angles γ and beamwidths θ for diffuse scatter at microwave frequencies. Note that for antenna beamwidths less than about 3^{o}, the maximum (sidelobe) delay spread is about 200 ns at an aircraft altitude of 30,000 feet.

*In three years of airborne testing [2.22], blade, dipole, and crossed slot UHF antennas were used to provide upper hemispherical coverage; at S-band, a $\pm$ 2^{o} beamwidth antenna was used. In [2.23], a 32-inch Cassegrain with a 3^{o} beamwidth at SHF was mounted on a KC-135.

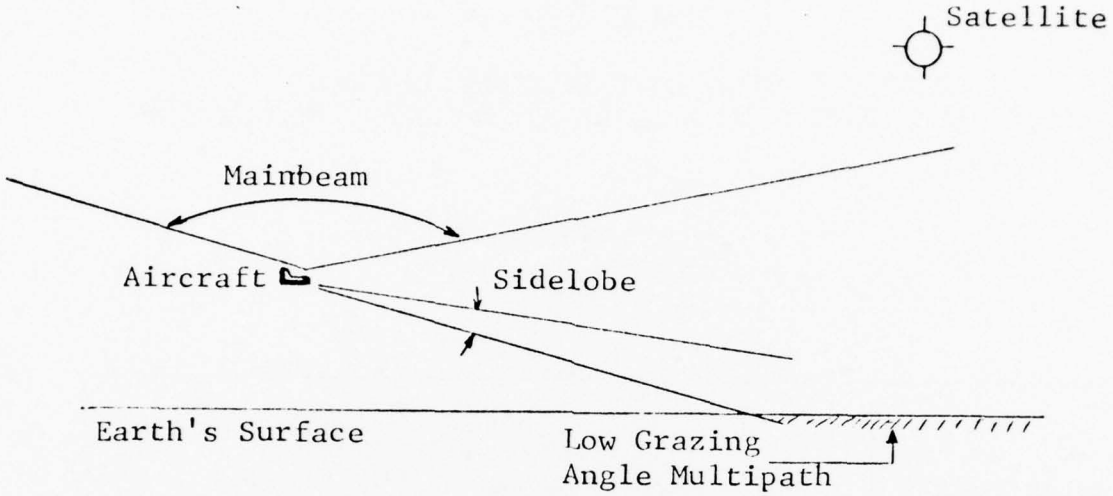

(a) UHF Antenna Coverage

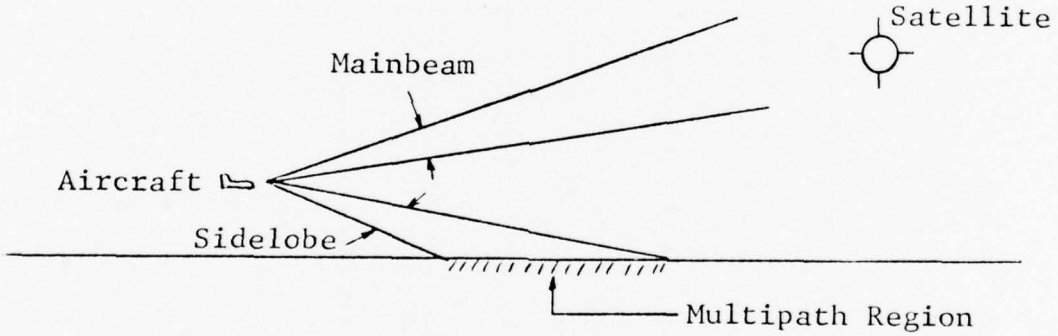

(b) Higher Frequency Microwave Antenna Coverage at High Elevation Angle

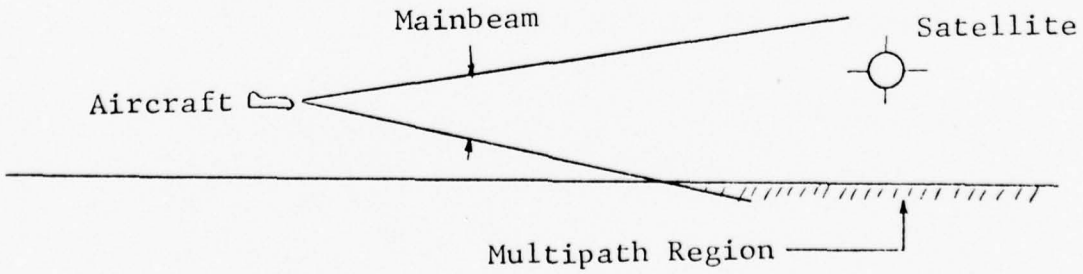

(c) Higher Frequency Microwave Antenna Coverage at Low Elevation Angle

Figure 2.8 Antenna Coverage on Military Aircraft-Satellite Links

TABLE 2-1

DELAY SPREAD OF DIFFUSE COMPONENT FOR
SIDELOBE ILLUMINATION ON AS LINK AT MICROWAVE FREQUENCIES

Specular Point Grazing Angle γ (Degrees)	Delay Spread Per 10 K Feet of Aircraft Altitude (Nanoseconds/10,000 Feet)				
	$\theta=1^o$	$\theta=2^o$	$\theta=3^o$	$\theta=4^o$	$\theta=5^o$
1	22	—	—	—	—
2	11	44	—	—	—
3	7	29	65	—	—
4	5	22	49	87	—
5	4	17	39	70	109
10	2	9	20	35	55

(Main Beam Illuminates surface in this region)

θ = Antenna elevation angle beamwidth.

If the main beam illuminates the earth's surface as it may when the satellite is near the horizon, the scattered power can be calculated from the scattering cross section, the surface roughness, and the $1/R^2$ losses. In calculating the multipath power, we have assumed worst-case rms surface slope α, i.e.,

$$\alpha = \alpha_{max} = \tan \gamma \tag{2.2}$$

(The rougher the surface, the larger the surface area over which scattering takes place and the larger the multipath spread.) When $\alpha > \tan \gamma$, a significant part of the surface becomes shadowed by the surface irregularities and the multipath power is typically reduced by an order of magnitude [2.24, p. 116]. The results of this calculation are shown in Table 2-2. It is seen that for grazing angles less than about 3^o, the multipath spread (defined here as the delay beyond the specular delay at which the multipath power drops to 1/e of its maximum value) is less than 200 ns.

Similarly, one may calculate the Doppler spreads for the cases of sidelobe illumination and mainbeam illumination of the surface at low grazing angles. The results of these calculations are shown in Tables 2-3 and 2-4. For an 8-GHz carrier frequency and Mach-.7, Doppler spreads of less than 10 Hz are predicted for a beamwidth of 3^o in the case of sidelobe illumination and for any beamwidth in the case of mainlobe illumination of the surface. Note that the Doppler spread decreases with decreasing grazing angle.

In the case of the AA and GA links, surface multipath will occur in addition to refractive multipath. The AA/GA links differ from the AS link, however, in that the multipath is always generated at low grazing angles and within the radio horizon. As a result of these differences, the surface scatter multipath on AA/GA has a specular component which is delayed only a few hundred nanoseconds from the direct path and shifted by at most 10 or 20 Hz. The multipath spread is worst for AA links. For AA links, the maximum value of multipath delay spread is shown in Figure 2.9 as a function of the specular point grazing angle for various antenna beamwidths. It is seen that aircraft at 30,000 feet with antenna beamwidths less than 3^o experience diffuse multipath with delay spreads of less than about 150 nanoseconds for grazing angles above 1^o. At angles below 1^o, the diffuse multipath power decreases due to shadowing and due to the tendency of the multipath to be specular near

TABLE 2-2

MULTIPATH SPREAD AT LOW GRAZING ANGLES FOR AN AIRPLANE-SATELLITE LINK AT MICROWAVE FREQUENCIES

Specular Point Grazing Angle	Nominal Multipath Spread ($\frac{1}{e}$ Width) Nanoseconds
1	70
2	130
3	195
4	260

TABLE 2-3

DOPPLER SPREAD OF DIFFUSE COMPONENT FOR
SIDELOBE ILLUMINATION ON AS LINK AT MICROWAVE FREQUENCIES

Specular Point Grazing Angle γ (Degrees)	Doppler Spread Per Mach # Per GHz of Carrier (Hz/Mach #/GHz)				
	$\theta=1^o$	$\theta=2^o$	$\theta=3^o$	$\theta=4^o$	$\theta=5^o$
1	0.17	—	—	—	—
2	0.34	0.68	— (Main beam illuminates surface in this region)	—	—
3	0.51	1.02	1.53	—	—
4	0.68	1.36	2.04	2.72	—
5	0.84	1.68	2.52	3.36	4.20
10	1.68	3.36	5.50	6.73	8.41

θ = Antenna beamwidth

TABLE 2-4

DOPPLER SPREAD OF DIFFUSE COMPONENT FOR
MAINBEAM ILLUMINATION ON AS LINK AT MICROWAVE FREQUENCIES

Specular Point Grazing Angle γ (Degrees)	Doppler Spread* per Mach # per GHz of Carrier (Hz/Mach #/GHz)
1	0.17
2	0.68
3	1.52
4	2.71
5	4.23

*Doppler spread calculated from specular point to horizon.

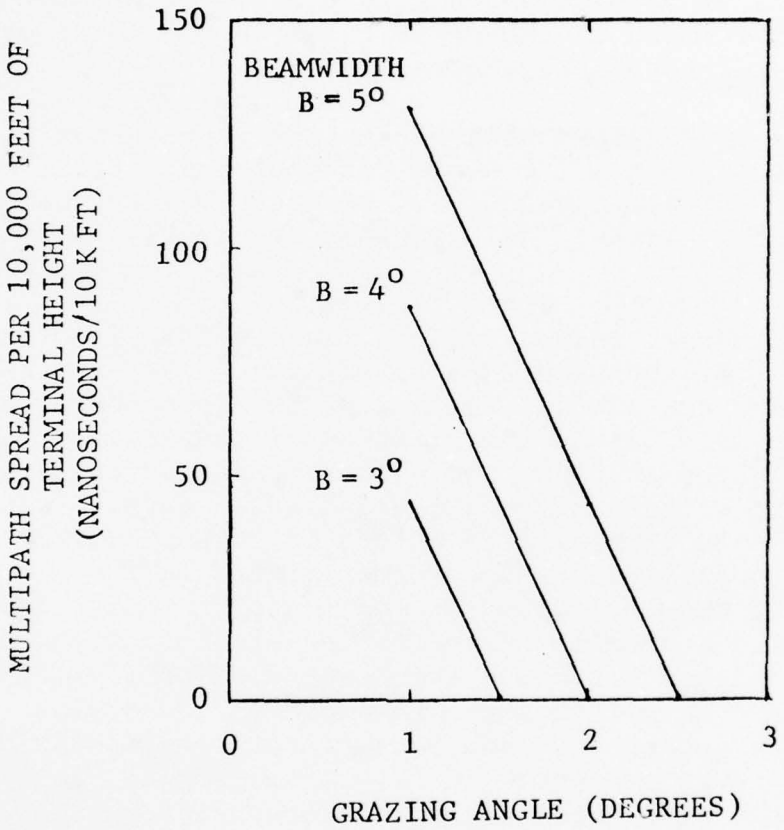

Figure 2.9 Maximum Diffuse Multipath Delay Spread on AA/GA Links

grazing incidence. It should be noted that when one terminal is lowered as in the GA case, the same beamwidth antenna can provide increased diffuse multipath discrimination.

Calculations of Doppler spreads indicate small values of the order of those found in the other cases, e.g., 10 Hz or less for 8 GHz, Mach-.7 and 3^{o} beamwidths.

In the case of GG links with parameters representative of those used in conventional microwave relay communication, multipath spreads and Doppler spreads will be much smaller than those quoted for the other links. Calculations are available in a report by CNR [2.15].

As a final channel characteristic, we consider ionospheric scintillation. This phenomenon is of relevance only for AS links in which the LOS pierces regions of the ionosphere which are perturbed anomalously in the vicinity of the equator. From an input-output point of view, the effect is one of causing amplitude and phase fluctuations, i.e., Doppler spread, with negligible multipath spread. The effect is quite important at UHF but will be negligible at the higher microwave frequencies, e.g., 8 GHz. The Doppler spread, in any case, is quite low — a few Hz at most. A detailed presentation of the current literature at UHF and higher microwave frequencies was performed at CNR under contract to DOT [2.25]. In addition, a model of scintillation was constructed and measurement recommendations were made. The model presented in [2.25] can be used to construct a realistic simulation and comparison with probing data well within the capabilities of the LOS simulator.

2.2 Channel Modeling, Simulation, and Measurement

Figures 2.1 and 2.2 break down the signal processing operations of an LOS channel into a cascade of component channels which may be grouped into two categories: propagation channels and equipment channels (transmitter channel, receiver channel, relay channel). The propagation channels are linear and, like all linear systems, may be represented in terms of canonic channel models such as tapped delay lines or parallel filter banks [2.26]. These canonic models can be used to provide the basic building blocks for channel simulation. However, some portions of the equipment channels are nonlinear and do not allow the use of the simple canonic model approach to simulation. Whenever linear portions of the equipment channel can be

combined with the propagation channel, their signal processing effects are included in the canonic model simulation; otherwise, separate nonlinear "black boxes" need to be provided.

Two special units to simulate equipment characteristics are provided: a phase jitter device and an adjustable nonlinearity. With the former, one may simulate oscillator instabilities. The latter may be used to simulate nonlinearities in a power amplifier. With the aid of this nonlinearity and the adjustable additive noise source, one may form a simple model of a satellite relay with different degrees of limiting to be used in cascade with a tapped delay line. The latter could be used to simulate the propagation channel and those contiguous transmitter and receiver linear filtering operations in cascade with the propagation channel.

In discussing channel simulation, it is important to recognize two basic types, each with its own role in modem evaluation: playback and synthetic channel simulation. Playback channel simulation is a two-stage process in which a channel system function is first measured and recorded for some length of time and then "played-back" or recreated in a canonic model simulator such as a tapped delay line. The basic forté of this type of simulation is that it involves no assumptions about the characteristics of the channel other than the maximum Doppler spread and maximum multipath spread, together with a specification of the bandwidth of the channel that it is desired to characterize. Its drawback is the time and expense of the flight tests required to conduct the channel measurements and the unpredictability of the time of occurrence of certain deleterious radio-propagation effects. The synthetic channel simulator must make assumptions about the stationary or nonstationary statistics of the time-varying complex gains on the taps of the simulator tapped delay line; but one may simulate ranges of propagation conditions at will, in particular conditions that are known to occur and must be considered in modem evaluation, but are difficult to "capture" in channel measurements.

We consider first the playback channel simulation process. For the purposes the of the present discussion, we present extremely simplified block diagrams for the channel measurement and playback in Figures 2.10(a) and (b), respectively. No heterodyning operations or multipath tracking operation have been explicitly indicated, and filters in cascade have been lumped together. Thus, in the prober/analyzer, Figure 2.10(a),

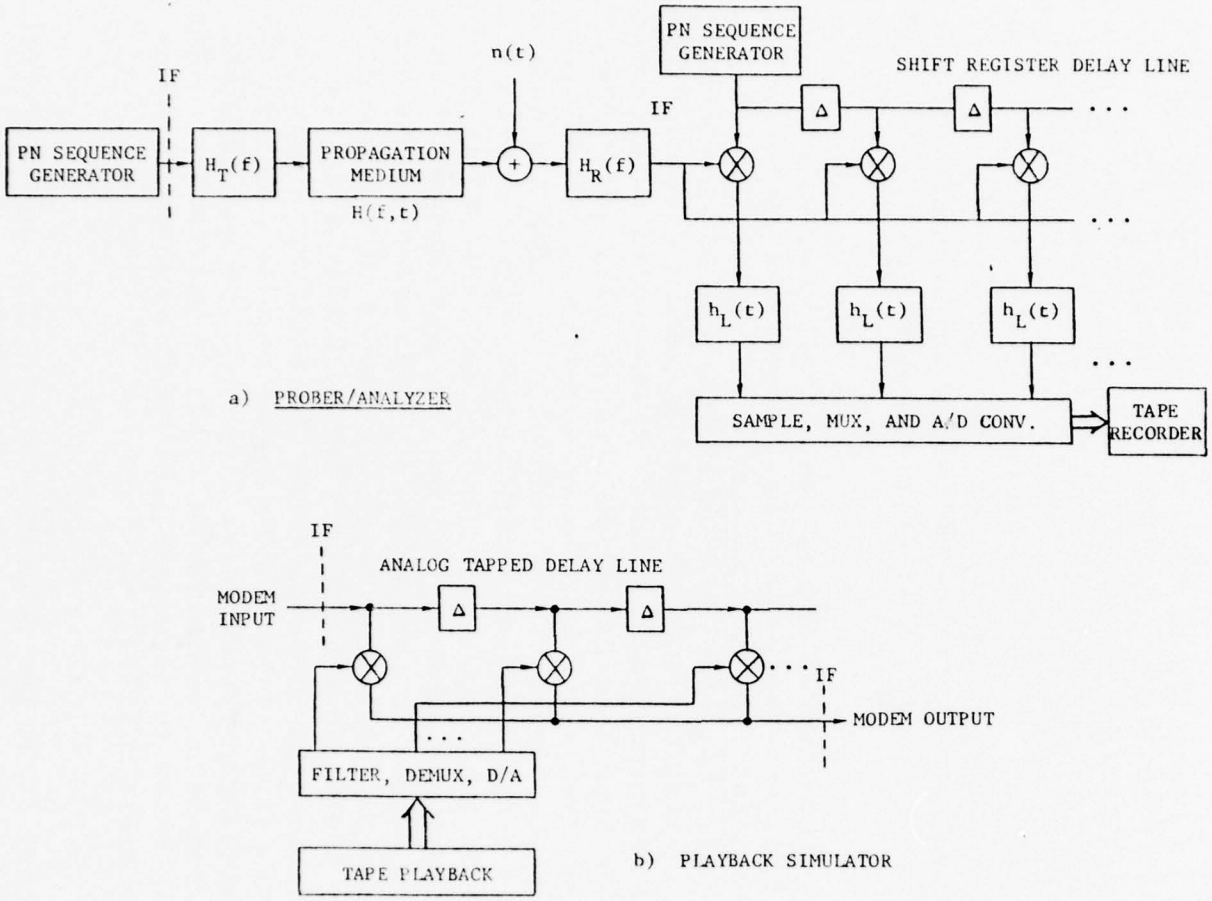

Figure 2.10 Simplified Signal Processing in Prober-Playback System

the transmitter and the receiver are represented by single filters, called transmitter and receiver filters, respectively. Since the playback system is a tapped delay line system, the probing equipment is designed to directly measure the channel impulse response.

The measurement technique used involves the transmission of a pseudo-random binary PSK ($0,180^o$) with the ($0,180^o$) states controlled by the (0,1) states of a maximal-length shift register sequence [2.27]. The received process is (complex) correlated with delayed replicas of the pseudo-random probing signal to produce lowpass in-phase and quadrature estimates of the channel impulse response. When a time-multiplexed correlator is used, as in the present design, the correlation with delayed replicas of the local PN sequence takes place in succession instead of in parallel.

The lowpass filters indicated in Figure 2.10(a) [$h_L(t)$] are just simple integrate-and-dumps for the analyzer. While the block diagram indicates parallel correlators, time-division multiplexing of this correlator is possible, as discussed in [2.20]. In the analyzer, a process of sampling, time-division multiplexing, and A/D conversion takes place prior to tape recording.

In playback, the reverse operation takes place – the tape is played back into a unit that demultiplexes, filters, and D/A converts the tape information into the lowpass in-phase and quadrature data required to drive the complex modulators at the tapped delay line output.

It should be emphasized that the above playback channel simulation concept assumes a <u>linear</u> system between IF interfaces of the radio. For each case of channel measurement, the radio must be examined to determine if this assumption will be violated for the particular input signals and operating conditions to be used in channel measurement. Thus, for a hardlimiting satellite repeater in an AS link, the nonlinearity need not be harmful if the multipath signal is buried in the ambient noise of the repeater amplifier, because then, in effect, linear operation is taking place for the signal. On the other hand, suppose a GG microwave link were probed with a PN signal whose bandwidth exceeded the IF and/or RF bandwidths of the transmitter. Amplitude modulation would appear on the output of the filters and on the input to the TWT. The TWT is driven nonlinearly and any amplitude modulation gets converted into phase modulation through

an AM/PM conversion effect. This modulation may degrade the effect of the channel measurement and must be examined carefully.

The oscillators used for IF to RF frequency translation may have poor short-term stability, and the spectral width of the transmitter carrier must then be regarded as adding to the Doppler spread of the propagation channel. Provided the low-pass filters in the analyzer are adequate to pass this extra spreading, no harm is done. However, as will be discussed below, it is desirable to keep the bandwidths of the lowpass filters as narrow as possible to minimize the effects of additive noise so that, in some cases, it may be desirable to stabilize the radio's local oscillator generation with new sources.

We have noted that the actual channel measured (neglecting nonlinearities) is the propagation medium in cascade with any linear filters and operations associated with the path from prober output to correlator output. One immediate consequence of this observation is that the impulse response measured must be longer than the multipath spread of the propagation medium. Provision must be made in the hardware for sampling this stretched impulse response. The amount of stretching depends upon the time constants of the transmitter and receiver filters and upon the pulse duration in the probing signal, Δ_0.

In [2.18] it is shown that for an analog correlator system the time-variant transfer function associated with the measured impulse response is given by:

$$K(f,t) = \left(\frac{\sin \pi f \Delta_0}{\pi f \Delta_0}\right)^2 H_T(f)\, H_R(f)\, H(f,t) \qquad (2.3)$$

where Δ_0 is the pulse width of the probing signal, $H_T(f)$ is the transfer function of the transmitter filter, $H_R(f)$ is the transfer function of the receiver filter, and $H(f,t)$ is the time-variant transfer function of the propagation medium. The squared term corresponds to the power spectrum of the probing signal. All of the filters are complex lowpass equivalent filters with zero frequency corresponding to the carrier frequency of the real filters. In our subsequent discussions we deal entirely with complex lowpass equivalents, where f=0 corresponds to the carrier frequency.

If the transfer function, Eq. (2.3), were to be identical to that of the propagation medium over a limited bandwidth W centered on the carrier frequency, then it is necessary that*

$$K(f) = \left(\frac{\sin \pi f \Delta_0}{\pi f \Delta_0}\right)^2 H_T(f)\, H_R(f) \approx 1 \quad ; \quad |f| < \frac{W}{2} \qquad (2.4)$$

where K(f) is a composite filter describing the filtering effect of the terminal equipment and the nonwhiteness of the prober spectrum. If the transmitter and receiver filters are wide in bandwidth and flat, only the prober power spectrum remains on the left side of Eq. (2.4). For the 100 Mb/s PN sequence, ($\Delta_0 = 10$ ns), and a desired W = 100 MHz, then $K[\pm(W/2)] = (2/\pi)^2 \approx 0.4$. Thus, the probing signal itself produces a droop at the band edges of approximately 8 dB, and the reproduced channel would normally be colored by this characteristic. An equalizer is provided in cascade with the simulator tapped delay line to remove this coloring of the played-back transfer function.

Recording the measured channel impulse response on magnetic tape involves sampling processes along two independent time axes. Sampling along the "age" or multipath axis is represented by the act of uniformly correlating delayed replicas of the local PN sequence (a replica of that transmitted) with the received signal, where the spacing of adjacent delayed replicas is $\Delta < \Delta_0$ seconds. Thus, the sampling rate of the impulse response along the multipath axis is $1/\Delta$ samples per second. Each correlator output is a "sample" of the impulse response along the multipath axis. If the channel were time-invariant, each "sample" would be fixed in time at a particular value of delay. In practice, the channel is time-variant and each correlator output is time-variant. The other independent sampling process occurs at the correlator outputs which are sampled to prepare the measurements for A/D conversion.

We are now in a position to appreciate the relationship between the size of the multipath spread and Doppler spread of the channel and the complexity of the simulator. As is well-known from sampling theory, accurate reconstruction of a continuous process from its uniform samples requires that the

---

*For simplicity, we do not indicate that a linear phase or delay is acceptable instead of unity for K(f) in the interval $|f| < W/2$.

sampling rate be sufficiently high, otherwise the filtering or interpolation process cannot eliminate crosstalk from aliases of the spectrum of the desired process. If one assumed that the channel impulse response at $t = t_0$ [Fourier transform of $K(f,t_0)$ vs. f] were of finite duration L_{tot} and, in addition, that the transfer function $K(f,t_0)$ had a bandwidth exactly equal to W, the bandwidth that the prober/analyzer is to characterize without distortion, then exactly WL_{tot} correlators (samples along the multipath axis) would be required for reconstruction of the impulse response at $t = t_0$. The cost of the simulator is a strong function of the number of correlators (or, equivalently, the number of taps) on the simulator tapped delay line. Thus, we see that for a given desired characterization bandwidth W, the simulator complexity and cost increases very nearly proportional to the multipath spread.

Of course, in practice, K(f,t) will be larger in bandwidth than W. This may be seen from the fact that [see Eqs. (2.3) and (2.4)] since $(\sin \pi f\Delta_0/\pi f\Delta_0)^2$ and H(f,t) cannot be bandlimited (the latter being the transfer function of an LOS propagation channel), either $H_T(f)$ or $H_R(f)$ would have to be a nonphysical filter with abrupt cutoff frequencies. Moreover, any attempt to make the product transfer function $H_T(f)H_R(f)$ have sharp skirts will cause the channel impulse response to "ring" and increase the system cost through increase of impulse response duration L_{tot}. Since the prober/analyzer has no control over the characteristics of the radio it must work with, the normal procedure is to employ a characterization bandwidth which is narrower than the filters in the radio. A special IF filter is then supplied at the input to the analyzer which dominates the product $H_T(f)H_R(f)$. This filter is optimized to provide an impulse response of minimum duration consistent with a specified attenuation of all alias energy below the desired transfer function at a specific sampling rate of the impulse response $1/\Delta$. Then Δ is adjusted to minimize the number of samples required to measure the desired multipath spread range. This double optimization has been carried out in the equipment and yields $\Delta/\Delta_0 = 0.75$.

As discussed above, each of the correlator outputs is sampled in time. The bandwidths of the correlator outputs are bounded by B_{tot}, the "total" Doppler spread of the channel. By this term we mean the bandwidth outside which there is negligible power (using an appropriate criterion for "negligibility"). Assuming the same sampling rate for each correlator, we see that each (complex) process must be sampled at a rate of at least

B_{tot} per second to allow reconstruction of the continuous process. Clearly, the amount of storage required and the rate of processing in the playback channel are directly proportional to the Doppler spread. Thus, the larger the channel's Doppler spread, the greater the system complexity and cost. Considering both sampling procedures, we find that if it is desired to characterize a channel for a bandwidth W over a time interval T, the number of samples that have to be stored is given by

$$N_{ST} = \alpha(B_{tot}L_{tot})(TW) \tag{2.5}$$

where α is a number lying between 1 and 2.

To keep the system complexity reasonable, provision must be made for separately and simultaneously measuring the surface multipath starting at the earliest arriving specular component and ignoring the "empty" region between the direct/refractive multipath and the surface multipath. By using this procedure, maximum utilization is made of the hardware in measuring and reproducing multipath. In effect, L_{tot} in (2.5) must then be interpreted as the sum of the multipath spreads for the direct/refractive multipath and the surface multipath.

The preceding discussion introduced some of the basic signal processing elements in the channel playback simulation system. However, practical utilization of this system requires the incorporation of additional features for the LOS channels which have moving terminals (GA, AA, AS). The changing path length causes both a time variation in path loss and a time variation in mean path delay for the direct path, refractive multipath, and surface multipath. To handle the time-variant delays, two tracking loops are used which adjust the timing of two separate PN sequence generators. The early tracker removes the time-variant group delay of direct/refractive multipath group while the late tracker separately removes the time-variant group delay of the surface multipath. Frequently, refractive multipath will be absent and the direct path alone will be tracked in the early group. The changing path delays also produce Doppler shifts. A Doppler tracking loop is provided to track out the Doppler shift of the direct/refractive multipath

group.* Otherwise, the output lowpass filters would have to be made very wide in bandwidth to accommodate this Doppler shift. The Doppler shift of the surface multipath group will differ from that of the direct/refractive multipath group; but, for channel measurement with airplanes flying at level height, the differential Doppler will be at most 10 - 20 Hz, and this shift is small enough to be absorbed by the analyzer lowpass filter bandwidth ranges. Therefore, no separate Doppler tracker has provided for the surface multipath.

In channel playback, ideally, the variable delays and Doppler shifts should be reinserted. It has been found prohibitively expensive to provide time variable delays covering the range of delays required. Moreover, as discussed in Section 2.3, there appears no need to have this feature, from a modem evaluation point of view. Differential and direct path Doppler may be set manually at measured values recorded in the log of the flight test. Differential delay will be fixed, but manually-selectable, from a range of values. Again, information from the log of the experiment would provide suitable values for this delay. Direct path delay would not be reproduced since it is irrelevant for modem testing.

Path loss variation will be significant only for the AA and GA links where variations of path length greater than 10:1 may occur during a channel measurement period, causing in excess of a 20-dB variation in average SNR during a measurement interval. To make maximum utilization of the dynamic range of the analog correlators employed in the analyzer, an AGC must be provided. Since the path loss variation will be slow, a long time constant is provided in the AGC. Cases may exist where the fading multipath could have low enough frequency components to be affected by the AGC, and provision must be made for recording the gain variations and reproducing them in the channel playback by means of a variable attenuator.

We consider now the synthetic simulation of the propagation channel. The same tapped delay line is used as in playback simulation, but now the complex tap gains must be generated synthetically.

---

*Actually, different frequency and time error discriminators are provided for tracking refractive multipath as opposed to tracking a resolvable direct path in order to optimize tracking performance under the fading dispersive conditions of refractive multipath.

The two major harmful propagation effects that require some complexity in implementation are refractive and surface multipath. From a mathematical-statistical point of view, these two propagation effects present a study of contrasts. The refractive multipath consists of a small number of individual paths while the surface multipath (aside from a possible specular component) consists of a very large number of small diffuse scattered components and has a continuous type of representation.

From a statistical point of view, the refractive multipath is far more nonstationary than the surface scatter. Consider an AG link. As the airplane passes near the layer of steep negative gradient in refractive index which causes the refractive multipath, multiple ray paths appear, move in delay relative to one another, coalesce, disappear, and new paths appear. As discussed in [2.16], the amplitudes and delays change much slower than the relative phases. Compare this behavior with the surface scatter in an AS link. The airplane antenna pattern is illuminating (through a main or sidelobe) a large portion of the surface of the earth. Many small reflections occur from the surface, and the law of large numbers gives some statistical regularity to the continuum of multipath components. No abrupt changes will be noticed unless the terrain or airplane antenna orientation changes abruptly. Over the ocean, statistical regularity will be the rule rather than the exception.

From these comments it should be evident that the character of the complex tap gain functions used for synthetic simulation will be quite different for refractive and surface multipath. We now present the mathematical foundations upon which the generation of the complex tap gain functions is based for these two multipath modes. First we discuss the character of the impulse responses. Then, via integrals previously developed by Bello [2.26], relate the character of the complex tap gains of the tapped delay line model to the impulse response characteristics of the refractive and surface multipath.

If $z(t)$ and $w(t)$ are the complex envelope representations of the input and output of a linear time-variant channel with impulse response $g(t,\xi)$ and transfer function $T(f,t)$, then we have the input-output relationships

$$w(t) = \int z(t - \xi)\, g(t,\xi)\, d\xi \tag{2.6}$$

$$w(t) = \int Z(f)\, T(f,t)\, e^{j2\pi ft}\, df \tag{2.7}$$

where $Z(f)$ is the spectrum of $z(t)$ and $T(f,t)$, $g(t,\xi)$ are related by Fourier transforms

$$T(f,t) = \int g(t,\xi)\, e^{-j2\pi f\xi}\, d\xi \tag{2.8}$$

$$g(t,\xi) = \int T(f,t)\, e^{j2\pi f\xi}\, df \tag{2.9}$$

Neglecting small amplitude and phase scintillation due to volume scattering, it is shown in [2.16] that the impulse response and transfer function of refractive multipath are given by

$$g(t,\xi) = \sum_{k=1}^{K} a_k(t)\, e^{-j2\pi f_0 \tau_k(t)}\, \delta[\xi - \tau_k(t)] \tag{2.10}$$

$$T(f,t) = \sum_{k=1}^{K} a_k(t)\, e^{-j2\pi f_0 \tau_k(t)}\, e^{-j2\pi f \tau_k(t)} \tag{2.11}$$

Equation (2.10) is just the expression for the (complex envelope of the) impulse response of a channel consisting of K paths having real time-varying amplitudes $a_k(t)$ and time-varying delays $\tau_k(t)$. The exponential term accounts for the time-varying phase shift (i.e., Doppler shift) produced at mid-band (f_0 Hz) by the changing path delay. Although τ_k is slowly changing, f_0 can be a very large number (up to 12 GHz in the present case) so that even very small changes in τ_k (fractions of a nanosecond and greater) can cause radians of phase shift and even several complete rotations of $\exp\{-j2\pi f_0 \tau_k(t)\}$. On the other hand, for bandwidths of interest, f in $\exp\{-j2\pi f \tau_k\}$ is of the order of 12.5 - 50 MHz (relative to midband), so that the same variations that make $\exp\{-j2\pi f_0 \tau_k(t)\}$ rotate many times could cause only a few degress change in $\exp\{-j2\pi f \tau_k\}$. If the delay separations between the refractive paths and the carrier frequencies are large enough as the airplane moves the various factors, $\exp\{-j2\pi f_0 \tau_k(t)\}$ will appear like a set of phasors of incommensurate frequencies rotating relative to one another several cycles apart, while the relative amplitudes and delays seem frozen by comparison. Deep nulls will occur in the transfer function. On the other hand, when the delays get close or the operating frequency is low enough, the phases may change much less and the fading will be shallow.

Although the individual paths do not have complex Gaussian statistics, as should be clear from the above discussion, it is nonetheless true that the probability distribution of the envelope of a received carrier at deep fades has been observed to have the same slope as Rayleigh fading, i.e.,

$$\Pr\left\{|T(f,t)|\right\} \leq \alpha \sim \alpha^2 \tag{2.12}$$

As shown by Lin [2.28], the Rayleigh slope behavior is a general property of deep fades on wide classes of fading channels and is in large measure independent of the actual statistics of the individual paths. Thus, if narrowband channel simulation is of interest, where the fading is essentially flat and nonfrequency-selective, a fading simulation using complex Gaussian statistics would be useful. However, when the bandwidth to be characterized is broad, so that frequency selectivity is important and the individual path can separately affect modem performance (as in the current situation), the use of complex Gaussian modeling cannot be justified. This is the case at hand in the LOS simulator.

Consider now the case of surface multipath where the terrain or water [2.28] has some statistical regularity. The diffuse portion of the multipath return is virtually a continuum of differential-sized scatterers randomly phased and with different amplitude. This is the same type of statistical model applicable to troposcatter channel modeling [2.29],[2.30] — the complex Gaussian WSSUS (wide-sense-stationary-uncorrelated-scattering) channel model. For this model, the differential-sized path fluctuations at any delay have complex Gaussian stationary statistics, and fluctuations at different delays are independent. Mathematically, the WSSUS property is exhibited by the singular correlation function behavior:

$$\overline{g^*(t,\xi)g(t+\tau,\eta)} = Q(\tau,\xi)\,\delta(\eta-\xi) \tag{2.13}$$

where $Q(\tau,\xi)$ is called the tap gain correlation function.

Equation (2.13) states that fluctuations at different delays are completely uncorrelated no matter how close the delay separation. Physically this is clearly an idealization, but, for the bandwidths of interest, which in effect limit the resolvability of very small delays, this is exactly the way the channel behaves. The stationary complex Gaussian property is

attached to $g(t,\xi)$ as a function of t for fixed delay ξ, i.e., the complex gain fluctuations at a given delay. The relative strength of scattering as a function of path delay is given by

$$Q(\xi) = Q(0,\xi) \tag{2.14}$$

called the delay power spectrum. Clearly, the multipath spread of the channel may be defined in terms of the width of the delay power spectrum.

The Fourier transform of $Q(\tau,\xi)$ with respect to τ,

$$S(\xi,\nu) = \int Q(\tau,\xi)\ e^{-j2\pi\nu\tau}\ d\tau \tag{2.15}$$

is called the scattering function of the channel. This function can be interpreted at the power spectrum of the channel fluctuations for path delay ξ. By integrating $S(\xi,\nu)$ over ξ, one obtains [2.26] the power spectrum of a received carrier,

$$P(\nu) = \int S(\xi,\nu)\ d\xi \tag{2.16}$$

The Doppler spread of the channel can be defined in terms of the width of $P(\nu)$.

We now consider the character of the complex tap gain functions of the tapped delay line model corresponding to surface and refractive multipath. The derivation of the tapped delay line model [2.26] is based upon the assumption that the spectrum of the input signal complex envelope Z(f) is confined to a finite bandwidth, say $-(W/2) < f < (W/2)$. Then the time-variant transfer function outside this interval clearly does not affect the output signal since only the product $Z(f)T(f,t)$ occurs in (2.7). One may then replace $T(f,t)$ by a periodic function in f of period $W_0 > W, T_0(f,t)$, which is identical to $T(f,t)$ within $-(W/2) < f < (W/2)$, without changing the output complex envelope w(t). However, since this modified time-variant transfer function is periodic, it has a Fourier series expansion, and its Fourier transform on the frequency variable $g_0(t,\xi)$ may be shown [2.26] to have the discrete representation

$$g_0(t,\xi) = \sum_{-\infty}^{\infty} g_k(t)\ \delta\left(\xi - \frac{k}{W_0}\right) \tag{2.17}$$

where $g_k(t)$ are the (time-variable) Fourier coefficients in the expansion of $T(f,t)$.

Equation (2.17) leads to the input-output representation

$$w(t) = \sum_{-\infty}^{\infty} g_k(t)\ z\left(t - \frac{k}{W_0}\right) \tag{2.18}$$

which is identical to the output of a uniformly tapped delay line with taps spaced $1/W_0$ seconds apart and with time variable complex tap "gain" $g_k(t)$ applied to the tap providing delay k/W.

In [2.29], W_0 was chosen equal to W, which leads to the two equivalent expressions for the k^{th} tap complex gain:

$$g_k(t) = \int \text{sinc}\left[W\left(\xi - \frac{k}{W}\right)\right]\ g(t,\xi)\, d\xi \tag{2.19}$$

$$g_k(t) = \frac{1}{W}\int_{-W/2}^{W/2} T(f,t)\ e^{j2\pi\frac{kf}{W}}\, df \tag{2.20}$$

where

$$\text{sinc } W\xi = \frac{\sin \pi W \xi}{\pi W \xi} \tag{2.21}$$

The question of the number of taps needed in the tapped delay line model to provide adequate representation of the channel is equivalent to the well-known question is spectral analysis: How many Fourier components are needed to represent a record of a random process? "Window" functions are used on the random process to minimize the number of Fourier components. Equations (2.19) and (2.20) correspond to the use of a rectangular window function which does not minimize the number of Fourier components. By choosing $W_0 > W$ and defining

$$T_0(f,t) = H(f)\, T(f,t) \tag{2.22}$$

where H(f) is a "window" transfer function which is satisfactorily close to unity over $|f| = W_0/2$, we may minimize the number of tap gains needed to represent the channel. One may show that with (2.22) the complex tap gains are now given by the expressions

$$g_k(t) = \int \frac{1}{W_0} h\left(\xi - \frac{k}{W_0}\right) g(t,\xi)\, d\xi \tag{2.23}$$

$$g_k(t) = \frac{1}{W_0} \int_{-W_0/2}^{W_0/2} H(f)\, T(f,t)\, e^{j2\pi \frac{k}{W_0} f}\, df \tag{2.24}$$

Consider now the characteristics of the complex tap gain functions for a complex Gaussian WSSUS surface multipath link. First, because of the linear relationship (2.23) between the complex tap gain $g_k(t)$ and the complex Gaussian system function $g(t,\xi)$, $g_k(t)$ is complex Gaussian. The strengths and cross correlations between these tap gain functions are readily found to be

$$\overline{g_k^*(t) g_\ell(t+\tau)} = \frac{1}{W_0^2} \int h^*\left(\xi - \frac{k}{W_0}\right) h\left(\xi - \frac{k}{W_0}\right) Q(\tau,\xi)\, d\xi \tag{2.25}$$

$$\overline{g_k^*(t) g_k(t+\tau)} = \frac{1}{W_0^2} \int \left| h\left(\xi - \frac{k}{W_0}\right)\right|^2 Q(\tau,\xi)\, d\xi \tag{2.26}$$

$$\overline{|g_k|^2} = \frac{1}{W_0^2} \int \left| h\left(\xi - \frac{k}{W_0}\right)\right|^2 Q(\xi)\, d\xi \tag{2.27}$$

If the delay power spectrum $Q(\xi)$ is smooth and does not change much over an interval of delay variation equal to the duration of $h(\xi)$, then we see that

$$\frac{\overline{g_k^*(t) g_\ell(t)}}{\sqrt{\overline{|g_k(t)|^2}\ \overline{|g_\ell(t)|^2}}} \approx \frac{\int h^*\left(\xi - \frac{k}{W_0}\right) h\left(\xi - \frac{\ell}{W_0}\right) d\xi}{\int |h(\xi)|^2\, d\xi} \tag{2.28}$$

$$\overline{g_k^*(t) g_k(t+\tau)} \approx \frac{1}{W_0} Q\left(\tau, \frac{k}{W}\right) \frac{1}{W_0} \int |h(\xi)|^2\, d\xi \tag{2.29}$$

$$\overline{|g_k|^2} \approx \frac{1}{W_0} Q\left(\frac{k}{W}\right) \frac{1}{W_0} \int |h(\xi)|^2 \, d\xi \tag{2.30}$$

Thus, in general, even in the limit of a "smooth" $Q(\xi)$, the tap gains are correlated with the correlation function proportional to the sampled autocorrelation function of the window function, while their strengths are proportional to samples of the delay power spectrum.

In the particular case of an ideal rectangular window function [see (2.19) and (2.20)], however, the sampled autocorrelation function in (2.29) is identically zero at the sample points, yielding

$$\overline{g_k^*(t) g_\ell(t+\tau)} \approx \begin{cases} 0 & ; \quad k \neq \ell \\ \frac{1}{W} Q\left(\tau, \frac{k}{W}\right) & ; \quad k = \ell \end{cases} \tag{2.31}$$

Thus, the independent complex Gaussian tap gain model may be used for surface multipath in the limit, as the bandwidth characterized, W, becomes large enough so that the delay power spectrum $Q(\xi)$ varies little in a delay interval $1/W$. The above analysis constitutes a justification for the use of this model for surface scatter simulation. Note, from (2.15), that the power spectrum of the fluctuations in $g_k(t)$, consistent with (2.31), is proportional to the scattering function evaluated at $\xi = k/W$, i.e., $S(k/W, \nu)$.

Strictly speaking, then, the power spectra of the synthetic complex tap gain fluctuations should be adjusted to match the scattering function. This matching procedure would be a very expensive undertaking and, in fact, would not significantly add to the utility of the synthetic simulator in "exercising" modems. Moreover, consider the following heuristic argument. For high-speed data transmission where the channel essentially looks "frozen" for the duration of a few bits, error rate performance depends only on the delay power spectrum $Q(\xi)$. On the other hand, in high-speed data transmission the first harmful

effects of fast fading are noticed in the channel measurement process (e.g., extraction of phase references in coherent and differentially coherent detection and predetection combining) and are determined by the Doppler power spectrum. Thus, for high-speed data transmission, one may replace the actual scattering function by a simpler scattering function,

$$S(\xi,\nu) = S(\xi)\, P(\nu) \tag{2.32}$$

and yet have the error rates due to multipath and fast fading be essentially identical. Moreover, as discussed in [2.30], these effects are dependent, to first order, on a single first-order parameter of the Doppler spectrum, the rms Doppler spread B. This parameter is simply twice the standard deviation of the power spectrum when it is made to look like a probability density function by normalizing it to unit area. As a result of these considerations, the synthetic surface multipath simulator has complex tap gain functions with identical unimodal power spectra. Front panel controls allow selection of the desired rms Doppler spread.

We now consider the behavior of the complex tap gain functions for the case of refractive multipath.

Using (2.10) in (2.19) we find that the tap gain function for refractive multipath takes the form

$$g_\ell(t) = \frac{1}{W_0} \sum_{k=1}^{K} a_k(t)\, e^{-j2\pi f_0 \tau_k(t)}\, h\left[\frac{\ell}{W_0} - \tau_k(t)\right] \tag{2.33}$$

This expression contains K terms, each corresponding to a particular discrete moving path of the multipath structure. To simplify the discussion, let us examine a single moving path and drop the k subscript. This moving path is characterized by the two time-variant parameters, delay $\tau(t)$ and amplitude $a(t)$. It has a discrete tapped delay line model representation with the ℓ^{th} complex tap gain given by

$$g_\ell(t) = \frac{1}{W_0}\, a(t)\, e^{-j2\pi f_0 \tau(t)}\, h\left[\frac{\ell}{W_0} - \tau(t)\right]$$

$$= \frac{1}{W_0}\, a(t)\, e^{-j2\pi f_0 \tau(t)}\, [h(\xi) - \tau(t)] \qquad \xi = \frac{\ell}{W_0} \qquad (2.34)$$

We see that $g_\ell(t)$ at a given time instant is just a sampled version of the window function which has a delay and complex amplitude determined by the value of a(t) and $\tau(t)$ at that time instant. The complex tap gains are completely correlated in complete contrast to the tap gains for surface multipath.

A convenient picture describing the variation of the tap gain with time for a single path is of a slowly moving and slowly amplitude changing window function moving along an axis with pickets every $1/W_0$, as shown in Figure 2.11 for a triangular window function. For simplicity, only the amplitude change a(t) is indicated in this figure by the dashed line connecting the peaks of the triangle. The tap gain function $g_\ell(t)$ is obtained by "sitting" on $\xi = \ell/W_0$ and watching the complex values observed as the triangle moves.

The complete refractive multipath structure is obtained by adding up the moving window functions for each path. Thus, $g_\ell(t)$ would be the summation of complex samples from the delayed moving window functions for each path. It should be clear at this point that independent complex Gaussian tap gain functions cannot be expected to represent refractive multipath. CNR has provided a true refractive multipath simulation. Complex tap gains are generated for up to seven moving paths, as described in Eq. (2.33), by the use of a minicomputer into which is fed (via digital tape) the time variable amplitudes and delays of the paths previously computed according to some desired scenario.

The synthetic simulation of ionospheric scintillation involves the use of one complex multiplier to insert time-variant amplitude and phase fluctuations on the direct path, because this phenomenon is not frequency-selective. The same minicomputer is used to generate these fluctuations. In [2.25], it is shown that an appropriate model for the ionospheric fluctuations consists of in-phase and quadrature Gaussian fluctuations of different mean strength, with the relative strength dependent on the operating frequency and intensity of the anomalous ionospheric electron density.

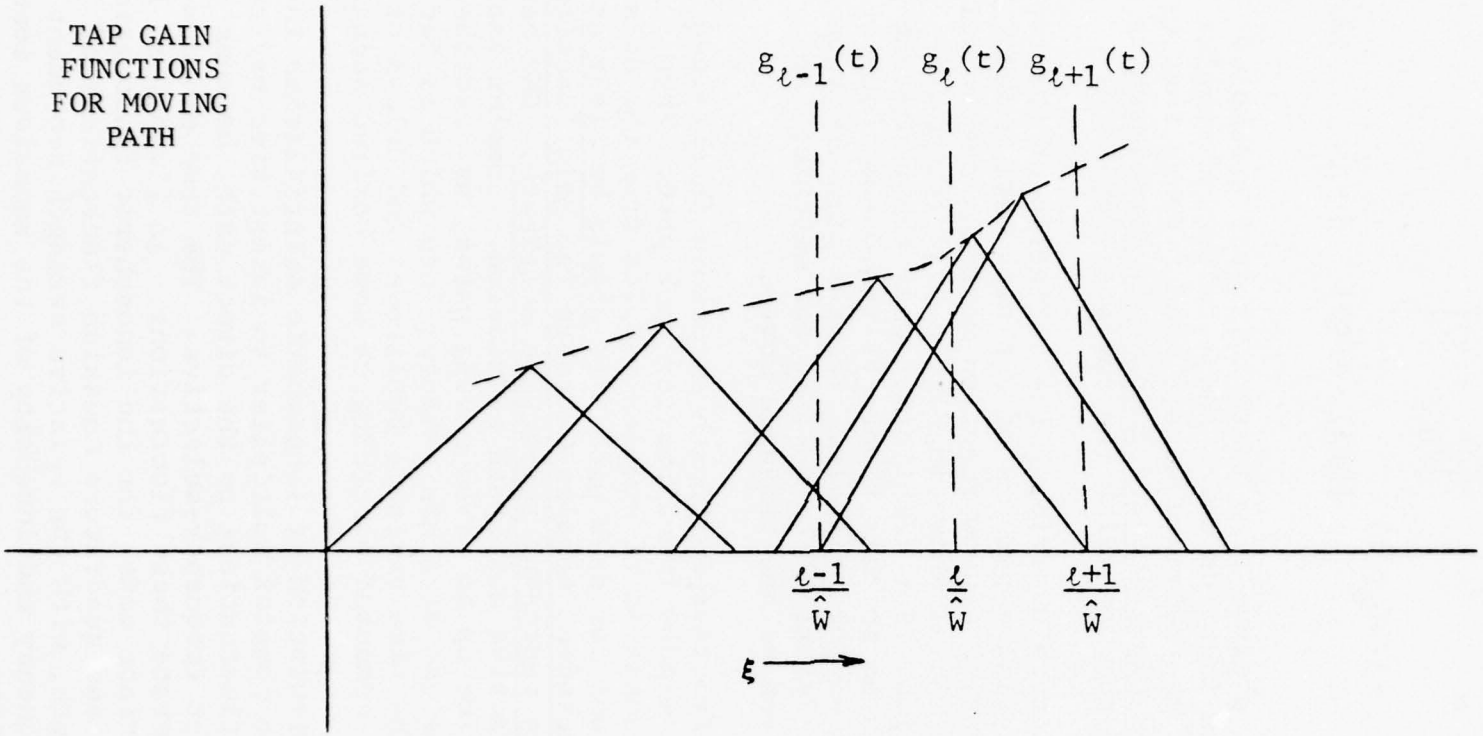

Figure 2.11 Illustration of Tap Gain Functions for a Moving Path

is acceptable instead of unity for $K(f)$ in the interval $|f| < W/2$.

2.3 Effect of Simulator Nonidealities on Modem Error Rate Reproducibility

The function of the wideband LOS simulator is to test digital modems so as to determine, in the laboratory, the effect on performance that LOS radio channel characteristics would have if the modem were actually field-tested at some future date. In designing the simulator, this objective was kept in mind because it allowed placement of practical design constraints on the simulator and kept the cost of development from being increased unnecessarily. Thus, for example, in channel playback simulation, it is only necessary to reproduce the channel characteristics with sufficient fidelity to reproduce modem error rate behavior. Design nonidealities and channel perturbations which have an imperceptible effect on modem error rate performance may be ignored. We consider first the effect of undesired additive noise on modem performance and then the effect of undesired signal distortions. Both spread-spectrum and nonspread-spectrum modems are considered.

Undesired additive noise contributions may enter into the simulator in two different ways. First we note that, in channel measurement with the prober/analyzer, additive noise at the analyzer input will result in noise contributions to the measured channel tap gains. Then, in channel playback, the simulator will produce a spurious output due to these noise contributions. The effect of the noise in the tap gains may be modeled as a dispersive "noise" channel in parallel with the desired played-back channel. Another way that noise enters into the simulation is via thermal noise effects in the simulator itself. This level has been specified to be no greater than -50 dBm in a 100-MHz bandwidth at the output. For the nominal output signal level of 0 dBm, this constitutes a 50-dB SNR.

Consider the effect of additive noise in the simulator and consider conventional digital communication techniques used in radio communications, e.g., FSK, PSK, DPSK. At high SNR, the error rate performances of these techniques are within a range of 3 dB, with binary PSK being best and noncoherent FSK worst. For noncoherent FSK*, bit error rates of 6.3×10^{-15} and 9.6×10^{-23} occur for SNR's of 18 and 20 dB, respectively, where SNR is defined as the ratio of signal power to the noise power

* $Pe = \frac{1}{2} \exp\left(-\frac{SNR}{2}\right) = \frac{1}{2} \exp\left(-\frac{10^{SNR(dB)}}{2}\right)$

in a bandwidth equal to the bit rate. From this calculation we see that additive noise, per se, can be as high as -18 dBm without causing a significant bit error rate. The effect of such a system noise level is to cause an irreducible error probability of 6.3×10^{-15} for the noncoherent FSK modem. That is to say, a curve of error rate vs. SNR obtained by adjusting the noise level in the simulator would show a bottoming-out as SNR's approach and exceed 18 dB. At an apparent input SNR of 12 dB, the actual SNR will be 11 dB. This one dB shift is undesirable since it occurs at SNR's where significant errors occur ($Pe = 1.1 \times 10^{-4}$ at SNR = 12 dB). A system noise level of -24 dBm would produce a shift of 0.5 dB at an input SNR of 15 dB ($Pe = 5.6 \times 10^{-8}$). Clearly, the -50 dBm specified in the simulator is more than adequate to remove the effects of simulator noise on modem performance even at signal levels lower than -20 dBm.

In the case of DCS microwave links, consideration is being given to transmission of 2 bits/sec/Hz of bandwidth with saturating power amplifiers. Such modem techniques require more SNR for the same error rate than the conventional modems mentioned above, sometimes as much as 10 dB greater [2.16]. In such a case, one would like the system SNR to be 34 dB or greater. Clearly, the simulator reaches this objective also.

For the case of PN spread-spectrum modems, the basic signaling elements are orders of magnitude wider in bandwidth than the bit rates. Thus, the SNR in a bandwidth equal to the bit rate is correspondingly orders of magnitude larger for a given system noise than for the case of a conventional modem. As a consequence, we have assumed that if system level noise is small enough for conventional modem error rate reproducibility, it is more than small enough for the case of spread-spectrum modems. This phenomenon appears true for all nonidealities. That is to say, if an equipment nonideality is small enough not to affect conventional modem error rate reproducibility, it is more than small enough for the case of spread-spectrum modems.

Consider now the case of noise introduced in the prober/analyzer. When the channel is probed, there will always be a background of Gaussian receiver noise. Thus the measured impulse response will actually consist of a desired impulse response and a "noise" impulse response. The resulting played-back channel will behave as the parallel combination of two channels – the desired channel and a "noise channel". The following useful theorem has been proven by Bello [2.31]:

If channel probing takes place with a received probing signal having power P and noise bandwidth B_T in the presence of receiver noise of one-sided power density N_0, then the noise channel acts like a surface multipath channel in which the ratio of the average strength of the desired played back channel transfer function to the noise played back channel transfer function is given by:

$$\frac{S_{ch}}{N_{ch}} = \frac{P}{N_0} \cdot \frac{T}{K} \cdot \frac{1}{B_T \Delta} \tag{2.35}$$

where it has been assumed that the prober demodulator consists of K adjacent correlator taps Δ seconds apart in delay, with an integrate-and-dump filter having a total integrate time T* for extracting the tap gain estimate at the correlator output. The noise scatter channel has a uniform rectangular delay power spectrum of duration $K\Delta$ and a Doppler power spectrum of shape $|H_L(\nu)|^2$, where $H_L(\nu)$ is the transfer function of the tap gain low pass filtering including all low pass filtering up to the input to the complex modulators of the tapped delay line.

Since the noise channel fluctuations and the modem signal are statistically independent, and since the noise fluctuations are complex Gaussian, one may show that the effect of the noise channel in producing error rates for a given S_{ch}/N_{ch} can be equal in some cases (e.g., binary PSK) to that produced by additive noise for an SNR equal to the value of S_{ch}/N_{ch}. However, it must be recognized that the noise channel produces intersymbol interference and is a <u>multiplicative</u> effect. Thus, a change in the modem signal level leaves S_{ch}/N_{ch} unchanged. In addition, a reduction in bit rate (as in the case of a spread spectrum modem), which increases the SNR for a given system noise level, will leave S_{ch}/N_{ch} unchanged.

---

*This integrate time is selectable as a multiple of the PN sequence period, depending on the Doppler spread of the channel, i.e., $T = IT_0$, where $I = 1,2,4,8,16,32$.

If the only significant nonideality present in the system was that due to noise received in the prober/analyzer, one could argue that an S_{ch}/N_{ch} of at least 24 dB would be satisfactory as in the case of SNR. However, there are a large number of possible multiplicative perturbations in the overall system, and it is necessary to consider the cumulative effect of all these perturbations in assigning tolerable levels. Thus, the following sources of multiplicative perturbations may be identified:

- Amplitude and group delay distortion in filters
- Amplitude and group delay distortion in acoustic delay line
- Amplitude and phase insertion errors in complex modulators and tapped delay line
- Leakage through complex modulators
- Phase shifts on tapped delay line produced by temperature changes
- Aliasing crosstalk due to sampling impulse response in prober/analyzer
- DC components at the correlator outputs of the prober/analyzer
- Crosstalk components at the correlator outputs produced by pseudo-noise sequence signal probing and correlation
- Aliasing crosstalk and distortion appearing in recovery of complex tap gains from sampled versions

We consider each of these disturbances. Consider first amplitude and group delay distortions in filters. One may regard the distortions as being produced by a "distortion" channel with transfer function D(f) in parallel with the desired distortion-free transfer function. This distortion channel, being a linear filter, has a representation in terms of a tapped delay line. Thus, one may always regard the distortion as being produced by a set of discrete echoes, i.e., discrete nonfading multipath. For a given small peak amplitude or group delay ripple departure from ideal, one may argue heuristically that a single echo which produces such a peak departure provides a worst case as far as affecting modem error rate behavior. A multiple path model providing the same peak distortion would have the sum of the peak values of the complex

path gains bounded by the peak distortion in the transfer function. But multiple paths spaced farther apart than the symbol durations would produce intersymbol interferences which would add independently. Thus, with a single path model providing the same peak distortion, the peak value of total intersymbol interference will occur 50% of the time for binary PSK but less often with a multiple path model, and the error rate with the single path model would be larger.

Consider then the sizes of the single interfering path which produces various peak distortions and the impact of this distortion on error rate for a binary PSK system. For a path 18, 24, and 30 dB below the direct path, we find peak amplitude ripples of 1.02, 0.52, and 0.27 dB in the transfer function amplitude and group delay ripples of $\tau/8$, $\tau/16$, and $\tau/32$ seconds where τ is the delay of the path relative to the direct path. The distortion specification in the work statement calls for a peak amplitude ripple of 0.5 dB, which corresponds to a disturbing echo or path 24 dB below the direct path. From a modem performance point of view, the echo produces an interfering pulse 24 dB below the desired pulse and changes the detector output by $\pm$0.5 dB. For low error rates, the error rate will be dominated by the 0.5-dB reduction in signal strength. In summary, then, the effect of a peak distortion of $\pm$0.5 dB in the amplitude characteristic, or $\pm(\tau/16)$ in the group delay characteristic, is bounded by 0.5 dB in the modem error rate vs. SNR behavior at high SNR. To select the worst-case path delay τ, one should choose the minimum value of τ yielding the maximum interference; namely, τ equal to the duration of one bit. Thus, at 100-Mb/s binary PSK, a peak group delay ripple of $\frac{5}{8}$ ns can be expected to produce, at most, a 0.5-dB degradation.

As far as amplitude and group delay distortion in the acoustic delay line is concerned, the same arguments just proposed for filter distortion clearly apply, as they do for any linear system.

In dealing with the type of distortion introduced by the lumped filters in the simulator, however, it must be recognized that some distortions follow characteristic slow changes over the passband that are not simply characterized by "ripple" in group delay and amplitude. For these cases, one must carry out error rate performance calculations specialized to the types of distortion as have been carried out by Sunde [2.33]. Because of the fact that the major group delay and amplitude distortions of the lumped filters occur at the band edges where

the power level of the data signal is low, it is found that much larger distortion in amplitude and group delay are actually tolerable before significant SNR performance degradation occurs. The effective analyzer/simulator filtering has been designed using [2.33] in order to keep the corresponding distortions from causing significant performance degradation.

Complex modulators are used in the tapped delay line to vary the amplitude and phase of the tap output according to an appropriate time-variant complex gain obtained either by playback of the measured and stored channel or by synthetic generation. These modulators have been built to have a wide dynamic range. However, practical limitations will prevent perfect linearity. Thus, as the input complex gain changes over a set of values, the actual complex gain inserted on the tap output will differ from the input slightly in its amplitude and phase or in its in-phase and quadrature components. The cumulative effect of these small insertion errors for the whole set of tap outputs will result in a distortion of the reproduced or synthetic transfer function.

One may model this distortion by a "distortion channel" in parallel with the undistorted channel, where the tapped delay line model of this distortion channel has complex gains equal to the in-phase and quadrature components of the insertion errors at each tap. Making the reasonable assumption of independent insertion errors at each tap, we see that the distortion channel transfer function has characteristics similar to those of the "noise" channel discussed previously. However, in one important respect the distortion channel differs from the noise channel: the level of distortion depends on the level of the desired multipath signal generated by the distortion-free tapped delay line model. A strong multipath signal will considerably degrade digital transmission performance over an LOS link. Small perturbations in the multipath signal, caused by the distortion channel, represent a spurious multipath signal considerably below the actual multipath signa, and should have minor impact on error rate responsibility.

To estimate the level of this spurious multipath signal in relation to the desired multipath signal, we may make use of calculations by Bello [2.18] who shows that the strength of the spurious multipath signal relative to the desired multipath signal at the simulator output is given by $(\sigma_\theta^2 + \sigma_\epsilon^2)$ where $\sigma_\epsilon^2, \sigma_\theta^2$ are the mean-squared values for an assumed random distribution of insertion phase error (in radians) and loss error (in nepers)

on each tap. Thus we see that an rms phase insertion error of 2^{o} ($\pm$ 6^{o} peak errors for three standard deviations) produces a spurious multipath signal 29 dB below the desired multipath signal. Also, an rms error in insertion loss of 0.3 dB ($\pm$ 0.9 dB peak errors) produces the same level of spurious multipath signal. It should be realized that weak multipath signals, say 20 dB below the direct path signal, will have negligible effect on conventional digital modem performance, since such multipath will affect modem performance as random noise does. (Recall that, for a noncoherent FSK modem, $Pe = 9.6 \times 10^{-23}$ at 20-dB SNR.) The simulator, as implemented, utilizes 32 complex modulators. For the case of independent complex tap gain modulations on each tap (corresponding to worst-case surface multipath), the multipath output is enhanced by 15 dB relative to the strength of a single tap. For the output multipath signal to be 20 dB below the direct path signal then requires that the level of the input multipath modulation per tap be at a level of 35 dB below the direct path modulation (the latter being set at the maximum by the simulator). At this low input, the distortion multipath signal at the output is at a level 24 dB below the multipath signal ($\pm$ 0.5 dB rms insertion loss error domination) or 44 dB below the direct path.

The maximum level that surface multipath can be expected to have at the simulator output is that of the direct path signal. In such a case, the uniform multipath model, described above, will require tap modulations at a level 15 dB below the maximum modulation level. The distortion multipath signal would be at a level of 24 dB below the direct path and will be totally obscured by the valid multipath signal as far as affecting modem error rate.

In the case of refractive multipath, there will be a few discrete paths (rarely reaching 6 - 7 for the longer paths), but these can be comparable in size, or even larger than the direct path. As a result, the distortion multipath signal can be expected to be 30 - 40 dB lower than the valid multipath signal at the simulator output. Again, since the valid multipath signal is dominating the error rate behavior by interference with the direct path, the small distortion component 30 - 40 dB below the mutlipath will have negligible additional effect on modem error rate behavior.

We consider now the effect of temperature change on the tapped delay line. A temperature change will cause the length of the delay line to change, which is mathematically equivalent

to a time scale change of a channel snapshot impulse response. From elementary Fourier theory, we know that if a change in time scale occurs in a function h(t), there is a corresponding inverse scale change in the transform H(f), i.e.,

$$h(t) \rightarrow h[(1+\alpha)t] \Longrightarrow H(f) \rightarrow \frac{1}{1+\alpha} H\left(\frac{f}{1+\alpha}\right) \qquad (2.36)$$

A thermal coefficient of expansion for the delay line is typically $4 \times 10^{-5}/^{o}C$, i.e., $\alpha \approx 4 \times 10^{-5}$ per ^{o}C. Thus, if the band center of the reproduced channel were at f_0 and a change in temperature of ΔT ^{o}C occurred, the band center would shift by Δf, given by

$$\Delta f \approx 4 \times 10^{-5} \Delta T f_0 \qquad (2.37)$$

Table 2-5 shows some representative calculations assuming a band center at 400 MHz and temperature changes of ± 0.5 ^{o}C and ± 5 ^{o}C. Since a range of ± 5 ^{o}C seems reasonable for the laboratory environment of the simulator, there should not be any need for an oven.

The harmfulness of frequency shifts of the channel transfer function on modem error rate reproducibility is not simply calcultated. However, by adopting a somewhat different point of view, we can use previous arguments to determine when it is negligible. This point of view regards the frequency shift of the transfer function as having been caused almost entirely by the uniform phase shift introduced between adjacent taps of the delay line by the slight change in delay. This may be proven by expressing the impulse response h(t) in the complex envelope form

$$h(t) = e^{j2\pi f_0 t} h_0(t) \qquad (2.38)$$

The change in time scale is so small that its effect on $h_0(t)$ is imperceptible. However, since f_0 is so large ($f_0 = 1$ Gc, say), the change in time scale does affect the exponent, changing the impulse response effectively to

$$h(t) \longrightarrow e^{j2\pi f_0 t} e^{j2\pi f_0 \alpha t} h_0(t) \qquad (2.39)$$

TABLE 2-5

CENTER FREQUENCY SHIFTS IN PLAYED-BACK CHANNEL AND CUMULATIVE PHASE SHIFTS OVER 200-ns DELAY PRODUCED BY TAPPED DELAY LINE AMBIENT TEMPERATURE CHANGES

	Temperature Change	
	$\pm$ 0.5°C	$\pm$ 5°C
Phase Shift* for 200-ns Delay at 400 MHz	$\pm$ 0.59°	$\pm$ 5.92°
Band Center* Frequency Shift Caused in Simulator	$\pm$ 8 kc	$\pm$ 80 kc

*Assumed delay line coefficient of thermal expansion $4 \times 10^{-5}/°C$.

which is exactly a frequency shift. However, note that for the tapped delay line representation

$$h_0(t) = \sum g_k \, \delta(t - k\Delta) \tag{2.40}$$

where Δ is the delay between taps (7.5 ns for the design). Equation (2.39) says that the complex envelope has been changed as follows:

$$h_0(t) \rightarrow e^{j2\pi f_0 \alpha t} \quad h_0(t) \rightarrow \sum g_k \, e^{j2\pi f_0 k\Delta} \, \delta(t - k\Delta) \tag{2.41}$$

which exhibits the described phase shift property between taps. Table 2-5 shows that over the length of the delay line (233.5 ns) a phase insertion error of less than 5.9^{o} will accumulate on the last tap, or less than 0.2^{o} per tap, if the temperature stays within $\pm 5\ ^{o}C$.

As discussed in the previous section, the process of using a tapped delay line model for channel playback simulation is a sampling process along the delay variable of the channel impulse response, and, like all sampling processes, introduces some alias crosstalk. To control this crosstalk, a filter is used at the input to the multipath analyzer to limit the spectrum of the received signal prior to correlation processing. Unfortunately, this filter must also satisfy the conflicting requirement of not distorting the channel in the reproducible bandwidth (e.g., 100 MHz). The filter design problem is simplified by making the sampling interval, i.e., spacing between taps on the delay line, as small as possible. However, the cost of the simulator increases linearly with the number of taps so every attempt is made to keep the tap spacing as large as possible consistent with a maximum level of alias crosstalk and inband distortion. It was found that a choice of tap spacing equal to 3/4 the duration of a PN sequence chip (e.g., 7.5 ns for 10-ns probing) and a sixth-order Butterworth filter of the proper bandwidth allowed the alias crosstalk to be limited to 40 dB below the desired channel transfer function and the inband distortion to be negligible provided an appropirate equalizer is used in the simulator to counteract the spectral shaping of the PN sequence transmitted spectrum. From our previous discussions we see that this level of crosstalk will be totally negligible in its effect on modem error rate reproducibility. Table 2-6 presents some parameters for a set of sixth-order Butterworth-Thompson

TABLE 2-6

SIXTH-ORDER BUTTERWORTH-THOMPSON FILTER DESIGNS WHICH GIVE 40-dB ALIAS ATTENUATION IN THE BAND $\pm \frac{1}{2}(1/\Delta_0)$ FOR TAP SPACING $\Delta = 0.75\ \Delta_0$

m	Bandwidth of Filter from f = 0 to -3 dB Gain in Units of $\frac{1}{\Delta_0}$	Filter Gain at Frequency of $\frac{1}{2\Delta_0}$	Magnitude of Group Delay Difference Between f = 0 and $f = \pm\frac{1}{2}\left(\frac{1}{\Delta_0}\right)$ in Units of Λ_0
0.0 (Butterworth)	0.904	0.00	0.036
0.2	0.879	- 0.50	0.024
0.4	0.816	- 0.89	0.014
0.6	0.749	- 1.21	0.013
0.8	0.698	- 1.48	0.006
1.0 (Bessel)	0.662	- 1.68	0.015

Δ_0 = Prober chip duration (10 ns or 40 ns for 100-MHz and 25-MHz characterization)

filters [2.32] that reduce the alias crosstalk to -40 dB for a tap spacing of 3/4 Δ_0 (Δ_0 = 10 ns for 100-MHz characterization). Butterworth-Thompson filters are indexed on a parameter m which ranges from 0 (Butterworth filter) to 1 (Bessel filter). The 3-dB bandwidth, gain at the edges of the characterization bandwidth($\pm$ 1/2 Δ_0 about band center), and group delay difference between midband and edges of characterization bandwidth are presented for values of m = 0, 0.2, 0.4, 0.6, 0.8, and 1.0. Note that the amplitude distortion is negligible for the Butterworth filter and the group delay distortion only 0.36 ns for the 100-MHz characterization.

The existence of an IF filter with transfer function H(f) in the analyzer and a rectangular "chip" of duration Δ_0 in the prober implies an inherent single-path transfer function [see (2.4) and the surrounding discussion]:

$$K(f) = \left(\frac{\sin \pi f \Delta_0}{\pi f \Delta_0}\right)^2 H(f) \qquad (2.42)$$

Figure 2.12 presents the Fourier transform of K(f) or channel impulse response k(t), for the Butterworth and Bessel filters listed in Table 2-6. The dashed triangle indicates the single-path channel impulse response without any IF filter. Note that, in the case of the Butterworth filter, the impulse response duration increases by around 1.5 Δ_0 beyond the 2 Δ_0 of the triangle, while the increase is only around 0.6 Δ_0 for the Bessel filter. It should be recognized that this spreading subtracts from the multipath spread measurement capability of the prober/analyzer. In the present design, the spreading is small. However, any attempt to increase the tap spacing significantly forces the bandwidths of the filters to be reduced considerably to achieve the -40 dB alias crosstalk. This bandwidth narrowing rapidly extends the "tail" of the system impulse response. Figure 2.13 illustrates this behavior for a tap spacing of 0.8 Δ_0 with a fourth- and sixth-order Butterworth filter.

Analog correlators suffer from certain dynamic range limitations. At the small signal end of the range, the limitation of the correlators is in the apparance of low-level dc components. Because there are only two complex analog correlations, which are time-division-multiplexed, the same spurious dc is fed to up to 16 multiplexed correlator outputs corresponding to a particular analog correlator. The two pairs of 16 correlator outputs are interlaced. Consider the effect on

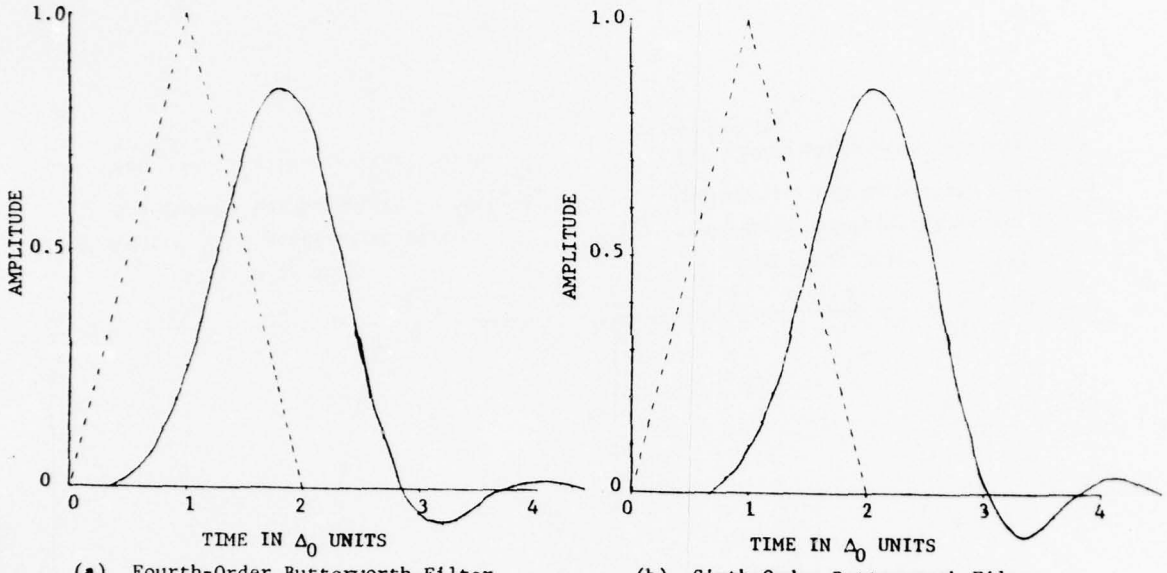

(a) Fourth-Order Butterworth Filter
One-sided - 3 dB bandwidth = $0.584\left(\frac{1}{\Delta_0}\right)$
for - 40 dB alias crosstalk with
$\Delta = 0.8\ \Delta_0$

(b) Sixth-Order Butterworth Filter
One-sided - 3 dB bandwidth = $0.664\left(\frac{1}{\Delta_0}\right)$
for - 40 dB alias crosstalk with
$\Delta = 0.8\ \Delta_0$

Figure 2.12 Prober/Analyzer Equipment Impulse Response for Two Filters in Table 2-6

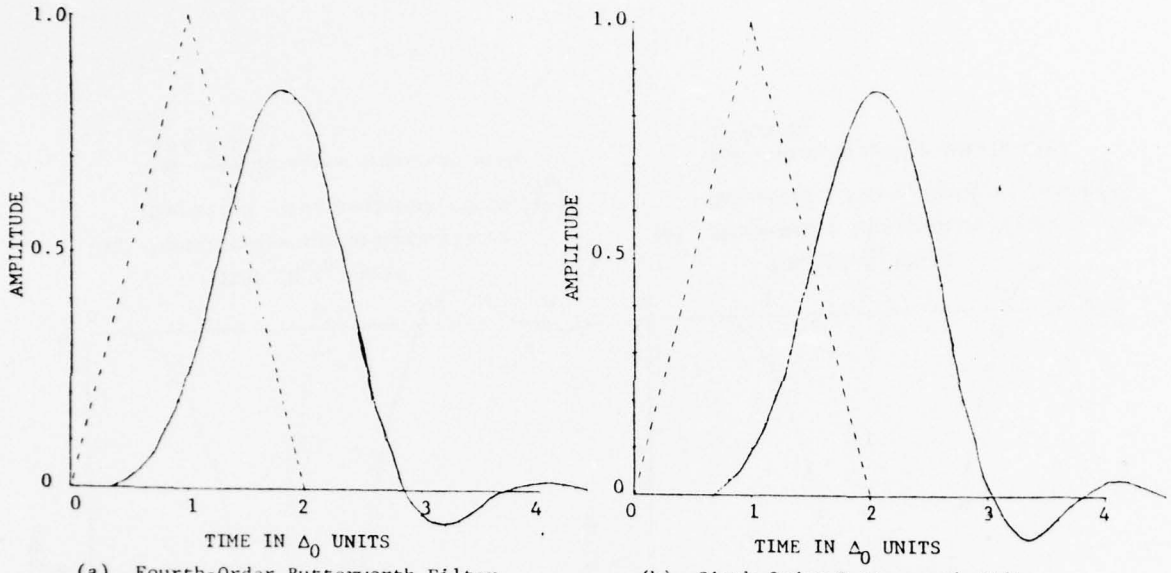

(a) Fourth-Order Butterworth Filter
One-sided - 3 dB bandwidth = $0.584\left(\frac{1}{\Delta_0}\right)$
for -40 dB alias crosstalk with
$\Delta = 0.8\ \Delta_0$

(b) Sixth-Order Butterworth Filter
One-sided - 3 dB bandwidth = $0.664\left(\frac{1}{\Delta_0}\right)$
for -40 dB alias crosstalk with
$\Delta = 0.8\ \Delta_0$

Figure 2.13 Prober/Analyzer Equipment Impulse Response for Tap Spacing $\Delta = 0.8\ \Delta_0$

the reproduced transfer function of a spurious dc γ on one set of 16 correlator outputs. Mathematically, the corresponding distortion transfer function is:

$$D(f) = \gamma \sum_{k=1}^{16} e^{j2\pi f2\Delta} \approx 16\gamma \frac{\sin \pi f 32\Delta}{\pi f 32\Delta} e^{j\theta} \qquad (2.43)$$

Thus, at the center of the band, the distortions add coherently to produce a level 16 times, or 24 dB, larger. However, this perturbation damps out away from the center of the band according to a ($\sin \pi f32\Delta / \pi f32\Delta$) behavior. The other set of 16 taps produces an effect of the same size, but phased differently. In the worst case, it may add directly, producing a net perturbation 30 dB higher than the dc on a single correlator output.

While such a distortion is large in the vicinity of the center of the band, its effect on modem error rate can be surprisingly small because, in analyzing the statistics of the intersymbol interference produced, it becomes evident that the coherency effect is largely negated by the data randomness. On the other hand, any carrier component of the modem near the center of the band will certainly be grossly affected unless the dc component is very small. To keep the perturbation at the band center to within $\pm$ 0.5 dB requires that the dc component be 54 dB down in the worst case. Unless the modem uses some special signaling element near the center of the band, e.g., a carrier component for phase reference extraction, this is an unnecessarily severe specification.

The analyzer meets the -54 dB specification at each correlator output for all modes of operation of the prober/analyzer except the maximum Doppler spread mode. Except in this mode, 180° reversals are inserted into the multiplexed correlation operations on alternate correlations, and a compensating reversal is used at the correlator output. In this way, the spurious dc components alternate in sign on adjacent taps in each set of 16, and their contribution cancels at the midband. The ripple builds up to a maximum at a frequency $\pm$ ($1/2\Delta$) on each side of midband. For Δ= 7.5 ns, $\pm$ ($1/2\Delta$) corresponds to $\pm$ 66 2/3 MHz. Since the reproducible bandwidth lies in the interval $\pm$ 50 MHz about midband, this ripple is attenuated at the edge of the reproducible bandwidth by around 22 dB. Thus, dc components 35 dB down from maximum at the multiplexed correlator outputs will still only produce perturbations which, under the worst combination of conditions, correspond to a perturbation

35 - 30 + 22 = 27 dB down. Moreover, as pointed out above, in examining the effect of intersymbol interference, it is more sensible in evaluating the effect on modem error rate to regard the dc components as producing a spurious multipath signal at a level 35 dB below the direct path.

It has been shown that two types of spurious components, called dc crosstalk and harmonic crosstalk, are introduced into the correlator outputs of the multipath analyzer by the correlation process. The former is caused by the small carrier component transmitted by the PN sequence prober (the number of 1's and 0's of a PN sequence differ by one) and produces an identical component at all correlator output proportional to the time-variant transfer function of the channel at midband. The latter consists of components at harmonics of the PN sequence fundamental frequency. Both have bandwidths of the order of the Doppler spread of the channel.

Since the dc crosstalk is the same for all taps, its effect on the played-back transfer function is the same as the dc unbalance of the correlator output discussed above. However, one may not cancel this term out by alternately changing the PN sequence phase $\pm 180^{\circ}$. The major perturbation occurs at band center. From Eq. (5.51) of [2.18], one may show that this maximum perturbation at band center has a magnitude of

$$\frac{\Delta_0}{\Delta} \cdot \frac{K}{N} \tag{2.44}$$

where Δ_0 is the PN sequence pulse duration, Δ is the tap spacing, K is the number of taps used, and N is the length of the PN sequence. For the prober/analyzer parameters chosen, this perturbation is 35 dB below the value of the played-back transfer function at midband and, in addition, is correlated with it. Thus, at midband, it causes at most a perturbation of 0.15 dB in the multipath signal transfer function. When one recalls that such a localized perturbation is considerably less harmful from the point of intersymbol interference than that caused by a single path, it is concluded that dc crosstalk effects may be ignored.

The upper bound for harmonic crosstalk appears at the output of the integrate-and-dump (I&D) circuit following the correlator. This I&D integrates over exactly one period of the locally-generated PN sequence, and thus has nulls in its transfer function at harmonics of the PN sequence fundamental

frequency. These nulls tend to cancel the harmonic crosstalk components, but the nonzero Doppler spread of the components prevents complete cancellation. Assuming an rms Doppler spread B, one may compute that the q^{th} harmonic crosstalk component on any correlator output normalized to the desired multipath signal at the playback tapped delay line output is given by

$$\frac{S_{harm,q}}{S_{ch}} = \frac{2}{N}\left(\frac{BT_0}{q}\right)^2 \tag{2.45}$$

where T_0 is the period of the PN sequence.

Due to the sampling process following the I&D, the harmonic crosstalk components get folded into the lowpass region of the correlator output. Making the worst-case assumption that all components appear around dc, the total normalized harmonic crosstalk per correlator output becomes

$$\frac{S_{harm,tap}}{S_{ch}} = \frac{2}{N}\left(\frac{BT_0}{2}\right)^2 2\sum_{1}^{\infty}\frac{1}{q^2}$$

$$= \frac{2}{N}\left(\frac{BT_0}{2}\right)^2 \frac{\pi^2}{3} \tag{2.46}$$

Finally, assuming independent crosstalk fluctuations on each tap, the output signal due to harmonic crosstalk normalized to the desired multipath signal is given by

$$\frac{S_{harm}}{S_{ch}} = \frac{2K}{N}\left(\frac{BT_0}{2}\right)^2 \frac{\pi^2}{3} \tag{2.47}$$

Assuming a worst-case Doppler spread of 1 kHz, Eq. (2.47) yields a harmonic crosstalk contribution 50 dB below the multipath signal. A Doppler spread of 10 kHz would increase this by 20 dB to a level 30 dB below the multipath signal. Thus, it is also clear that harmonic crosstalk will have negligible effect on modem error rate reproducibility.

We consider now the introduction of degradation into the simulation caused by the sampling and reconstruction process that takes place for each measured complex tap gain. Due to the time-division-multiplexing process and the need to provide

settling time for the analog integrate-and-dump, the interval between samples of a particular complex tap gain, τ_s, is much larger than the total integrate time T associated with that tap gain measurement. The spectrum of the sampled signal contrains aliases of the desired spectrum centered at multiplex of $\pm 1/\tau_s$ Hz. Figure 2.14 shows two of these aliases straddling the desired lowpass tap gain process.

To extract the desired signal, the equipment includes a linear interpolator which acts like a filter with transfer function $(\sin \pi f\tau_s / \pi f\tau_s)^2$, as shown in Figure 2.14. This filter suppresses considerably the aliases while passing the desired signal with small distortion.

Calculation of the total distortion power after interpolation relative to the desired signal power, assuming a Gaussian-shaped signal spectrum, yields the values indicated in Table 2-7 as a function of the ratio of the rms Doppler spread to the sampling rate. Even at a Doppler spread as high as 0.354 times the sample rate, the level of distortion indicated on the table is 17.6 dB below the desired signal. Thus, the total distortion effect on the simulator output is a distortion signal 17.6 dB below the multipath signal. Operation at such a high value of Doppler spread in relation to the sampling rate is not likely to be needed since the highest sampling rate of the system for 32 measured samples of the impulse response (i.e., 32 correlators) is approximately 2 kHz, yielding a value of rms Doppler spread of around 700 Hz to produce the -16.7 dB alias distortion. Such large Doppler spreads are not predicted by the models available. Thus, under expected channel conditions, the alias distortion can be made negligible since it drops rapidly with Doppler spread, e.g., at a 354-Hz Doppler spread, the alias distortion drops to a value 33.2 dB below the multipath signal when the sampling rate is at the maximum.

We explore next the effect that the lack of inclusion of time-variant delays in the channel simulation has upon modem error rate reproducibility. Consider first the direct path alone. Let the transmitted signal be given by

$$x(t) = \mathrm{Re}\left\{z(t)\, e^{j2\pi f_0 t}\right\} \tag{2.48}$$

where z(t) is the complex envelope of the transmitted signal and f_0 is the center frequency of the transmitted signal. Making

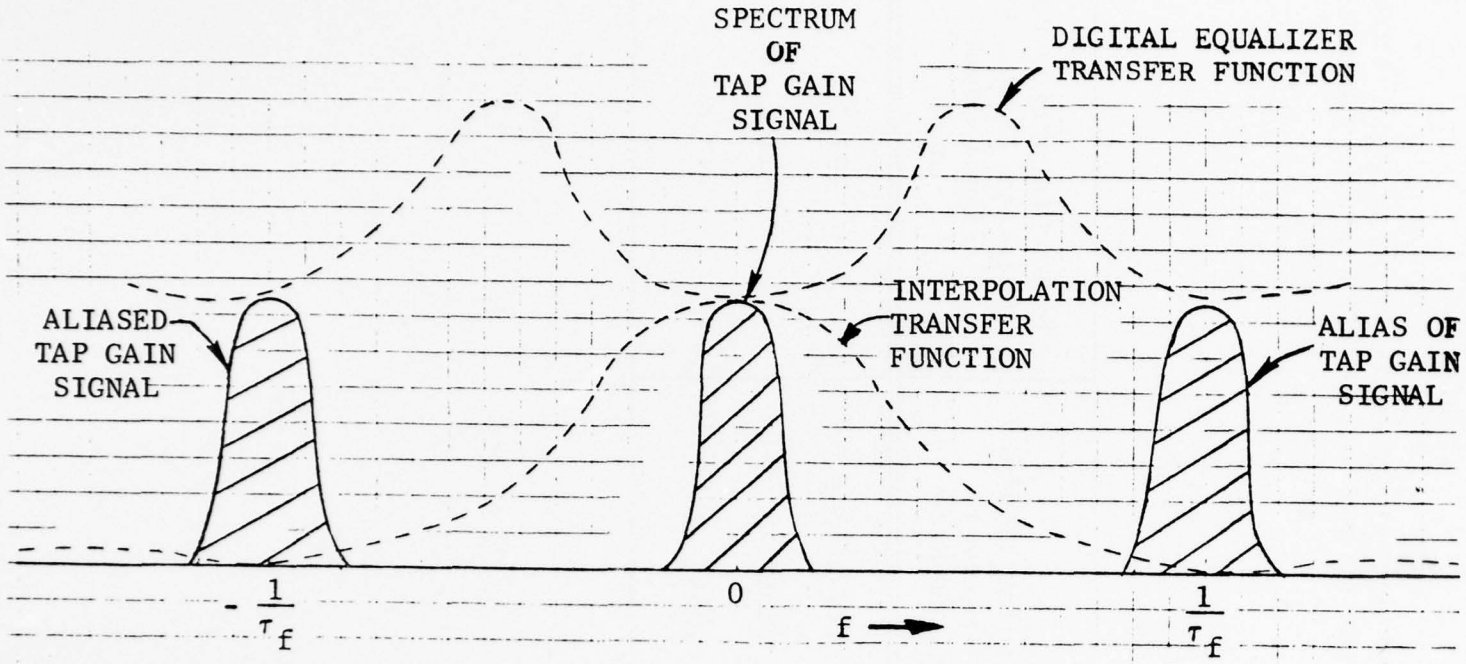

Figure 2.14 Illustration of Equalization and Interpolation in Reconstruction of a Tap Gain Signal from its Played-Back Samples

TABLE 2-7

RESIDUAL ALIAS DISTORTION RELATIVE TO DESIRED SIGNAL POWER AS A FUNCTION OF THE RMS DOPPLER SPREAD NORMALIZED TO THE SAMPLING RATE

RMS Doppler Spread Normalized to Sampling Rate	Total Distortion Power Relative to Desired Signal Power in dB
.177	-33.2
.250	-25.2
.354	-17.6

the valid assumption that a linear variation of delay with time characterizes the delay $\tau(t)$ over intervals of time long compared to many data bits,

$$\tau(t) = \tau_0 + \frac{v}{c}t \tag{2.49}$$

where v is the rate of change of the line-of-sight path, c is the velocity of light, and τ_0 is the delay at $t = 0$. The received signal in the absence of noise is given by

$$\begin{aligned} y(t) &= x[t - \tau(t)] \\ &= \mathrm{Re}\left\{ z\left(t - \frac{v}{c}t - \tau_0\right) e^{-j2\pi f_0 \frac{v}{c}t} \; e^{-j2\pi f_0 t} \right\} \end{aligned} \tag{2.50}$$

where the term $\exp(-j2\pi f_0 \frac{v}{c}t)$ may be recognized as providing the Doppler shift $-f_0 \frac{v}{c}$ Hz.

Apart from the Doppler shift, which is provided for in the simulator, the effect of the time-variant delay is to cause a change in time scale of the transmitted signal by the very small amount $-(v/c)$. For a Mach-1 speed v, this corresponds to approximately one part in 10^6. From the point of view of digital modems whose output complex envelope timing is controlled by a crystal oscillator, such a change in time scale produces an effect identical to a change of one part in 10^6 in the frequency of the crystal oscillator.

The only types of military modems whose output complex envelope timing is not completely controlled by a crystal oscillator are those which employ spread-spectrum pulse-forming networks at the transmitter and a corresponding matched filter at the receiver. These modems may exhibit a change in time scale of the order of $1/10^6$ in the received pulse as compared to the matched filter impulse response. However, if such a time scale change can cause perceptible degradation in a modem, that modem will likely never be built, because small temperature changes will cause much greater changes in time scale of the impulse response of the matched filter in the receiver. We have already pointed out that a typical time-scale change for cable is of the order of $4 \times 10^{-5}/^{\circ}C$. For acoustic surface wave matched filters, the change is much larger. In a sense, the

effects of time-scale change on modem performance caused by time-variant delay in a radio channel will be lost in the effects of temperature fluctuations.

If no temperature sensitivity is assumed, it may be shown that, if the time-bandwidth product of the spread-spectrum pulse satisfies the inequality

$$W_{RMS} T_{RMS} \ll \frac{2}{\pi \frac{v}{c}} \tag{2.51}$$

where W_{RMS} and T_{RMS} are the rms bandwidth and time duration, respectively, of the pulse

$$W_{RMS} = 2\sqrt{\frac{\int f^2 |P(f)|^2 \, df}{\int |P(f)|^2 \, df}} \tag{2.52}$$

$$T_{RMS} = 2\sqrt{\frac{\int t^2 |p(t)|^2 \, dt}{\int |p(t)|^2 \, dt}} \tag{2.53}$$

then no perceptible degradation can occur. In defining W_{RMS} and T_{RMS}, it is assumed that the pulse p(t) is centered at $t = 0$ and its spectrum P(f) is centered at $f = 0$.

Considering that v/c is of the order of 10^6, it is clear that time-bandwidth products approaching 100,000 would be needed before any possibility of degradation might occur! To our best knowledge, such large TW products are not practical for the impulse response of matched filters with the present state-of-the-art of fabrication techniques. Thus, time-scale change induced by relative motion of the terminals does not need to be provided in the simulation of a single line-of-sight path apart from simulation of the Doppler shift at the band center. Moreover, since the more general multipath situation can be broken up into a set of discrete paths with the aid of the tapped delay line model, it is clear that exactly the same conclusion is reached for the general channel with multipath.

AD-A056 374 CNR INC NEEDHAM MA F/G 20/14
WIDEBAND LINE-OF-SIGHT CHANNEL SIMULATOR.(U)
JUN 78 P A BELLO, D GOLDFEIN, K P JAUNISKIS F30602-75-C-0242
UNCLASSIFIED RADC-TR-78-118 NL

2 OF 2
AD
A056374

END
DATE
FILMED
9 -78
DDC

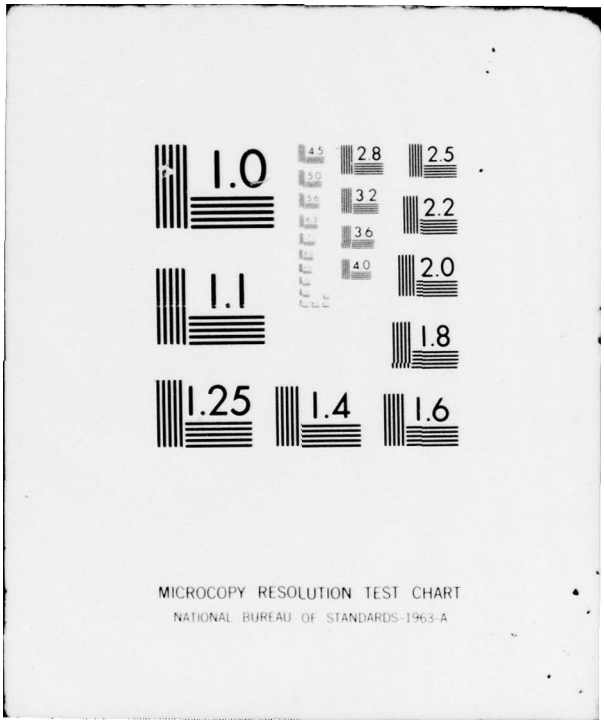
1.0
1.1
1.25
1.4
1.6
1.8
2.0
2.2
2.5
2.8
3.2
3.6
4.0
4.5
5.0
5.6
MICROCOPY RESOLUTION TEST CHART
NATIONAL BUREAU OF STANDARDS-1963-A

In conclusion, reviewing the potential harmful effects of the many small simulator nonidealities, it becomes clear that, as far as modem error rate reproducibility is concerned, the only impediments to modem error rate reproducibility possible with the prober/analyzer/simulator, as specified herein, are connected with measuring a channel in which one of the following three effects occurs:

(1) The ambient noise level is too high in channel measurement [see Eq. (2.35)].

(2) The Doppler spread exceeds the sampling rate capacity of the system (Table 2-7).

(3) The propagation channel multipath spread exceeds the measurement capability of the system.

Every reasonable effort has been made to reduce the limitations imposed by (1), (2), and (3). Moreover, the propagation analyses summarized in Section 2.1 show that, on the basis of reasonable scenarios for military links, the ranges of multipath and Doppler spreads measurable by this equipment is more than adequate for refractive multipath and reasonably adequate for surface multipath although, in the latter case, the unknowns of propagation channel modeling limit an assessment of adequacy. In any case, the prober/analyzer is sufficiently flexible to be able to identify channels for which (1), (2), or (3) occurs, and thus provides guidance for expansion of the system capability, if necessary. Table 2-8 defines the basic envelope of performance capability for the three conditions listed above.

TABLE 2-8

MAXIMUM RMS DOPPLER SPREAD (IN Hz) AND REQUIRED SIGNAL POWER/ NOISE POWER DENSITY (IN dB) AS A FUNCTION OF MEASURED MUTLIPATH SPREAD FOR REPRESENTATIVE OPERATING MODES OF THE PROBER/ANALYZER*

Mode	Multipath Spread†									
	37.5 ns [6]††		52.5 ns [8]		112.5 ns [16]		202.5 ns [28]		233.5 ns [32]	
	(Hz)	(dB)	(Hz)	(dB)	(Hz)	(dB)	(Hz)	(dB)	(Hz)	(dB)
I	3193.5	85.4	2513.4	86.7	1398.3	89.7	839	92.1	697.4	92.7
II	1571.8	82.4	1256.7	83.7	699.2	86.7	419.5	89.1	348.7	89.7
III	785.9	79.4	628.4	80.7	349.6	83.7	209.7	86.1	174.3	86.7
IV	392.9	76.4	314.2	77.7	174.8	80.7	104.9	83.1	87.2	83.7
V	196.5	73.4	157.1	74.7	87.4	77.7	52.4	80.1	43.6	80.7
VI	98.2	70.4	78.5	71.7	43.7	74.7	26.2	77.1	21.8	77.7

*When the Doppler spread reaches the value indicated, the total distortion power due to lowpass filter is at a level 17.6 dB below the desired signal. For a reduction of Doppler spread by 0.707 or 0.5, the aliased power reduces to 25.2 or 33.2 dB below the desired signal, respectively. When the signal power/noise power density is at the indicated value, the played-back channel will have an output noise contribution 30 dB below the desired playback channel output for the 100-MHz characterization.

†These multipath spread values are for the 100-MHz characterization. For 25-MHz characterization, the same multipath spread would be measured with 1/4 the number of impulse response samples. Only the first two columns are then applicable for playback with the multipath spread changed to 150 and 210 ns from 37.5 and 52.5 ns, respectively.

††Numbers in brackets are the total number of impulse response samples spaced 7.5 ns apart measured for the multipath, including direct path.

REFERENCES

[2.1] F. Ikegami, "Influence of an Atmospheric Duct on Microwave Fading," IRE Trans. on Antennas and Propagation, July 1959, pp. 252 - 257.

[2.2] M. S. Wong, "Refraction Anomalies in Airborne Propagation," Proc. of the IEEE, Vol. 46, September 1958, pp. 1628 - 1638.

[2.3] N. W. Guinard, et al., "Propagation Through an Elevated Duct: Tradewinds III," IEEE PGAP, July 1964, pp. 479 - 490.

[2.4] B. R. Bean and E. J. Dutton, Radio Meteorology, National Bureau of Standards Monograph 92, 1 March 1966.

[2.5] B. R. Bean, et al., "A World Atlas of Atmospheric Radio Refractivity," Essa Monograph No. 1, U. S. Government Printing Office, Washington, DC, 1966.

[2.6] H. T. Dougherty, "A Survey of Microwave Fading Mechanisms, Remedies, and Applications," Essa Technical Report ERL 69-WPL4, U. S. Government Printing Office, Washington, DC, March 1968.

[2.7] E. E. Gossard, "The Reflection of Microwaves by a Refractive Layer Perturbed by Waves," IEEE Trans. on Antennas and Propagation, May 1962, pp. 317 - 325.

[2.8] C. C. Watterson, J. R. Juroshek, and J. L. Demmer, "SHF Bandwidth Study, Phase III," NBS Report 8842, U. S. Department of Commerce, NBS, Boulder, Colorado.

[2.9] M. C. Thompson, Jr., H. B. Janes, L. E. Wood, and D. Smith, "Phase and Amplitude Scintillation of Microwave Signals Over an Elevated Atmospheric Path," Report of NASA Contract Order No. L-31028, ITS, Boulder, CO, 10 May 1971.

[2.10] O. E. DeLange, "Propagation Studies at Microwave Frequencies by Means of Very Short Pulses," BSTJ, January 1952, pp. 91 - 103.

[2.11] A. B. Crawford and W. C. Jakes, Jr., "Selective Fading of Microwaves," BSTJ, January 1952, pp. 68 - 90.

[2.12] G. M. Babler, "A Study of Frequency-Selective Fading for a Microwave Line-of-Sight Narrowband Radio Channel," BSTJ, Vol. 51, No. 3, March 1972.

[2.13] G. M. Babler, "Selectivity Fading Non-Diversity and Space Diversity Narrowband Microwave Radio Channels," BSTJ, Vol. 52, No. 2, February 1973.

[2.14] K. Bullington, "Phase and Amplitude Variations in Multipath Fading of Microwave Signals," BSTJ, Vol. 50, No. 5, July-August 1971, pp. 2039 - 2053.

[2.15] P. A. Bello, J. K. DeRosa, and C. J. Boardman, "Line-of-Sight Wideband Propagation," Final Report by CNR, Inc. on Contract No. F30602-73-C-0013 for Rome Air Development Center, May 1973.

[2.16] P. A. Bello, C. J. Boardman, D. Chase, and J. K. DeRosa, "Line-of-Sight Technical Investigations," Final Report by CNR, Inc. on Contract No. F30602-73-C-0244 for Rome Air Development Center, June 1974.

[2.17] J. K. DeRosa, "Tropospheric Refractive Multipath on LOS Links," CNR Executive Software Package No. 9-24.

[2.18] P. A. Bello, C. J. Boardman, D. Chase, and J. K. DeRosa, "Impact of Satellite Aeronautical Channel on Modem Specifications," Final Report by CNR, Inc. on Contract No. FAA-RD-74-54 for DOT/FAA, March 1974.

[2.19] P. A. Bello, D. Chase, J. K. DeRosa, L. J. Weng, and M. G. Bello, "Impact of Satellite Aeronautical Channel on Modem Specification, Phase II: Oceanic Multipath and Modem Concepts," Final Report by CNR, Inc. on Contract No. DOT-TSC-516-2 for DOT/FAA, March 1974.

[2.20] P. A. Bello, J. K. DeRosa, and C. J. Boardman, "Line-of-Sight Wideband Propagation," Final Report by CNR, Inc. on Contract No. F30602-73-C-0013 for Rome Air Development Center, May 1973.

[2.21] P. Beckmann and A. Spizzichino, The Scattering of Electromagnetic Waves From Rough Surfaces, Pergamon Press, 1963.

[2.22] A. L. Johnson and M. A. Miller, "Three Years of Airborne Communication Testing Via Satellite Relay," AFAL Report TR-70-156, November 1970.

[2.23] NATO/AGARD, "Antennas for Avionics," Conference Proc. No. 139, AD-782-310, November 1973.

[2.24] T. P. McGarty, "Models of Multipath Propagation Effects in a Ground-to-Air Surveillance System," Lincoln Lab. Tech Note 1974-7.

[2.25] P. A. Bello, J. K. DeRosa, and L. W. Pickering, "Impact of Satellite Aeronautical Channel on Modem Specifications, Phase III: Preliminary Satellite Wideband Test Plan," Final Report No. DOT-TSC-516-3, prepared for DOT/FAA by CNR, Inc., July 1974.

[2.26] P. A. Bello, "Characterization of Randomly Time-Variant Linear Channels," IEEE Trans. on Comm. Systems, Vol. CS-11, No. 4, December 1963, pp. 360 - 393.

[2.27] R. M. Lerner, "Signals With Uniform Ambiguity Functions," IRE Convention Record Pl.4, March 1958, pp. 27 - 36.

[2.28] S. H. Lin, "Statistical Behavior of a Fading Signal," BSTJ, December 1971, pp. 3211 - 3270.

[2.29] P. A. Bello, "A Troposcatter Channel Model," IEEE Trans. on Comm. Tech., Vol. COM-17, No. 2, April 1969, pp. 130 - 137.

[2.30] P. A. Bello, L. J. Jankauskas, and L. W. Pickering, "Equivalence Measurement Studies," Final Technical Report on RADC Contract No. F30602-73-C-0267 by CNR, Inc, April 1975. RADC-TR-75-95, Volumes I & II (A010004) & (A010005)

[2.31] P. A. Bello, D. Chase, J. K. DeRosa, L. W. Pickering, et al., "Impact of Satellite Aeronautical Channel on Modem Specifications," Report No. DOT-TSC-516-3, March 1974.

[2.32] Y. Peless and T. Murakami, "Analysis and Synthesis of Transitional Butterworth-Thompson Filters and Bandpass Amplifiers," RCA Review, March 1957, pp. 60 - 94.

[2.33] E. D. Sunde, Communications Engineering Theory, John Wiley & Sons, 1969. See Chapter 7.

SECTION 3

DESCRIPTION OF EQUIPMENT

Three separately packaged units are described in this report: the simulator, the analyzer, and the prober. Tables 3-1, 3-2, and 3-3 review the basic specifications for each of the three separate units.

Because of the flexibility of the equipment and the wide range of radio links which can be measured or simulated, there is no simple generalized operating procedure or configuration. Specific procedures for the measurement and simulation of radio propagation conditions, defined and described in Section 2, are presented in the Operations Manual.

3.1 Analyzer

The channel prober generates a 25- or 100-MHz chip rate PN sequence which is phase-modulated on an IF carrier at 70, 300, or 700 MHz and transmitted from either a ground site or an aircraft. The multipath analyzer accepts the IF output from a receiver at 70, 300, or 700 MHz and estimates the delay line channel model tap gains for the radio transmission channel from the prober to the analyzer. The mutlipath analyzer will be located at a ground site whenever possible, but must be located on a test aircraft for analysis of AA and ASA LOS channels. In addition to estimating tap gains, the analyzer tracks mean Doppler shift and will track differential multipath delay between the direct path and the earliest surface scatter path.

In order to permit accurate playback simulation of the multipath channel differential delay, tracking is continuous, not quantized, and no step changes in differential delay will be required from the channel simulator.

The multipath analyzer interfaces to a radio receiver at IF and processes the received probing signal to generate, display, and record the tap gains for a tapped delay line model of the radio channel. An extremely broad range of operating parameters is provided to characterize the largest range of radio channels possible.

TABLE 3-1

PROBER SPECIFICATIONS

Output Frequency:	70, 300, or 700 MHz
Output Level:	+10 to -59 dBm in 1-dB steps
Chip Rate:	100 M chips/sec or 25 M chips/sec
PN Sequence Length:	2047 for 100 M chips/sec 511 for 25 M chips/sec
Modulation:	PN sequences 0,180^{o} modulated at chip rate No Modulation
Input Power:	150 watts @105 - 125Vac, 50 - 400 Hz
Dimensions:	22" wide x 24" deep x 9" high
Test Outputs:	Chip rate clock 100/25 MHz, Sequence sync, both 50 ohm ECL compatible

TABLE 3-2

ANALYZER SPECIFICATIONS

Input Frequency:	700, 300, or 70 MHz
Input Level:	-80 dBm to -20 dBm
Gain Control Range:	60 dB manual or 60 dB automatic (recorded for playback)
Dynamic Range of Correlators:	55 dB except in highest sampling rate mode where it exceeds 35 dB
Multipath and Doppler Spread Measurement Capability:	As specified in Table 2-8
Real-Time Display:	Monitor oscilloscope will display complex voltage for up to 32 correlator outputs
Tape Recorder:	• Direct path Doppler • Refractive multipath Doppler • Direct path delay • Refractive multipath delay • Surface multipath delay
Correlator Multiplexing:	Selectable from 2 to 32 correlators. These outputs can be recorded for both 25- and 100-MHz correlation modes.
Physical:	Size - 22" x 26" x 60" Power Requirements - 110VAC, 60 Hz, 20A

TABLE 3-3

SIMULATOR SPECIFICATIONS

Input	
Center Frequencies:	70, 300, 700 MHz
Signal Processing Bandwidth:	25 MHz minimum for 20-MHz input frequency. 100 MHz minimum for 300-MHz and 700-MHz input frequencies.
Input Signal Level:	-20 dBm to +10 dBm. Also adjustable over a 40-dB range in 1-dB steps by input attenuator.
Impedance:	50 ohms
Output	
Center Frequencies:	Same as Input
Output Signal Level:	In the synthetic mode, the output signal and noise can be attenuated over a 40-dB range. The output level assuming 0-dB attenuation at both input and output and 0-dBm input level will be 0 dBm.
Spurious Contributions:	-50 dBm max, with any one tap ON
System Noise:	-48 dBm $\pm$ 3 dB with any one tap ON
Two-Tone Intermodulation Distortion for 0-dBm Inputs:	-48 dBm max, with any one tap ON
Impedance:	50 ohms
Physical	One rack: 44" x 38" x 90" One rack: 22" x 38" x 90" Power requirements: 110Vac, 60 Hz, 3φ, 30A/φ
Environmental	Typical laboratory environment

TABLE 3-3 (Continued)

Complex Modulator	• Playback • Computer synthesized • Synthetic complex Gaussian • External modulation • Fixed 0^{o}, 180^{o}, 90^{o}, or -90^{o} • Off
Test Equipment and Modes	
Signal Sources:	CW at 300 MHz.
Precision Power Meter:	Required to adjust input and output levels and available for system test.
LED Fault Monitors:	Individual power supplies and major RF subsection fault-isolating indicators.

TABLE 3-3 (Continued)

Noise Generator	
Level:	-50 dBm to +10 dBm in 1-dB steps.
Gaussian:	± 6 standard deviation. 10% accuracy in density function.
Spectral Shape:	Flat over selected input bandwidth.
Jamming	
Level:	Controllable by input attenuator in 1-dB steps over 40-dB range.
Frequency Response	
Amplitude Response with One Tap On:	± 0.5 dB over 100 MHz.
Nonlinear Distortion	Variable in 19 discrete steps from OFF to maximum (hardlimiting).
Internal Frequency Control	
Frequency Offset:	1 kHz in 1-Hz steps
Doppler Shift:	± 125 kHz in 1-Hz steps
Differential Doppler Shift:	± 125 kHz in 1-Hz steps
Phase Control (Jitter)	
Internal:	Sinusoidal up to 360^{o} and up to 1-kHz rate in 10-Hz steps.
External:	Up to 360^{o} and bandwidth up to 3 kHz.
Differential Delay	0.1, 0.2, 0.3, 0.4, 4.1, 8.1, 12.1, and 16.1 μs.
Tapped Delay Line	31 taps spaced 7.5 ns ± 25 ps.

Figure 3.1 is a block diagram of the multipath analyzer. The basic signal processing functions for a single tap sample are shown in Figure 3.2. Figure 3.2 has been simplified to eliminate the carrier and delay tracking loops and most of the IF signal processing.

The multipath analyzer time-division multiplexes two complex correlators to measure up to 34 complex tap gains. The tap gains are spaced 0.75 PN sequence chip apart on a tapped delay line channel model. The analyzer can operate at either 100-MHz or 25-MHz chip rates. The set of tap gains can be clustered into one of two groups, with 2 to 34 taps in the first (early or E) group and 0 to 32 taps in the second (late or L) group. Optimal channel characterization for playback through the simulator will be provided with a maximum total number of 32 tap positions sampled.

The analyzer contains tracking loops to keep the E and L tap groups centered in delay on the desired multipath signals and to track out the E path mean Doppler shift.

An AGC is included to track slow changes in received signal level to allow the optimal use of the analyzer and playback mode simulator with Air-Ground, Air-Air, and Satellite-Air radio channels with widely varying path losses.

Two PN sequence lengths and a range of correlator integration times are provided to allow the delay ambiguity, Doppler characterization bandwidth, and tap gain estimate SNR to be optimized for the radio channel being characterized.

The sampled tap gain output and AGC level from the analyzer is recorded as encoded digital data on an instrumentation tape recorder. The analyzer includes a real-time display which is used to evaluate system performance and to assist in signal acquisition.

Figure 3.3 is a picture of the analyzer; the tape recorder used for recording channel characterization data is not shown.

3.2 Prober

The prober/analyzer system uses external transmitters and receivers as its radio channel interface. The prober generates the IF signals which are required by the multipath analyzer.

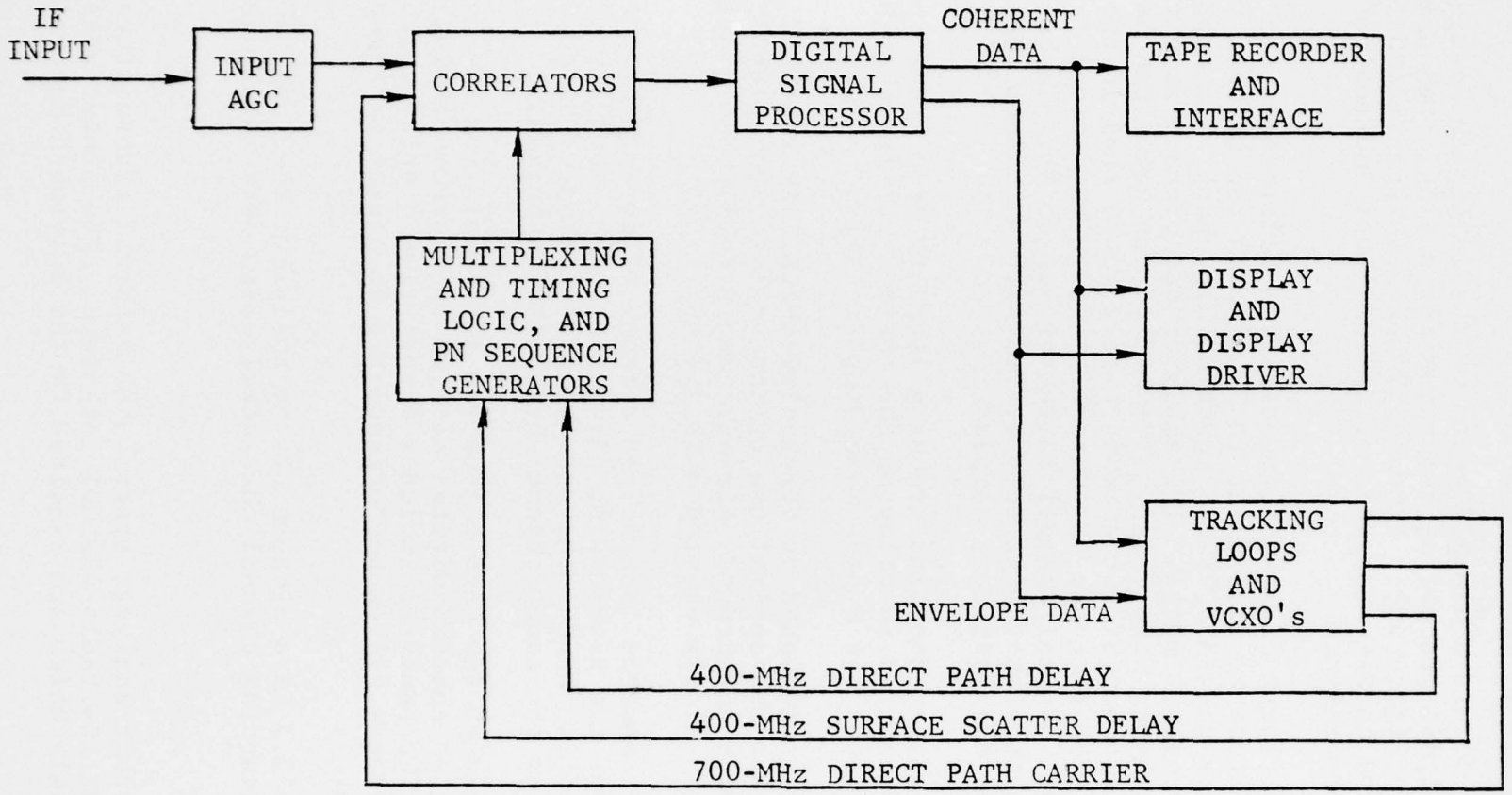

Figure 3.1 Block Diagram of Multipath Analyzer

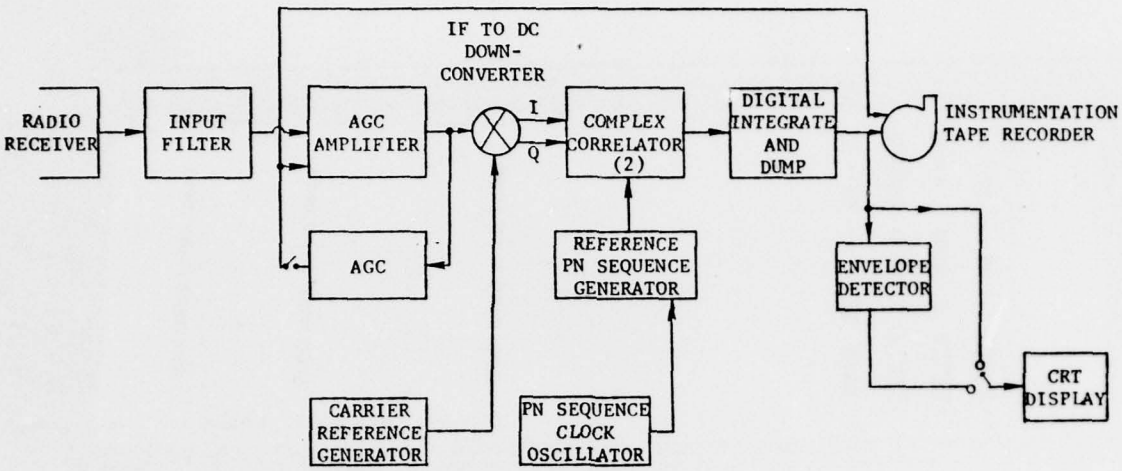

Figure 3.2 Simplified Multipath Analyzer Signal Processor Diagram

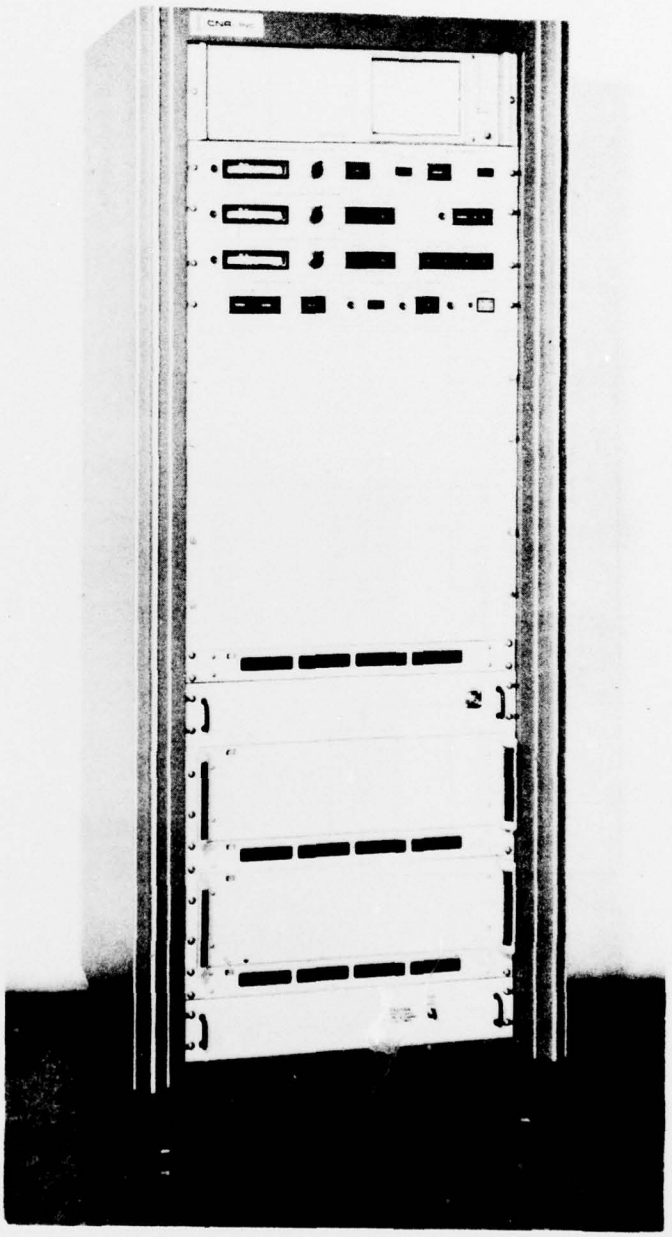

Figure 3.3 Analyzer

The channel prober provides only 511-bit and 2047-bit PN sequences. The 511-bit sequence is always used at the 25-MHz chip rate, and the 2047-bit sequence is always used at 100 MHz. The prober also incorporates a fault detection circuit which senses the presence of modulation and the IF output level. If either is disabled, a LED fault indicator is illuminated. Figure 3.4 shows the prober.

3.3 Simulator

Figure 3.5 is an overall block diagram of the simulator. The input section accepts the primary input at a 70-, 300-, or 700-MHz frequency. The input section also accepts a jamming signal at the same set of input frequencies, and generates an additive noise signal. A controllable nonlinear distortion element and the direct path signal gain multiplier are included. The section contains switches and attenuators for mode and level control, and provides several test and monitor inputs and outputs.

The analog signal processor section includes delay lines and tap gain multiplier arrays to simulate multipath propagation. Differential Doppler shift between two propagation paths is introduced here. Separate equalizers are provided at both the 25- and 100-MHz characterization bandwidths to maintain flat system response for channel playback. These are switched out for synthetic channel simulation.

The output section includes summing circuits and a down-converter to generate the composite multipath plus noise plus jamming plus direct path output signal. Test and monitor inputs and outputs are also provided.

The reference and local oscillator section synthesizes several fixed and variable oscillator frequencies for the up- and downconverters in the input and output section, and for differential Doppler simulation. Phase noise simulation control signals are introduced here. The oscillators provide extreme spectral purity for accurate radio channel simulation and playback.

The digital signal processing section includes the linear interpolator and linearizer sections and several signal sources. The linearizer provides a digital control signal mapping to provide linear tap gain response. The linear interpolator

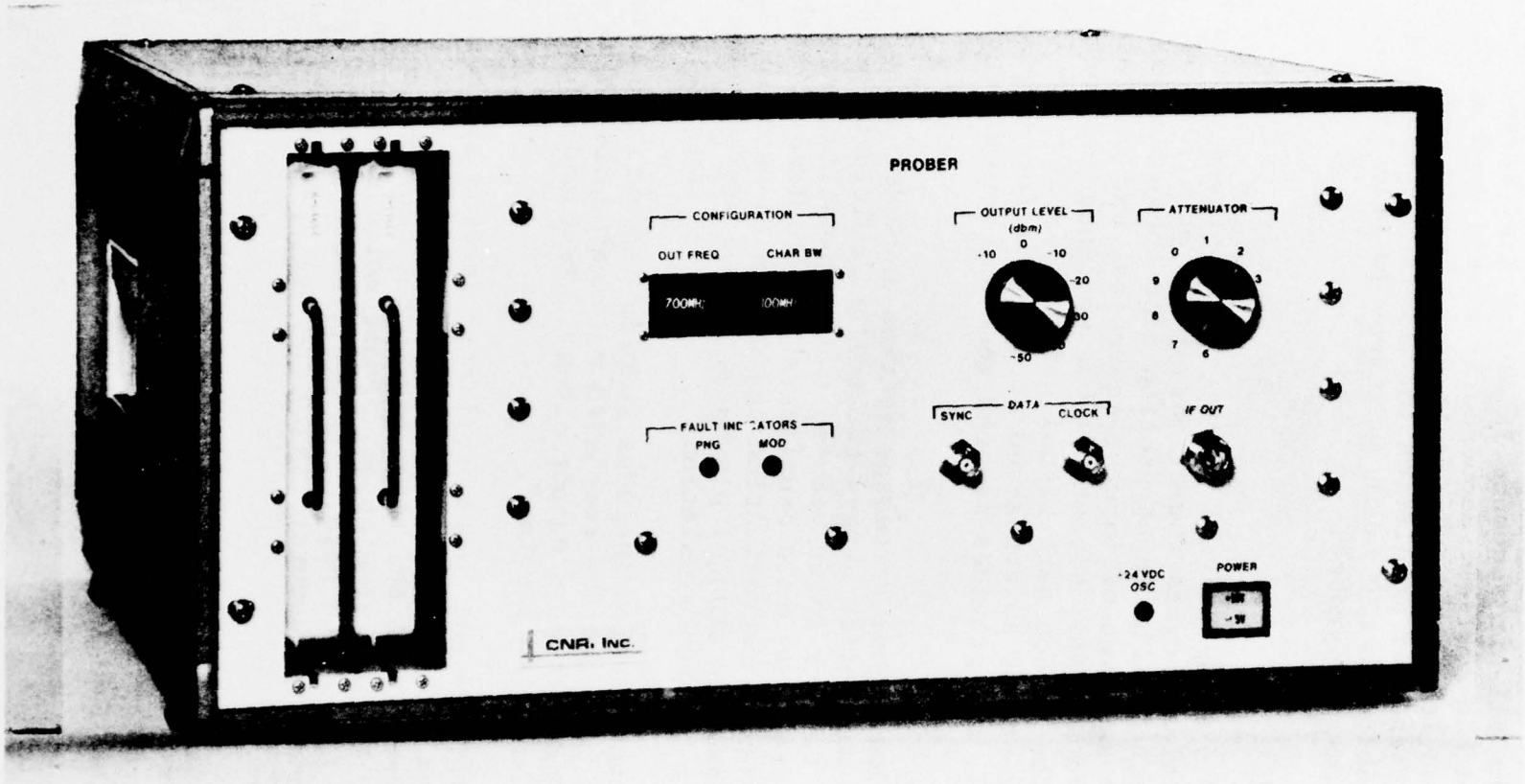

Figure 3.4 LOS Channel Prober

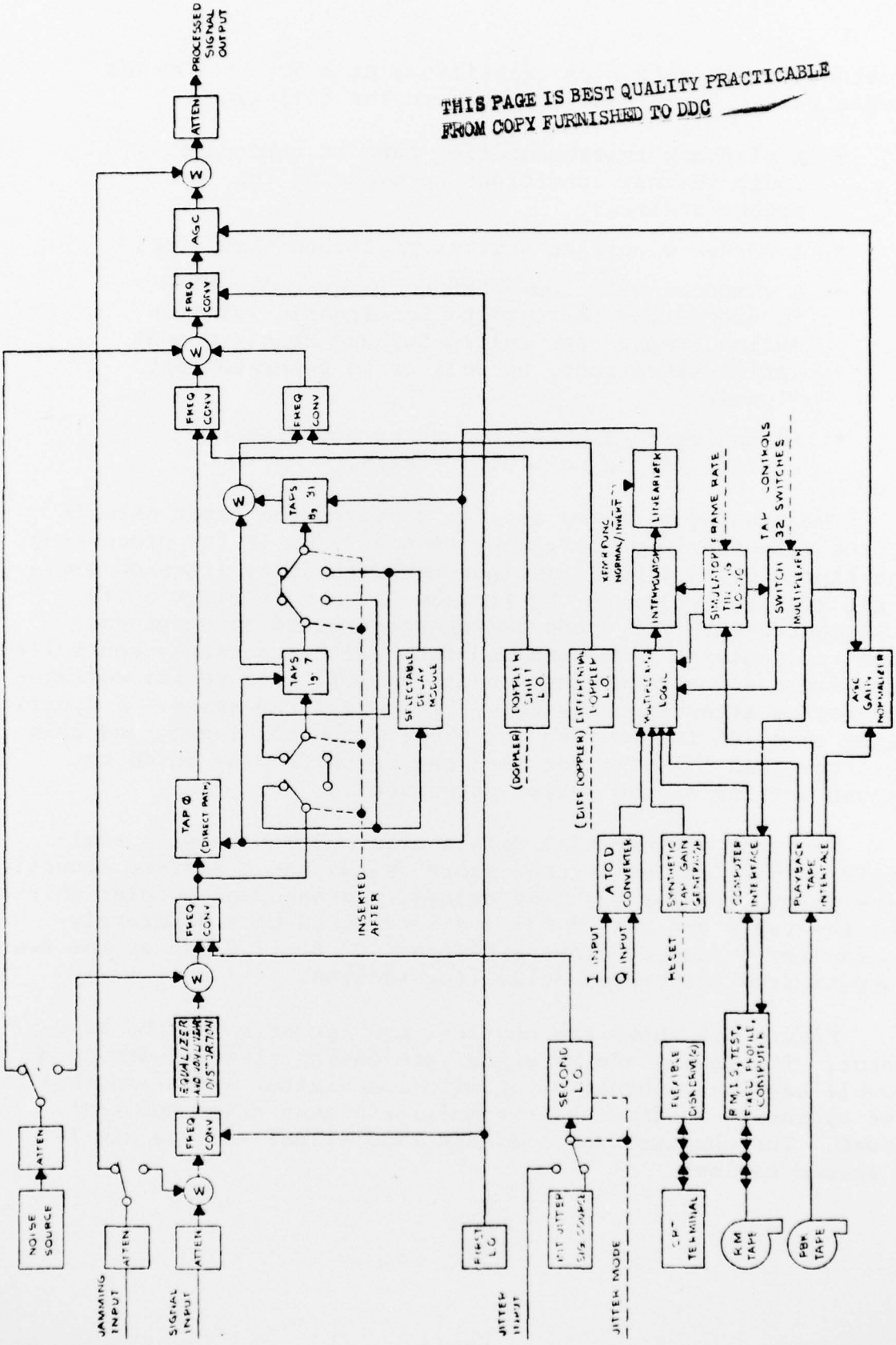

Figure 3.5 Functional Block Diagram of LOS Simulator

provides smooth gain step transitions at a 50- to 100-kHz sample rate. The signal sources are the following:

- A playback instrumentation tape to reproduce radio channel conditions recorded by the prober/analyzer.
- A hardware surface scatter multipath simulator.
- A computer with low-speed computer tape which is programmed to simulate ionospheric scintillation, refractive multipath, and static propagation situations, as well as to generate test signals.
- An analog-to-digital converter for direct control of tap multiplier units.

The simulator analog section converts the input signals at the selected input frequency to a 400-MHz IF for processing. The tapped delay line is implemented with delay lines of semi-rigid coaxial cable and the (complex) tap multiplier units implemented with PIN diode voltage-controlled attenuators. Each tap contains a complex modulator with separately controlled In-phase and Quadrature components as well as a series voltage-controlled attenuator to scale the overall tap gains. A dynamic range of 60 dB is provided for the I/Q control input, and this relative gain of different taps can be shifted by 60 dB by manual setting of the series attenuator.

The long differential delays are implemented with semi-rigid coaxial cables for the short delays and a Surface Acoustic Wave delay line for the long delays. Independent Doppler shifts for the tap 0 and taps 1 - 31 are introduced by a separately-controlled frequency conversion from 400 to 1700 MHz at the two outputs from the tapped delay line sections.

Figure 3.6 shows the physical configuration of the simulator. The analog and RF signal processing elements are in a double bay rack cabinet along with the digital signal sources for syntheitc surface scatter multipath generation and test modes. The computer and playback tape signal sources are in a second cabinet.

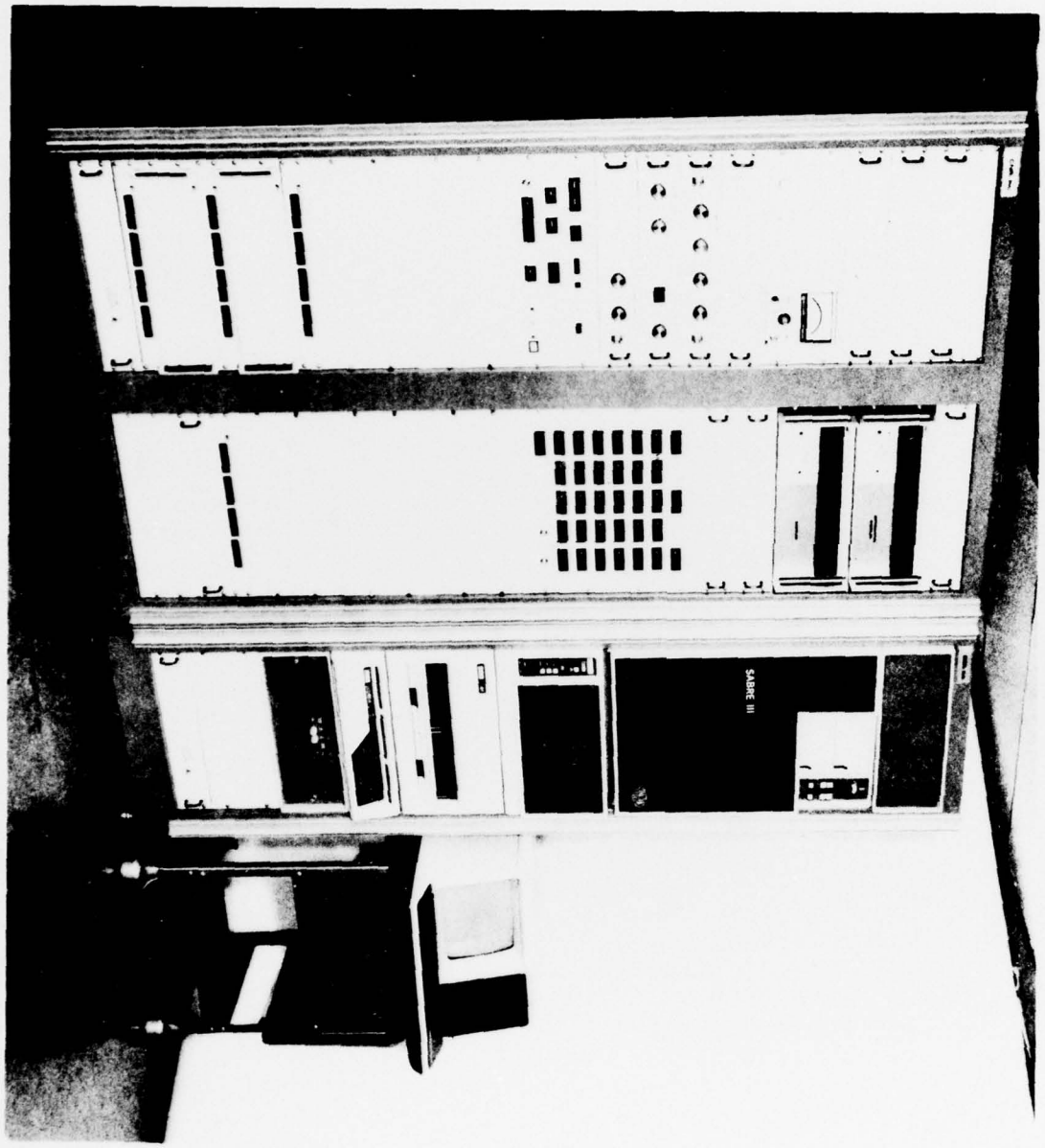

Figure 3.6 LOS Simulator

MISSION
of
Rome Air Development Center

RADC plans and conducts research, exploratory and advanced development programs in command, control, and communications (C^3) activities, and in the C^3 areas of information sciences and intelligence. The principal technical mission areas are communications, electromagnetic guidance and control, surveillance of ground and aerospace objects, intelligence data collection and handling, information system technology, ionospheric propagation, solid state sciences, microwave physics and electronic reliability, maintainability and compatibility.